

UNIVERSITY OF NAPLES FEDERICO II

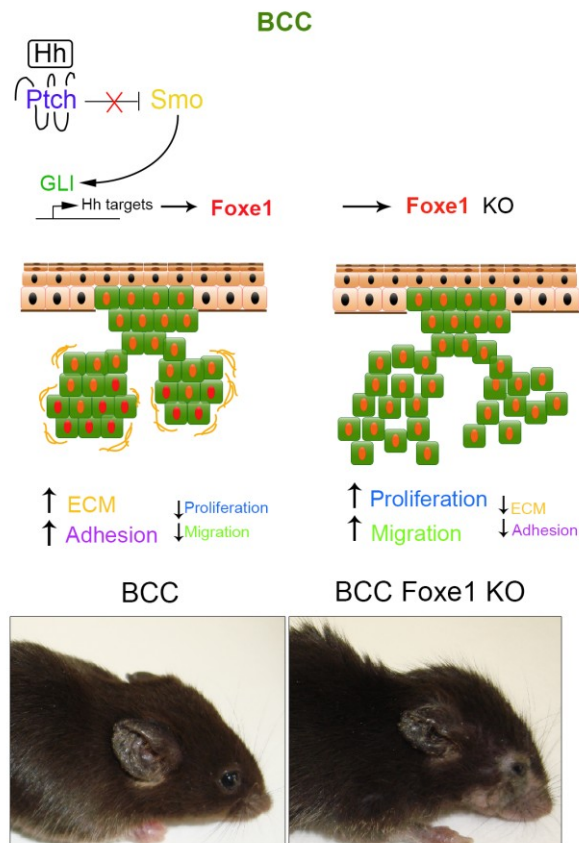
DOCTORATE IN
MOLECULAR MEDICINE AND MEDICAL BIOTECHNOLOGY

XXXII CYCLE



Federica Feo

IDENTIFICATION OF FOXE1 BIOLOGICAL FUNCTIONS IN NON-MELANOMA SKIN CANCERS (NMSC)



Year 2020

UNIVERSITY OF NAPLES FEDERICO II

DOCTORATE IN
MOLECULAR MEDICINE AND MEDICAL BIOTECHNOLOGY

XXXII CYCLE



IDENTIFICATION OF FOXE1 BIOLOGICAL FUNCTIONS IN NON-MELANOMA SKIN CANCERS (NMSC)

Tutor
Prof. Caterina Missero

Candidate
Dr. Federica Feo

Coordinator
Prof. Vittorio Enrico Avvedimento

Year 2020

TABLE OF CONTENTS

LIST OF ABBREVIATIONS USED	5
ABSTRACT	6
1. BACKGROUND.....	7
1.1 The epidermis	7
1.2 The hair follicle	9
1.3 Regulation of HF morphogenesis	12
1.4 Shh Pathway	13
1.5 Human skin cancers	15
1.6 Cutaneous Squamous Cell Carcinoma (SCC)	16
1.7 Basal Cell Carcinoma (BCC).....	17
1.7.1 Subtypes of BCC	19
1.7.2 BCC cell origin	21
1.8 FOX genes	22
1.9 FOXE1/TTF-2	24
1.10 FOXE1 in cancer	26
1.11 Foxe1 expression in skin	27
1.12 FOXE1 expression in NMSCs	32
1.13 Tbx1, another transcriptional regulator involved in BCC	37
2. AIMS OF STUDY	38
3. MATERIALS AND METHODS.....	39
3.1 Cell culture.....	39
3.2 Primary mouse keratinocytes isolation and cell cultures	39
3.3 Retroviral preparation	39
3.4 Retroviral infection	40
3.5 Lentiviral preparation	40
3.6 Lentiviral infection	40
3.7 Western Blot	41
3.8 RNA isolation and RT-qPCR	41
3.9 Microarray data analysis	42
3.10 Cell proliferation assay (BrdU assay)	43
3.11 Wound Healing Assay	43
3.12 Boyden Chamber cell migration assay	43

3.13 Tumorsphere assay with Matrigel coating.....	43
3.14 Tumorsphere assay with Ultra-low attached plates	44
3.15 Adhesion assay	44
3.16 Histology and Immunostaining	44
3.17 Mouse genotyping	44
3.18 Tumour induction	46
4. RESULTS.....	47
4.1 Identification of Foxe1 putative target genes in WT keratinocytes and BCC cells.....	47
4.2 FOXE1 negatively regulates keratinocyte proliferation.	55
4.3 FOXE1 expression impairs cell migration and affects cell adhesion in cultured NMSC cell lines.....	59
4.4 Tbx1 positively regulates cell migration in BCC cells.....	64
4.5 Depletion of Foxe1 expression in K5-Gli2 model results in severe tumorigenic skin lesions.	66
4.6 Foxe1 depletion in BCC leads to more disorganized skin lesions in SmoM2 expressing BCCs.....	71
5. DISCUSSION	77
6. LIST OF PUBLICATIONS.....	80
7. REFERENCES	81

LIST OF ABBREVIATIONS USED

BCC Basal Cell Carcinoma

SCC Squamous Cell Carcinoma

NMSCs Non Melanoma Skin Cancers

HF Hair Follicle

IFE Interfollicular Epidermis

HFSCs Hair Follicle Stem Cells

ORS Outer Root Sheath

IRS Inner Root Sheath

FOXE1 Forkhead Box E1

TTF-2 Thyroid Transcription Factor-2

TACs Transit Amplifying Cells

SCs Stem Cells

HFSC Hair Follicle Stem Cells

HH Hedgehog signaling pathway

GLI2 GLI Family Zinc Finger 2

K5 Keratin 5

K17 Keratin 17

ABSTRACT

FOXE1 is a thyroid-specific transcription factor belonging to the family of the Forkhead box (FOX) proteins, an evolutionarily conserved group of transcriptional regulators with a central role in a variety of developmental and physiological processes. Alterations in the FOX genes function is often associated to cancer. FOXE1 mutations are causative of the Bamforth-Lazarus syndrome, characterized by congenital hypothyroidism, cleft palate and spiky hair. Our findings have shown that in Basal Cell Carcinoma (BCC), the most common type of human cancer, the constitutive induction of the Sonic Hedgehog pathway leads to a strong upregulation of Foxe1 expression. In contrast, FOXE1 is absent in the more aggressive Squamous Cell Carcinoma (SCC), which is associated with a substantial risk of metastasis. Here we show that FOXE1 acts as a selective regulator of BCC formation, resulting in inhibition of cell proliferation and migration. We identified its putative targets genes in skin, revealing a positive correlation between Foxe1 expression and genes modulating the extracellular matrix structure and the cell-matrix interactions, actin cytoskeleton organization and regulation of cell adhesion. Accordingly, functional assays revealed that its expression negatively affects cell migration and increases cell adhesion. Moreover, we found that its expression is negatively correlated with cell cycle progression, resulting in an increased self-renewal capacity when depleted in BCC cells. Importantly, these *in vitro* findings correlate with studies *in vivo*. Using two distinct BCC mouse models, K5-Gli2 and K14-CreER; SmoM2, we demonstrate that Foxe1 is an important determinant of BCC architecture *in vivo* and that is likely to have a significant impact on BCC formation and maintenance by conferring at least in part the well-organized poorly invasive structure of this tumor. We propose a novel intriguing role for this transcription factor, which seems to play a negative contribution in skin tumorigenesis. These observations apparently odd for a gene overexpressed in cancer, may explain at least in part the relative slow proliferation rate and aggressiveness of BCC as compared to more invasive SCC.

1. BACKGROUND

1.1 The epidermis

The epidermis is the uppermost, multilayered compartment of the skin that serves as a protective barrier against external environmental insults, mechanical trauma and dehydration. The skin epidermis rests on the basement membrane rich in extracellular matrix, which separates the epidermis and its appendages from the underlying dermis. It is composed of 4-5 layers depending on the region of skin being considered. Those layers in descending order are the cornified layer (*stratum corneum*), granular layer (*stratum granulosum*), spinous layer (*stratum spinosum*) and basal layer (*stratum basale*). The stratified squamous epithelium of the epidermis is maintained by cell division within the basal layer. During the epidermal maturation keratinocytes, cellular component of the skin, undergo a series of morphological and physiological changes during epidermal maturation, giving rise to the complex architecture of the tissue (Fig.1). The cells of the basal layer remain attached to an underlying matrix through a series of adhesion molecules such as hemidesmosome, laminin and anchoring fibrils, and proliferate. Some of their daughter keratinocytes enter the spinous layer through asymmetric mitoses, where they exit the cell cycle, grow larger and establish robust intercellular connections (Simpson et al., 2011). The cells switch expression of basal layer specific keratins, Keratin5 and Keratin 14, to Keratin1 and Keratin10 (Krt1, Krt10) typical of the spinous layer (Fuchs and Green, 1980). The spinous layer also contains Langerhans cells, which are derived from a precursor in bone marrow and are involved in immune response. Above the spinous layer, keratinocytes contain numerous electron-dense keratohyalin granules packed with the protein profilaggrin in their cytoplasm, hence the name “stratum granulosum”. Filaggrin and loricrin are examples of markers of granular layer. The stratum corneum is the outermost layer of the epidermis. It is constituted by many layers of cells extremely flattened and imbricate each other. The stratified squamous epithelium is maintained by cell division within the basal layer. Differentiating cells slowly displace outwards through the spinous layer to the stratum corneum, where anucleate corneal cells are continuously shed from the surface (desquamation). In normal skin the rate of production equals the rate of loss, taking about two weeks for a cell to migrate from the basal cell layer to the top of the granular cell layer, and an additional two weeks to cross the stratum corneum (Rook and Burns, 2004). So the epidermis, like other stratified epithelia, has a self-renewing capacity throughout life, and this continuous turnover is mediated by stem cells in the basal layer of the interfollicular epidermis (Watt, 2002) and in the bulge region of the hair follicle (Cotsarelis et al., 1990). Keratinocytes move from the proliferative basal layer through the granular layer and continually replaced the cells of the outward layers. Indeed, as the body’s outer frontier, the epidermis is subject to repeated trauma that must be repaired after wounding (Shen et al., 2013). Within this layer, epidermal stem cells divide to self-renew and produce transient amplifying (TA) cells, which possess a more limited proliferative capacity. Transit amplifying cells (TACs) constitute the major cell type in the basal layer of the developing and mature epidermis and after few rounds of cell division they exit from the cell cycle, and initiate a terminal differentiation program, as they migrate outward toward the tissue surface.

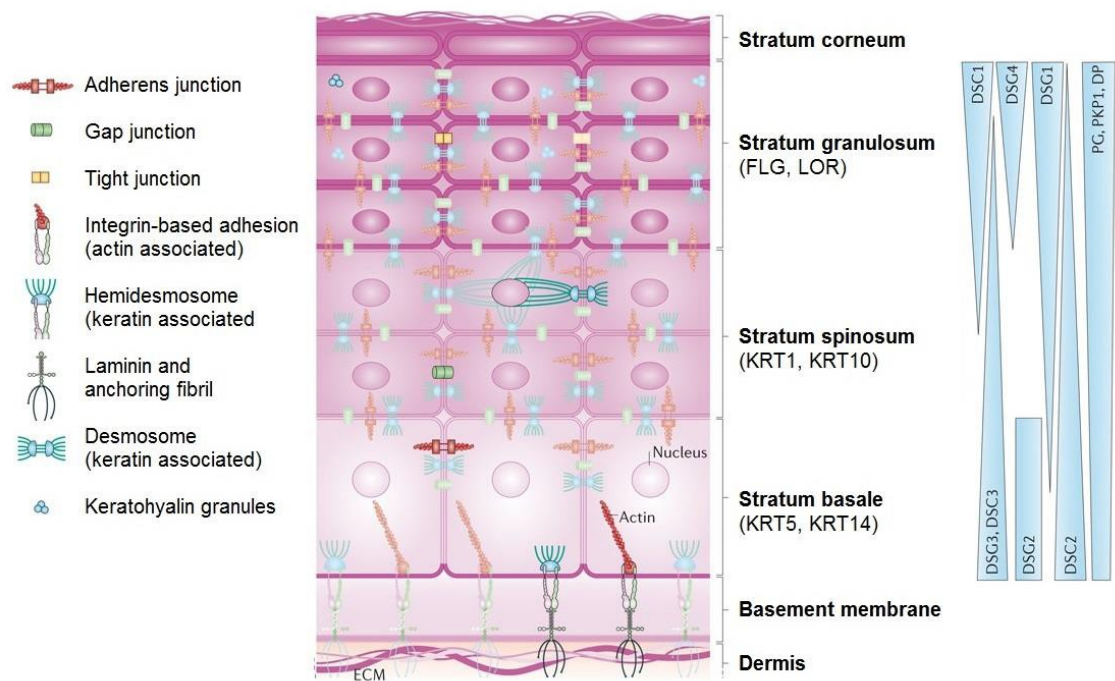


Figure 1. The epidermis. The epidermis is a stratified squamous epithelium composed by four layers resting on the basement membrane, which separates the epidermis from the underlying dermis. During epidermal maturation keratinocytes undergo a terminal differentiation driven by a gradual and sequential expression of specific cytoskeletal and junction proteins, which underlies the tissue morphogenesis. Desmogleins (DSG1, DSG2, DSG3, DSG4) and desmocollins (DSC1, DSC2, DSC3) are desmosomal cadherins that bind to plakoglobin (PG) and plakophilin (PKP) for the assembly of the desmosomes. Desmoplakin (DP) anchors keratin intermediate filaments to desmosomal plaques (adapted from Simpson et al., 2011).

1.2 The hair follicle

The hair follicle (HF) is a spatially and temporally well-defined mini-organ responsible for generating a hair composed of terminally differentiated, dead keratinocytes. In addition, HFs undergo cyclical bouts of tissue regeneration and hair growth, a process fuelled by stem cells. Its morphogenesis takes place early during embryogenesis and requires reciprocal interactions between the ectoderm and the mesenchyme, mediated by secreted ligands. The HF organogenesis process can be divided into three principal phases: the induction, the organogenesis and the cytodifferentiation. Each one of these phases is further divided into multiple stages (Schmidt-Ullrich et al., 2005). At the beginning of the HF development, an initial signal from the dermis allows the formation of a regular array of epithelial thickenings, called placodes. The signal involved in this process is probably the Wnt pathway. One of the clues that led to this hypothesis is that Lef1 (a transcription factor regulated by Wnt signalling) is expressed in the mesenchyme of the mouse hair follicle prior of its development and that it is necessary to this process (Millar SE, 2002) (Zhang Y et al., 2009). The formation of the regular pattern is owed to a balance between placode activators and repressors. Placode promote the clustering of dermal fibroblasts to form the dermal condensates, which become enveloped by follicular epithelial cells, to form the dermal papillae (DP) (Fuchs E, 2008). DP cells constitute the dermal niche that instructs hair follicle epithelial cell fate and differentiation. After embryonic follicular development, interactions between HF resident stem cells (HFSCs) and the underlying DP continue to regulate the cyclical regeneration of hair shafts in existing HFs throughout the life of the organism. The contact, between the dermal condensates and the epithelial cells, stimulates the epithelium to proliferate and generate the HF. During the hair follicle downgrowth, part of the developing hair germ cells loses contact with the dermal papilla and becomes the Outer Root Sheath (ORS). The remaining part, that maintains the contact with the dermal papilla and is made up of highly proliferative cells, is called Matrix. When the Matrix cells withdraw from the cell cycle, they move upward in concentric cylinders that adopt distinct differentiation programs: at first appear the Inner Root Sheath (IRS), and then the Hair Shaft (Fuchs E, 2001). The IRS is made up of three layers (from the outer to the inner: Henle, Huxley layers and IRS cuticle) and acts as a channel that guides the HS to the skin surface (Fuchs E, 2008). The HS is composed of terminally differentiated death keratinocytes, which are compacted to form a fiber (Schneider MR et al., 2009). Simultaneously, the outer root sheath starts to form a cylinder around the inner root sheath to create a bulbous peg structure. Additional appendages such as sebaceous glands and touch domes also develop during this phase (Fig.2).

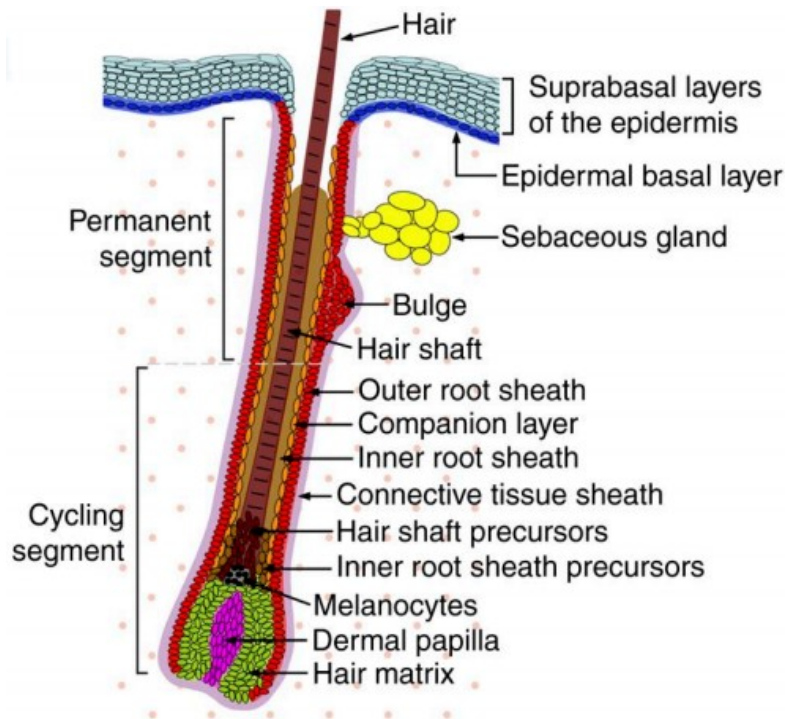


Figure 2. The anatomy of mature Hair Follicle. Schematic of the histology of a mature hair follicle (HF). The hair matrix consists of proliferating cells (green) encasing the dermal papilla (magenta). Upon differentiation, matrix cells produce the concentric rings of cells that generate the hair shaft (dark brown) and inner root sheath (IRS; light brown). The upper matrix contains melanocytes (black). The outer root sheath (ORS; red) is continuous with the basal layer (blue) of the epidermis. The companion layer (orange) separates the ORS from the IRS. The ORS contains follicular stem cells nested in the bulge niche underneath the sebaceous gland (yellow). The HF is surrounded by connective tissue sheath cells (CTS; violet). Dermal cells are shown as dots. In contrast to the HF permanent segment, the cycling lower segment undergoes phases of growth and degeneration (adapted from Gritli-Linde et al, 2007).

When matrix cells exhaust their proliferative capacity or the stimulus required for it, hair growth stops. At this time, the follicle enters a destructive phase (catagen), leading to the degeneration of the lower two-thirds of the follicle. The upper third of the follicle remains intact as a pocket of cells surrounding the old hair shaft. The base of this pocket is known as the Bulge, which is the natural reservoir of hair follicle stem cells (SCs) necessary to form a new hair follicle. After catagen, the bulge cells enter a quiescent stage (telogen). In the mouse, the first telogen lasts approximately one day, after which all the hair follicles synchronously enter a new cycle of regeneration and hair growth (anagen) (Fig.3).

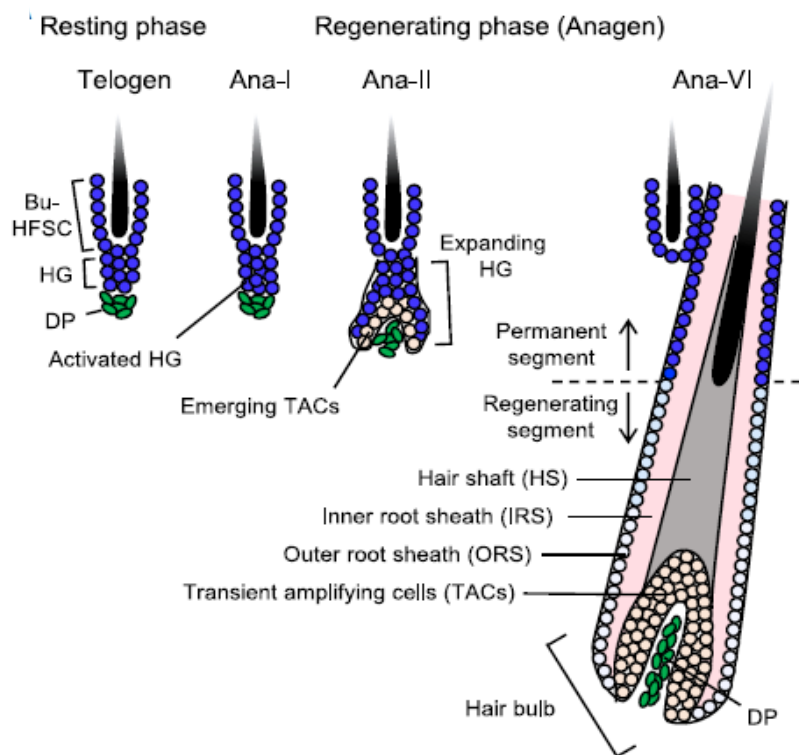


Figure 3. The Hair Cycle. Schematic depicting resting (telogen) and regenerating (anagen) phases of hair follicles. Bu-HFSC, HF stem cells residing in the bulge niche; HG, hair germ, a niche housing the primed HFSCs that will be activated at the start of the new hair cycle; DP, dermal papilla, specialized mesenchymal cells required to fuel the hair cycle (adapted from Yang, Adam et al. 2017).

1.3 Regulation of HF morphogenesis.

At the beginning of the HF development, an initial signal from the dermis allows the formation of a regular array of epithelial thickenings, called placodes. In mice, from embryonic day E14.5 to birth, hair placodes emerge in waves of spatially patterned cell clusters within the basal-epidermal plane. Canonical WNT signaling, mediated by β -catenin and LEF1, is essential for placode formation (Andl et al., 2002; Gat et al., 1998; Huelsken et al., 2001; van Genderen et al., 1994). Wnt ligands are expressed in the interfollicular epidermis as well as the hair follicle during all stages of follicle development, suggesting that the Wnt signaling is a main regulator of follicle development (Huelsken et al., 2001, Fuchs et al., 2001, Widelitz et al., 2008). The initial step appears to take place in the absence of cell divisions, as WNT-signaling epidermal cells cluster within the basal plane (Ahtiainen et al., 2014). The activation of canonical Wnt signaling induces SHH expression, indicating HH signaling activation during hair follicle development. While both signals occur within the bud, SHH signaling is genetically downstream of WNT-signaling, as it still occurs when SHH is absent, even though hair buds but do not progress further (Jamora et al., 2003; St-Jacques et al., 1998; Woo et al., 2012). It has been shown that the cutaneous *Wnt5a* disappears into the skin *Shh*^{-/-}, indicating that *Wnt5a* is downstream, or even to direct target of the HH signal (Reddy et al., 2001). *Wnt5a* suppresses expression of LEF-1, indicating the suppression of Wnt's canonical reporting, cooperation between *Wnt5a* and the negative regulators of HH signaling may be important for cell differentiation during the development of the hair follicle demonstrated crosstalk between the Wnt, HH and BMP signaling pathways during hair follicle development (Suzuki et al., 2009). Asymmetric distribution of WNT and SHH signaling and their mutual antagonism are used in the niche's place to govern SC (Stem Cell) specification and balance proliferation and differentiation, suggesting, from recent studies, that the molecular and cellular diversity is generated within the hair germ during the earliest divisions in the established WNT-activated placode (Ouspenskaia T., et al. 2016). At each step, stem cells and their progeny receive instructive signals and must change their chromatin landscape to generate the distinct lineages of the HF (Yang et al., 2017; Adam et al., 2018).

1.4 Shh Pathway

The Hedgehog (HH) signaling pathway is one of the fundamental signaling pathways that contributes to hair follicle development and follicle bulge stem cell maintenance, aberrant activation of HH signaling is associated with several tumor conditions. Shh expression during hair follicle morphogenesis is conserved between mice and humans. HH signaling is initiated by one of three spatiotemporally-confined ligands: Sonic Hedgehog (SHH), Indian Hedgehog (IHH), and Desert Hedgehog (DHH). Each HH ligand has distinct spatial and temporal expression patterns, but all activate HH signaling by binding to Patched (PTCH) 1 or 2. PTCH1 is considered to be the primary receptor for HH ligands. In the absence of HH, PTCH1 is localized in primary cilia and constitutively suppresses the activity of SMO, a seven-pass transmembrane-spanning protein that is a member of the G-protein-coupled receptor superfamily (Rohatgi et al., 2007). Suppressor of fused (SUFU) is a key negative regulator of the HH signaling pathway (Lee et al., 2007), in the absence of HH ligands, in fact, SUFU inhibits signaling by sequestration of GLI proteins in the cytoplasm. Graded levels of HH signaling trigger the expression of different sets of response genes, depending on the ratio of GLI activator (GLI-A) to repressor (GLI-R) forms. In vertebrates, the GLI family consists of three proteins, GLI1, GLI2, and GLI3 (Aberger et al., 2014). All GLI proteins contain an activator domain at their C-terminus; GLI2 and GLI3 also have an N-terminal repressor domain. Studies in mutant mice suggest that GLI2 is the major activator of HH signaling, whereas GLI3 is the major repressor. GLI1 most likely serves as a signal amplifier downstream of GLI2. When HH signaling is activated, SUFU–GLI2 complexes dissociate and GLI2 is activated. Gli2 knockout mice die at birth, whereas Gli1 knockout mice show normal development, unless one copy of Gli2 is also defective (Park et al., 2000). Constitutive activation of HH signaling has been observed in many cancers and promotes cancer cell proliferation, metastasis, and cancer stem cell maintenance. Somatic mutations of PTCH1 and SMO have been identified in patients with BCC and medulloblastoma.

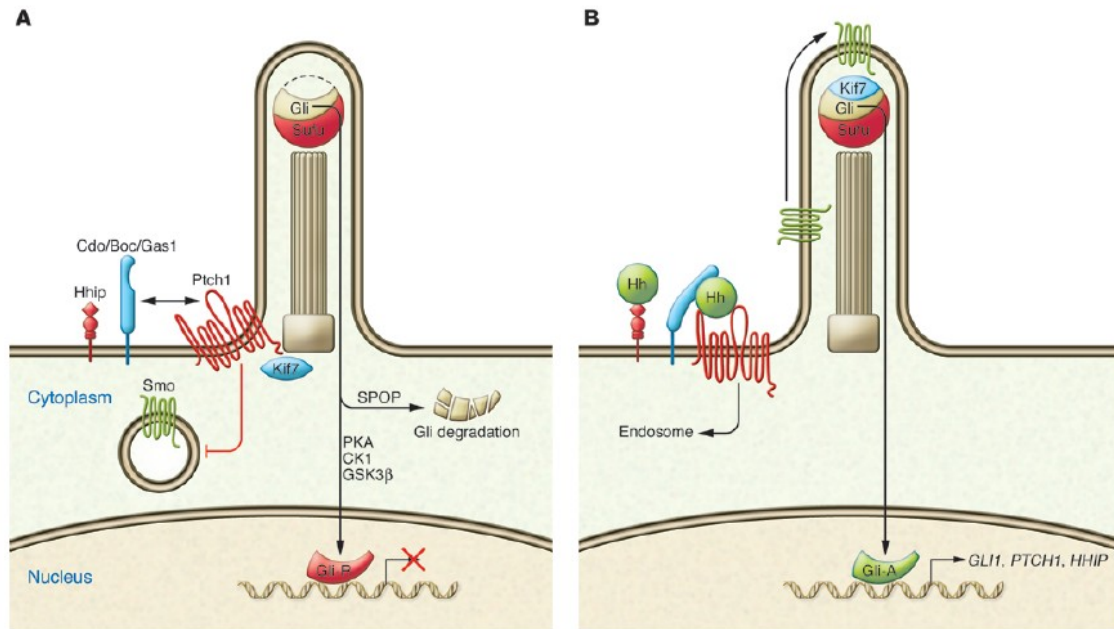


Figure 4. The Hh signaling pathway. A) In its “off” state, Ptch1 represses Smo activity. Gli2 and Gli3, effectors of the Hh pathway, are phosphorylated by a kinase cascade, which includes PKA, CK1, and GSK3 β , and are directed to the proteasomal degradation pathway via the SPOP complex. A fraction of the Gli2/3 protein is processed into a repressor form, Gli-R, which inhibits Hh target gene transcription. B) Hh ligand binding to Ptch1 abrogates its inhibitory effect on Smo, allowing Smo to translocate into the primary cilium and induce accumulation of the Gli-Sufu complex at the tip of the primary cilium. Activation of the Hh pathway results in accumulation of Gli-A and initiation of the transcription of Hh target genes such as PTCH1, GLI1, and HHIP (adapted from Kasper et al., 2012).

1.5 Human skin cancers

Skin cancer is the most common of all human cancers, manifested by the uncontrolled growth of abnormal skin cells. It occurs when unrepaired DNA damage to skin cells (most often caused by ultraviolet radiation from sunshine or tanning beds) triggers mutations, or genetic defects, that lead the skin cells to multiply rapidly and form malignant tumors. Skin cancers comprise two major categories. The first group includes the melanomas, which represent only a small percentage (about 5%) of all cancers that affect the skin but they are also the most aggressive form of skin cancer that can spread quickly to other parts of the body if not treated early. Cutaneous melanoma is a cancer that is derived from the tumor transformation of melanocytes. The skin cancers different from malignant melanomas are classified as Non-melanoma skin cancers (NMSCs). This group includes Basal Cell Carcinoma (BCC) and Squamous Cell Carcinoma (SCC), the two most common type of human malignancy. While malignant, these are unlikely to spread to other parts of the body and they may be locally disfiguring if not treated early. Their incidence is increasing at high rate worldwide. The need to understand the molecular mechanisms underlying these injuries is essential. The basal cell carcinoma (or basalioma) originate from basal cells, the keratinocytes present in the deepest layer of the epidermis, while squamous cell carcinoma from the most superficial epidermal cells, known as squamous cells. Basal cell and squamous cell carcinomas account for almost all (over 99%) of non-melanoma skin cancers, but there are other rare types of skin cancer such as Merkel cell carcinoma, Kaposi's sarcoma and cutaneous lymphoma. In addition, another rare form of skin cancer displays phenotypes of both BCC and SCC known as Basosquamous carcinoma (BSC). BSCs genetically likely originate as basal cell carcinomas that partially squamatize through an accumulation of ARID1A mutations and RAS/MAPK pathway activation (Tarapore E. and Atwood S. X., 2019).

1.6 Cutaneous Squamous Cell Carcinoma (cSCC)

Squamous cell carcinoma (SCC), the second most common form of skin cancer (Venza et al., 2010), is an uncontrolled growth of abnormal cells arising from the squamous cells in the epidermis, the skin's outermost layer. It is sometimes called cutaneous squamous cell carcinoma (CSCC). SCCs often look like scaly red patches, open sores, warts or elevated growths with a central depression; they may crust or bleed. They can become disfiguring and sometimes deadly if allowed to grow. More than 1 million cases of squamous cell carcinoma are diagnosed each year in the U.S. Incidence has increased up to 200 percent in the past three decades in the U.S., and more than 15,000 Americans die each year from the disease. This cancer can be particularly aggressive and have a higher tendency to metastasize. Although some cSCCs can arise from healthy skin, they often originate from early non-invasive lesions called actinic keratosis (AK). The progression from AK to cSCC can be viewed as a multistep process involving sequential DNA mutations, mainly UV-light-induced, in oncogenes and tumor suppressor genes (Missero and Antonini, 2014).

Several cancer-associated genes have been identified which contribute to formation and progression of cSCC. The tumor suppressor TP53 is very frequently mutated in cSCC, ranging from 44% to 79% in advanced cSCC. Mutations in p53 are found in SCC precursor lesions suggesting that this mutational event may represent an early step in human cSCC development. Some p53 mutations may have little detrimental effect and are found in non-neoplastic keratinocytes. Also the inactivation of NOTCH1 and NOTCH2 is frequent in cSCC, according to the close interconnection between this signaling and p53. The tumor suppressors CDKN2A and KMT2D are also mutated with a similar frequency (45% and 48%). RB1 and PTEN are mutated at a low frequency, such as gain-of-function mutations in RAS gene that are less frequent. Inactivation in these tumor suppressor genes is often associated with benign injury as papillomas or keratoacanthomas. Both interfollicular epidermis and the hair follicle stem cell compartment (HFSC) are competent to generate cSCCs (Missero C., 2016).

1.7 Basal cell carcinoma (BCC)

Basal Cell Carcinomas (BCC) is the most common type of cancer in human. Although in most cases it does not metastasize, BCC is a significant health issue because it usually appears in exposed skin, and it must be surgically removed to avoid expansion and disfiguration. Left untreated, though, they can reach large sizes and invade anything in their path including bone, cartilage, and vital structures such as the eye. BCCs are the most commonly diagnosed human cancer (750,000 BCCs are treated each year in the US) but the death rate from these carcinomas is very low, since they metastasize extremely rarely. The majority of BCCs occur sporadically, although the patients with a rare heritable disorder named basal cell nevus syndrome (BCNS) have a marked susceptibility to developing BCCs. The causative mutations occur in the 90% of sporadic BCCs in Patched 1 (PTCH1) gene, an inhibitor of the Hedgehog (HH) signaling pathway. Only rarely, activating mutations occur in the Smoothed (SMO) protein which presumably render SMO resistant to inhibition by PTCH. These mutations lead to a constitutive activation of HH which is found in most sporadic or inherited form of BCC. This deregulation of HH pathways predispose also to other human malignancies such as medulloblastoma, habdomyosarcoma and basaloid follicular hamartoma in skin. Ligand-independent activation of Hh signaling in epidermal cells is the primary event in sporadic BCC. These tumors express high levels of Gli1 and Gli2, PTCH and other HH target genes. Several animal models support the notion that uncontrolled Hh signaling is sufficient to drive BCC- or BCC-like tumorigenesis in mice (Daya-Grosjean, L. & Couve-Privat, S., 2005). The overexpression of positive regulators of the Hh pathway (Shh, oncogenic SMO, GLI1, Gli2) in skin (Oro et al., 1997; Xie et al., 1998; Grachtchouk et al., 2000; Nilsson et al., 2000; Grachtchouk et al., 2003), or gene deletion studies, to generate mice with a disrupted *Ptch1* allele mimicking the genetic defect in NBCCS patients (Aszterbaum et al., 1999). p53 loss contributes markedly to the development of BCC enhancing HH-driven tumorigenesis (Epstein, 2008). Intriguingly, superficial BCCs arise as *de novo* epithelial buds resembling embryonic hair germs, a condensate of cells whose development is regulated by canonical Wnt/b-catenin signalling. Similar to embryonic hair germs, human BCC buds showed increased levels of cytoplasmic and nuclear b-catenin and expressed early hair follicle lineage (EHFPs) markers. Wnt signalling pathway controls this genetic reprogramming of epithelial cells and its inhibition obtained *in vivo* with the conditional overexpression of the Wnt pathway antagonist Dkk1 in SmoM2-expressing mice (Xie, J. et al., 1998) potently inhibited epithelial bud and hamartoma development without affecting Hh signalling (Yang, Andl et al. 2008) and prevents the reprogramming in EHFPs and tumor initiation (Youssef et al., 2012), suggesting the requirement of activated Wnt signalling in BCC induction. In particular, it has been identified the transcriptional factor Sox9 as the principal downstream effector of Wnt/b-catenin signalling required for the long term self-renewal of oncogene-expressing cells and tumor formation (Larsimont, Youssef et al. 2015). Moreover, independently from influence by canonical Wnt or Hedgehog signalling on tumorigenic process, genetic aberrations in the Hippo (or YAP/TAZ) regulators promote BCC formation. YAP depletions in BCC tumors leads to effective impairment of the JNK-JUN signaling, a well-established tumor-driving cascade, by providing a lower fitness

to Yap-null dysplasia and thus reducing their capacity to progress to invasive BCC, in mice (Maglic, Schlegelmilch et al. 2018).

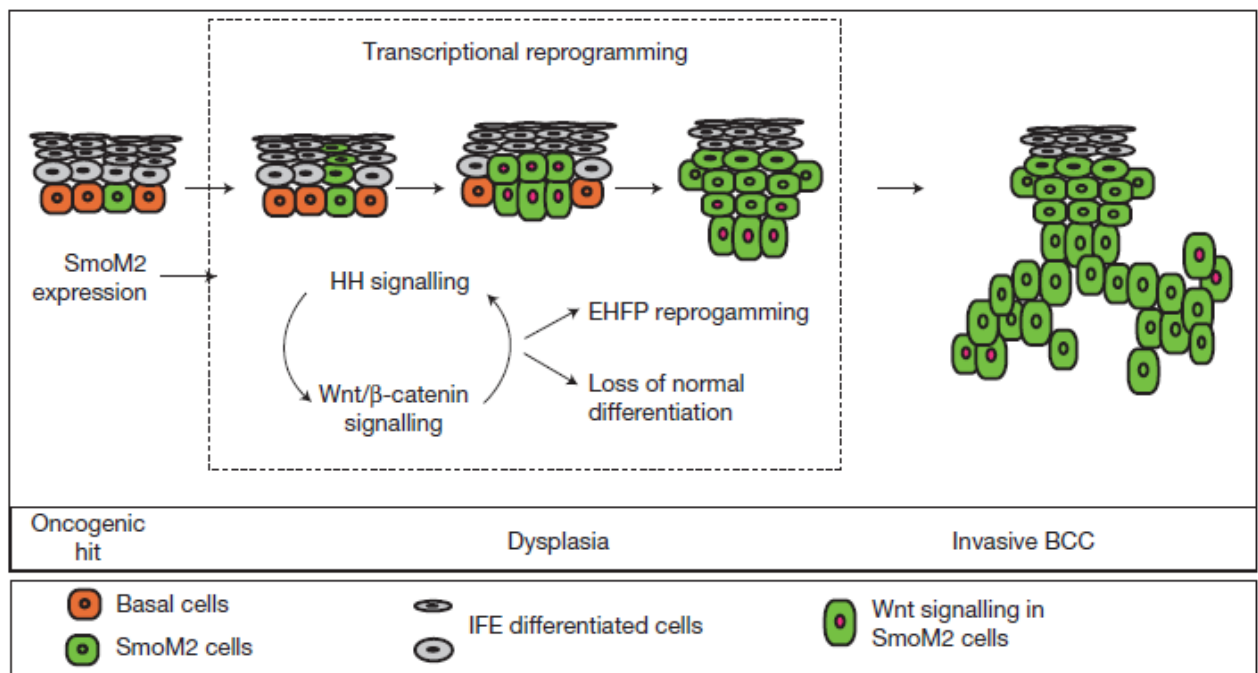


Figure 5. Human BCCs express markers of the Wnt/β-catenin and EHFP signatures. Model summarizing the mechanisms regulating the early step of BCC initiation. SmoM2 expression in tumour-initiating cells leads to a rapid and profound change in gene expression that induces a fate change in IFE progenitors, which stop to differentiate into suprabasal cornified cells and acquire a morphology and a gene expression profile presenting striking similarities with normal EHFPs before progressing into invasive carcinoma. SmoM2 expression in adult IFE cells rapidly activates the Wnt/β-catenin signalling pathway, which in turn regulates the embryonic hair follicle reprogramming of adult IFE cells and sustains HH signalling in a positive feedback loop to initiate BCC development (Youssef et al., 2012).

1.7.1 Subtypes of BCCs

Like many tumors, BCCs can be classified into several subtypes based on morphology and differentiation. They are distinguished as: superficial, nodular, micronodular, infiltrating, sclerosing, and fibroepithelial. Diversity in the phenotypic appearance of BCCs indicates that the cell of origin may be a stem or progenitor cell (Kasper, Jaks et al. 2012).

The superficial and nodular subtypes of BCC are indolent and are thought to arise from progenitor cells located in the epidermis and within the hair follicle, respectively. In contrast, the cellular origins of the more aggressive variants, including infiltrative, basosquamous, and morpheaform or sclerosing BCCs, are unclear. These aggressive subtypes frequently cause local tissue damage, are often not circumscribed by a basement membrane, and may be associated with fibroplasia, suggesting that stromal communication via paracrine signals may also be especially important in these tumors. How the seemingly diverse variations of BCC are manifest currently remains unclear. The hair follicle itself comprises at least eight related epithelial cell lineages, and both tumor morphology and behavior may be influenced by the particular cellular lineage that sustains the initial oncogenic hit to the Hh pathway. BCC-like lesions arising from different experimental mouse models of BCC often exhibit diverse morphologies with varying degrees of resemblance to human BCCs. These findings suggest that the nature of the genetic mutation may also affect BCC subtype. Finally, and perhaps most importantly, the amplitude of Hh pathway activation may underlie many of these variations. Indeed, studies in transgenic mice have suggested that high activation of Hh signaling can elicit BCC-like lesions that more closely resemble classical forms of nodular human BCCs, whereas low pathway activity induces the formation of tumors resembling benign basaloid hamartomas (Grachtchouk et al., 2003, 2011). In turn, the degree of Hh signaling likely impinges upon, and conversely may be affected by, synergistic activation of other pathways such as Wnt, epidermal growth factor receptor, phosphatidylinositol 3 kinase/mammalian target of rapamycin, and p53. Thus, cell of origin, the nature of the genetic mutation, the degree of Hh pathway activation, and synergy with other collaborating pathways are likely all key determinants of BCC morphology and behavior (Wong and Dlugosz 2014).

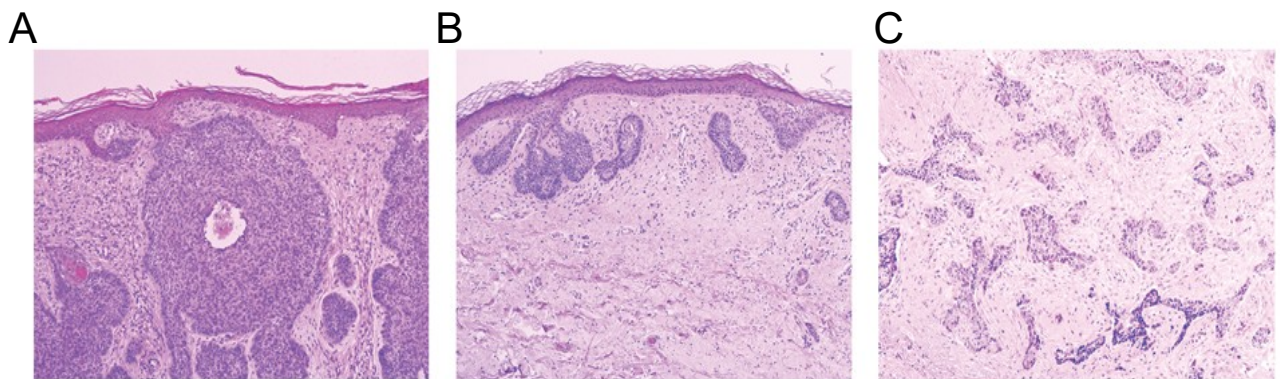


Figure 6. Major subtypes of human BCC. Microscopic (A, B, and C) appearance of nodular (A), superficial (B), and sclerosing (C) human BCCs. Original magnification, $\times 100$ (A, B, and C). Adapted from (Kasper, Jaks et al. 2012).

1.7.2 BCC cell origin

Several genetic approaches were used to investigate the identity of the cell lineage at the origin of BCC and more recently mouse models of BCCs, attempts to elucidate the cellular origin for these lesions. For instance, BCC-like tumors induced by an oncogenic form of Smo have been reported to arise primarily from the interfollicular epidermis, but not from hair follicle bulge stem cells, except upon wounding (Youssef et al., 2010; Kasper et al., 2011; Wong and Reiter, 2011) (Fig.7). In direct contrast, lineage tracing studies have suggested that bulge cells give rise to the majority of BCCs in irradiated *Ptch1* heterozygous mice (Wang et al., 2011). Additional studies have shown that BCCs induced by a truncated form of *GLI2* exhibit high-level pathway activation and can arise from both the epidermis and the hair follicle lower bulge or secondary hair germ (Grachtchouk et al., 2011). Notably, tumors originating from the epidermis resembled superficial BCCs, whereas nodular tumors were associated with the follicle, suggesting that cell of origin may indeed influence tumor subtype. these studies may also suggest that perhaps the cellular origin for BCC may not be fixed and immutable, but rather may depend on the nature of the genetic mutation and the degree of Hh pathway activation as well as on stromal context (Wong and Dlugosz 2014).

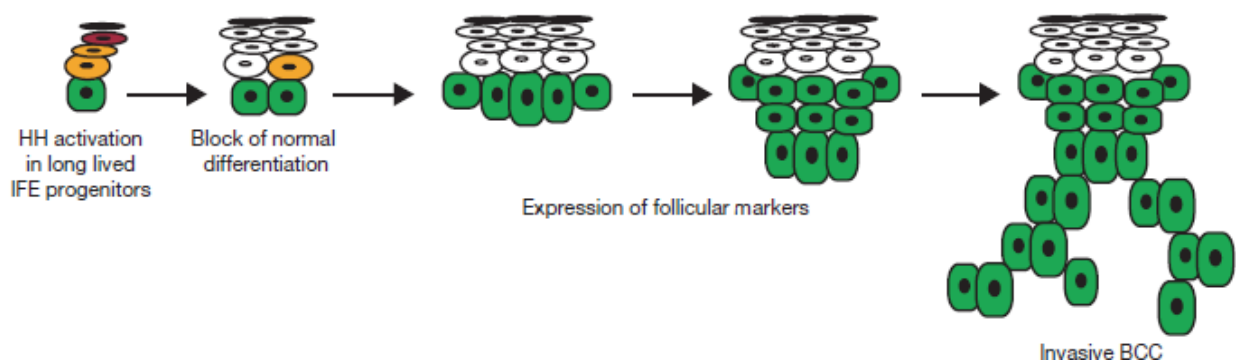


Figure 7. Model of BCC initiation in adult mice. Hedgehog (HH) activation in interfollicular long-lived progenitors induces a block of their normal differentiation and induces expression of hair follicle markers before progression into invasive BCC (Youssef et al., 2010.).

1.8 FOX genes

The forkhead (*fh*) gene was originally identified in a random mutagenesis screen performed in *Drosophila melanogaster* (Weigel et al., 1989). This study showed that *fh* is required for normal gut development, and that its absence results in a characteristic “forked head” appearance resulting from the homeotic transformation of the foregut into a head structure. Soon after this discovery, a number of related genes – termed Fox genes – were identified in multiple organisms, ranging from yeasts to humans. Fox genes control a wide variety of biological functions and are broadly expressed both during development and in adult life. Fox transcription factors are required for the normal specification, differentiation, maintenance and/or function of tissues such as the trophoderm, liver, pancreas, ovaries, intestine, lung, kidney, prostate, brain, thyroid, skeletal and heart muscle, skeleton, vascular tissue and immune cells (Zhu, 2016). In mammals, Fox transcription factors are categorized into subclasses A to S (Fig.8A) based on sequence similarity within and outside of the forkhead box (Hannenhalli and Kaestner, 2009; Kaestner et al., 1999). In many cases, the homozygous deletion of just one Fox gene leads to embryonic or perinatal lethality and, in humans, mutations in or the abnormal regulation of Fox genes are associated with developmental disorders and diseases such as cancer (Halasi and Gartel, 2013; Li et al., 2015; Wang et al., 2014). Fox transcription factors bind a similar DNA sequence, albeit with different affinities, due to their highly conserved DNA-binding motif. Forkhead genes encode a subgroup of the helix–turn–helix class of proteins and the arrangement of loops (or wings) connecting the b strands that flank one of the three helices (Fig.8B), gives rise to a butterfly-like appearance, hence their alternative name of ‘winged-helix’ transcription factors. The divergent sequences outside of the conserved DNA binding domain likely differentiate the function of these proteins, as do their distinct temporal and spatial gene activation patterns (Golson and Kaestner 2016). Moreover, in contrast to most helix–turn–helix proteins, forkhead proteins bind DNA as monomers. Hence, the binding sites, which typically span 15–17 bp, are asymmetrical. The sequence specificity has been determined for several representatives of this protein family through selection of binding sites from pools of short, random-sequence duplexes. A seven-nucleotide core corresponds to the major groove base contacts made by the recognition helix (helix 3) (Carlsson and Mahlapuu 2002).

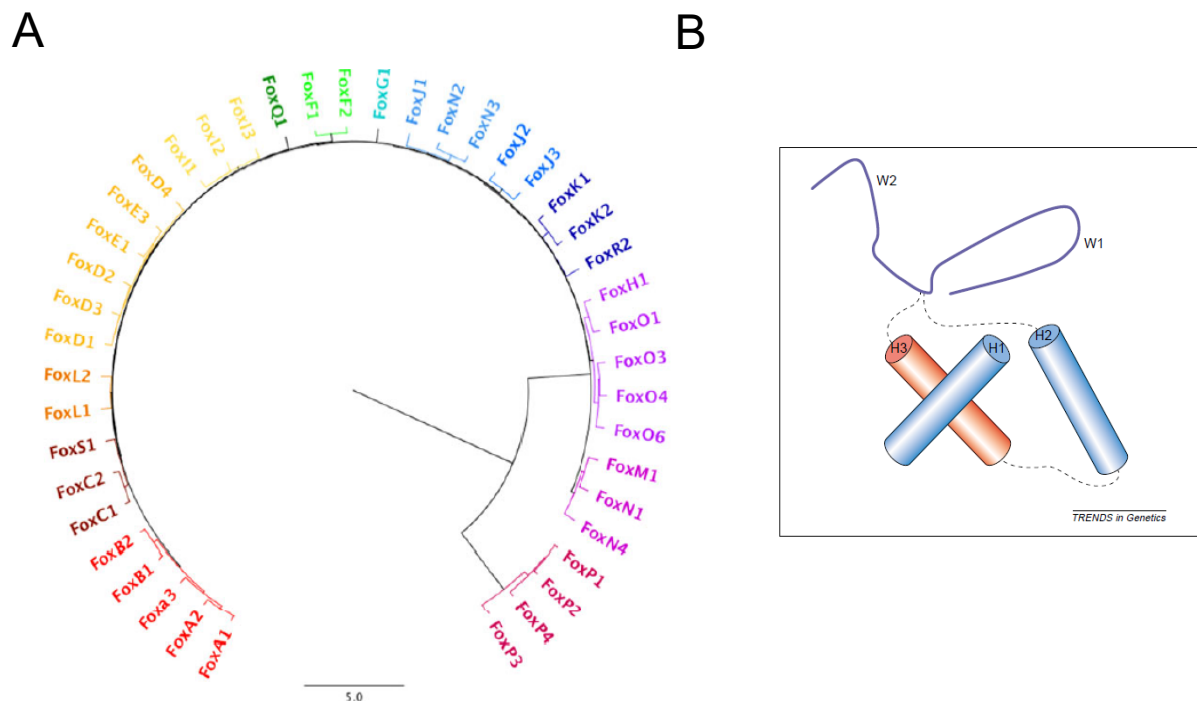


Figure 8. FOX genes. A) Phylogenetic tree of mouse Fox family members. (Adapted from Golson and Kaestner 2016). B) The forkhead domain. The three-dimensional structure of the forkhead domain derived from X-ray crystallography data for the HNF-3, FOXC2 and Genesis forkhead proteins. The α helices (H1–H3) and two wings (W1–2) are shown. The recognition helix H3 (red) lies in the major groove of DNA (adapted from Lehmann et al., 2003).

The binding domains of FoxA transcription factors, for example, have structural similarity to linker histones H1 and H5. These data suggest that the forkhead domain can promote gene activation directly, by opening up chromatin, and not just by bringing in a separate transcriptional activation domain. Forkhead proteins have been shown to act mostly as transcriptional activators but not exclusively so. In general, the described trans-activation and -repression domains lack distinctive features, such as enrichment for a particular amino acid. Little is known about the mechanisms through which forkhead proteins interact with the transcriptional machinery. In vitro, FOXF2 binds the general transcription factors. TBP and TFIIB, and in cotransfection experiments, FOXF2 acts synergistically with TFIIB (Hellqvist et al., 1998). In general, forkhead genes are distributed throughout the genomes and do not form physically linked clusters. The human genome also contains a few intronless sequences related to *FOXO* genes, *FOXO1b* and *FOXO3b*, that appear to be processed pseudogenes (Lehmann et al., 2003).

1.9 FOXE1/TTF-2

Foxe1 (formerly called TTF-2 for Thyroid Transcription Factor-2) was originally identified as a thyroid-specific nuclear protein that recognizes a DNA sequence present on both Tg (*Thyroglobulin*) and TPO (*Thyroid peroxidase*) promoters under hormone stimulation. This gene is located on mouse chromosome 4. The human ortholog FOXE1 is mapped to the q22 region of chromosome 9. This gene contains a single exon coding for a protein consisting of N-terminal region, highly conserved forkhead region, alpha helix poly-alanine channel and unique C-terminal residue. During mouse embryogenesis, Foxe1 is expressed in the foregut endoderm, in the craniopharyngeal ectoderm, involved in palate formation, and in the thyroid primordium. Human FOXE1 expression was detected in the oropharyngeal epithelium and thymus, late than in the mouse. Homozygous null mice with targeted disruption of Foxe1 exhibit severe cleft palate and sublingual or completely absent thyroid gland. Homozygous, human loss-of-function mutations located within the forkhead domain of FOXE1 cause the Bamforth–Lazarus syndrome (OMIM 241850), which includes congenital hypothyroidism, cleft palate and spiky hair, with or without choanal atresia, bifid epiglottis and ocular hypertelorism, depending on the severity of the mutation (Bamforth et al., 1989).

Studies in thyroid cells indicate that Foxe1 is required for the expression of thyroid-specific genes, such as Tg and TPO, thus explaining the variable pathologies associated with thyroid development and function. Moreover, the constant presence of cleft palate and the frequent choanal atresia, bifid epiglottis and ocular abnormalities observed in the Bamforth–Lazarus syndrome strongly suggest that FOXE1 controls downstream genes required, also, for craniofacial morphogenesis. Foxe1 mRNA is detected at E8.5 in all the endodermal cells of the floor of the foregut, including the thyroid anlage. Hence, at variance with *Titf1/Nkx2-1* and *Pax8*, the expression of which in the pharynx is strictly limited to the thyroid anlage, Foxe1 has a wider domain of expression. When the thyroid diverticulum forms and begins its migration, the expression of these factors is restricted to the thyroid primordium. In mouse thyroid, Foxe1 expression become not more detectable between E13 and E15, stage in which occurs the activation of differentiation markers like thyroperoxidase (TPO) and thyroglobulin (Tg). Their expression is induced by transcription factors *Pax-8* and *TTF-1*, respectively, which bind them promoters, even though the onset of their expression is at E9.5. This occurs because still at E14-15 the TPO and Tg promoters are bound by Foxe1, which play a negative role repressing their transcriptional activation by both *TTF-1* and *Pax-8*. This inhibition could be necessary to avoid the thyroid cells precursors to terminally differentiate before ending their migration. Between E9 and E13-14, thyroid cells precursors, indeed, migrate from the pharyngeal ectoderm till their final destination, in front of the trachea. It is only at E15, when is completed the migration process, thyroid follicular cells (TFCs) differentiate, when Foxe1 expression is down-regulated. This suggests that this transcription factor is involved either in promoting the migration process or in repressing differentiation of the TFCs until migration is terminated. Then, Foxe1 shows, during thyroid development, a biphasic expression which control the onset of differentiation (Zannini et al., 1997). For the rest of its life, a thyroid cell will be hallmarked by the simultaneous presence of *Titf1/Nkx2-1*, *Foxe1*, *Pax8*, and *Hhex*. According to this expression pattern, at later stages of development *Foxe1* is expressed in

the tissues derived from the pharyngeal arches and pharyngeal wall: thyroid, tongue, epiglottis, palate, and esophagus. In the adult, Foxe1 is still present in the thyroid, whereas the expression in the esophagus is faint. In ectoderm-derived structures, at an early stage of development, Foxe1 is present in the posterior stomatodeum, in the buccopharyngeal membrane, and in the cells of the roof of the oral cavity indenting to constitute Rathke's pouch, which will form the various components of the anterior pituitary. At later stages, Foxe1 mRNA expression in the pituitary is down-regulated, whereas it appears in the secondary palate, in the definitive choanae, and in the whiskers and hair follicles. In humans, FOXE1 (formerly called FKHL15) mRNA is also detected in adult testis and several other tissues (De Felice and Di Lauro 2004). Mice lacking both copies of Foxe1 suffer from neonatal hypothyroidism characterized by a sublingual small ectopic or completely missing thyroid gland and cleft palate. Although, the initiation of thyroid primordium formation at early stages of embryogenesis and functional differentiation of the TFC precursors are not impaired (De Felice et al., 1998) (Fig.9).

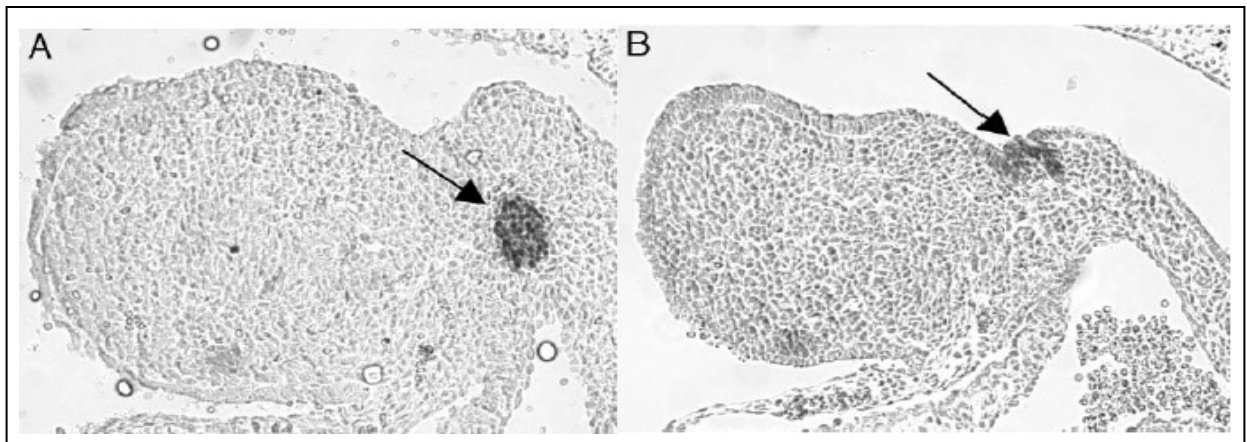


Figure 9. Foxe1 is required for thyroid precursor cells migration. Sagittal sections of *Foxe1*^{+/+} (A) and *Foxe1*^{-/-} (B) E11 mouse embryos stained with an anti-Titf1/Nk2-1 antibody. The *arrows* point to the thyroid bud. In the mutated embryo, the thyroid bud is still on the floor of the primitive pharynx (adapted from De Felice and Di Lauro 2004).

1.10 FOXE1 in cancer

The relationship of FOXE1 with malignant tumors has been explored for a long time. At present, many studies have found that FOXE1 gene played a role in skin squamous cell carcinoma, leukemia, pancreatic cancer, breast cancer, thyroid cancer and head squamous cell carcinoma and other tumors. Recently, it has been reported a function of tumor suppressor gene for Foxe1 in early stages of Papillary Thyroid Carcinoma (PTC), where its specific silencing causes an increase in cell proliferation, migration and invasion (Ding et al., 2019). In colorectal cancer (CRC) the methylation-mediated silencing of Foxe1 expression was shown to be a potential prognostic factor (Sugimachi, Matsumura et al. 2016). Moreover, recent studies identified that two risk alleles for PTC are associated with reduced FOXE1 expression, consistent with its pro-differentiation role in the thyroid development and in the adult thyroid (Lidral AC et al., 2015, He H et al., 2015).

However, genome-wide association studies have indicated an association between SNPs in FOXE1 locus and the susceptibility to thyroid carcinomas (Takahashi M, et al. 2010, Landa I et al., 2009, Gudmundsson et al., 2009) as well as the increased expression of FOXE1 in PTC. At the same time, it has been demonstrated that Foxe1 overexpression alone, in thyroid, is not related in thyroid cancer development and that that proper Foxe1 dosage is essential for achieving normal structure and function of the thyroid (Nikitski, Saenko et al. 2016). Meta-analysis revealed that common variations of FOXE1 (rs965513, rs944289 and rs1867277) were risk factors associated with increased differentiated thyroid carcinoma (DTC) susceptibility (Chen and Zhang 2018).

FOXE1 variations have been associated, also, with susceptibility to other types of cancers. In pancreatic cancer, the loss of afadin leads to increased formation of the Dvl2-FOXE1 complex in the Snail gene promoter region, which activates Snail gene transcription, thereby promoting pancreatic cancer metastasis. Moreover, FOXE1 was identified as the direct functional target of miR-422a and involved in human hepatocellular carcinoma (HCC) tumorigenesis and metastasis (Zhang et al., 2015). Moreover, in skin cancers FOXE1 seems to be a crucial player in development of cutaneous SCC, where, with high frequency, its promoter results hypermethylated resulting in a complete absence or downregulated gene expression (Venza I. Et al., 2009).

1.11 Foxe1 expression in skin

Our research group have provided for the first time a detailed characterization of Foxe1 expression in embryonal and post natal skin. As reported (Brancaccio et al., 2004) (Fig.10), during HF development, Foxe1 shows a dynamic pattern of expression that begins after E17.5, at first in few cells located above the forming dermal papilla. At P0, Foxe1 shows a similar localization but in a higher number of follicles. In the mature HF, Foxe1 expressing cells are located in the lower portion of the ORS and specifically in the portion surrounding the bulb, whereas the expression of this transcription factor is not present in the upper part of the hair follicle or in the epidermis.

In postnatal skin, we demonstrated that *Shh* and Foxe1 expression showed similar changes in expression during the hair cycle. Indeed, their expression ceases in telogen and is up-regulated in early anagen. It is possible because Foxe1 is a direct GLI2 target in human epidermis, an activator of *Shh* signaling pathway (Eichberger et al., 2004). By immunohistochemical analysis, we demonstrated that Shh/Gli signaling is required for Foxe1 expression *in vivo*. Moreover, we assessed the role of Foxe1 in hair follicle morphogenesis and maintenance, analyzing the skin of mice carrying a homozygous deletion of Foxe1. The results demonstrated that Foxe1 null mice at birth did not reveal any differences compared to wild-type skin; thus, Foxe1 is not required for early stages of hair follicle morphogenesis, as also suggested by its late expression. As Foxe1 null mice die at birth, skin grafts experiments allowed us to evaluate effects of Foxe1 absence on later stages of hair follicle morphogenesis. Foxe1 null skin grafts showed an aberrant hair formation with the production of thinner and curly pelage hairs, a downgrowth of HF impaired causing disorientation, misalignment and aberrantly shaped of HF. However, internal structure of the hair follicle as well as the differentiation programs appears unaffected (Brancaccio et al., 2004) (Fig.11). Taken together these findings indicate that Foxe1, although is unlikely to be involved in proliferation and differentiation of hair follicle keratinocytes, is essential for correct hair follicle orientation and downgrowth in late steps of hair follicle morphogenesis.

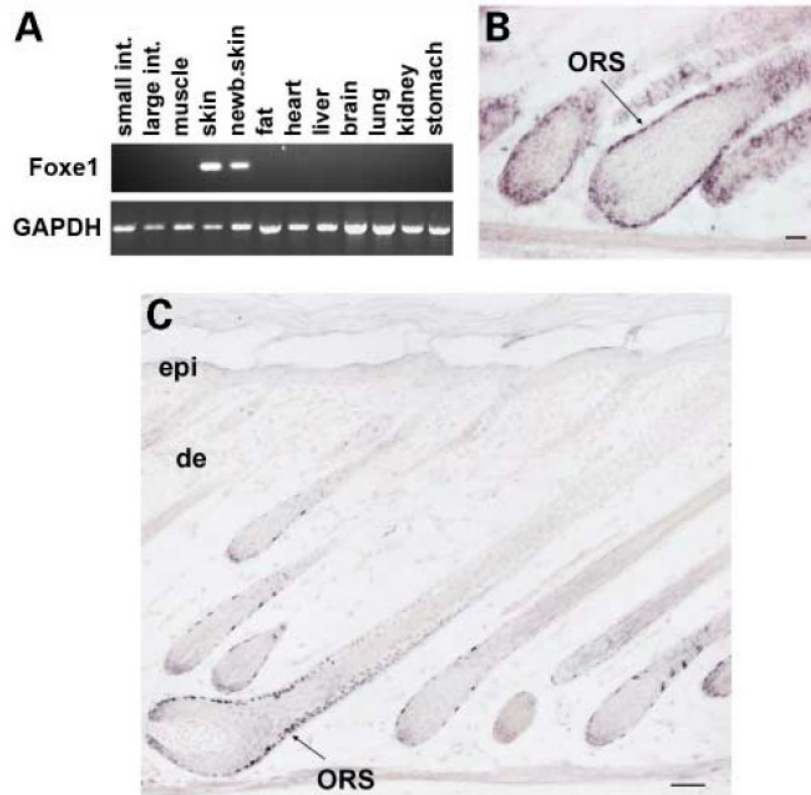


Figure 10. Foxe1 is specifically expressed in the hair follicle. A) RT-PCR analysis of total RNA prepared from various adult mouse tissues using Foxe1-specific oligonucleotide primers reveals specific expression in adult skin (skin) and newborn skin (new.skin) (upper panel). GAPDH is used to normalize the amount of cDNAs (lower panel). B) RNA in situ hybridization of mouse skin sections at postnatal day 10 (P10) using a DIG-labeled antisense probe for mouse Foxe1. Note the discrete pattern of Foxe1 expression in the ORS of the hair follicle (see arrow). In situ hybridization using a Foxe1 sense probe gave no detectable signal under the same conditions (not shown) (Brancaccio et al., 2004).

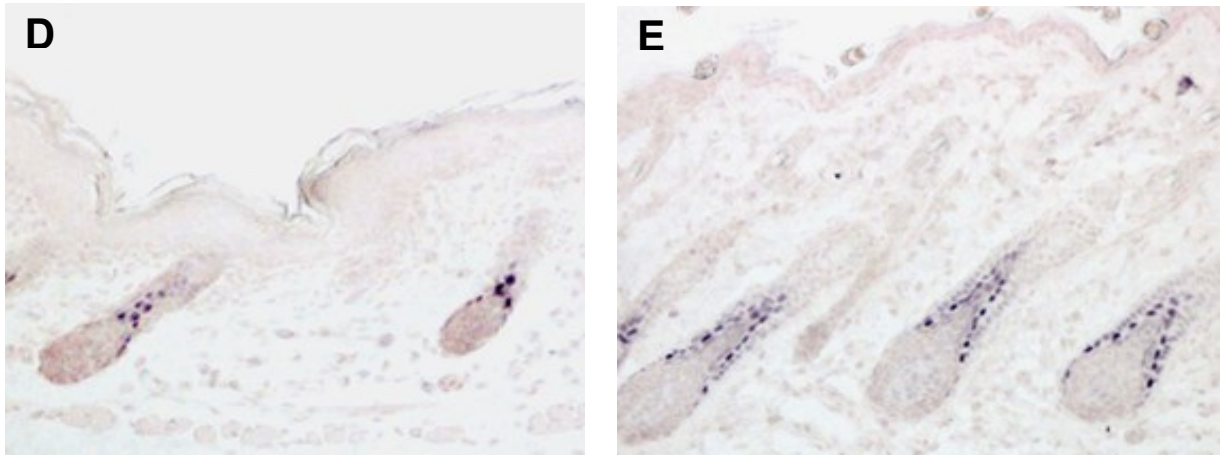


Figure 10. C–E) Immunohistochemical staining of longitudinal sections of mouse skin at P0, P5 and P23 using anti-Foxe1 polyclonal antibodies and an alkaline phosphatase reporter system. At P0 and P23 Foxe1 protein expression is localized in few epithelial cells located just above the bulb, whereas at P5 and during the entire growth phase it is confined to the nuclei of the lower ORS at P5 and in the hair follicle. Arrows indicate sites of Foxe1 expression. Arrowheads in (D) indicate immature hair follicle in which Foxe1 is not expressed. In (E) Foxe1 expressing cells are located in the undifferentiated compartment as shown by staining of adjacent sections with ORS and IRS markers (data not shown). No Foxe1 expression is detected in other hair follicle compartments, in the epidermis (epi) or in the dermis (de). Scale bars: 20 μ m. (Brancaccio et al., 2004).

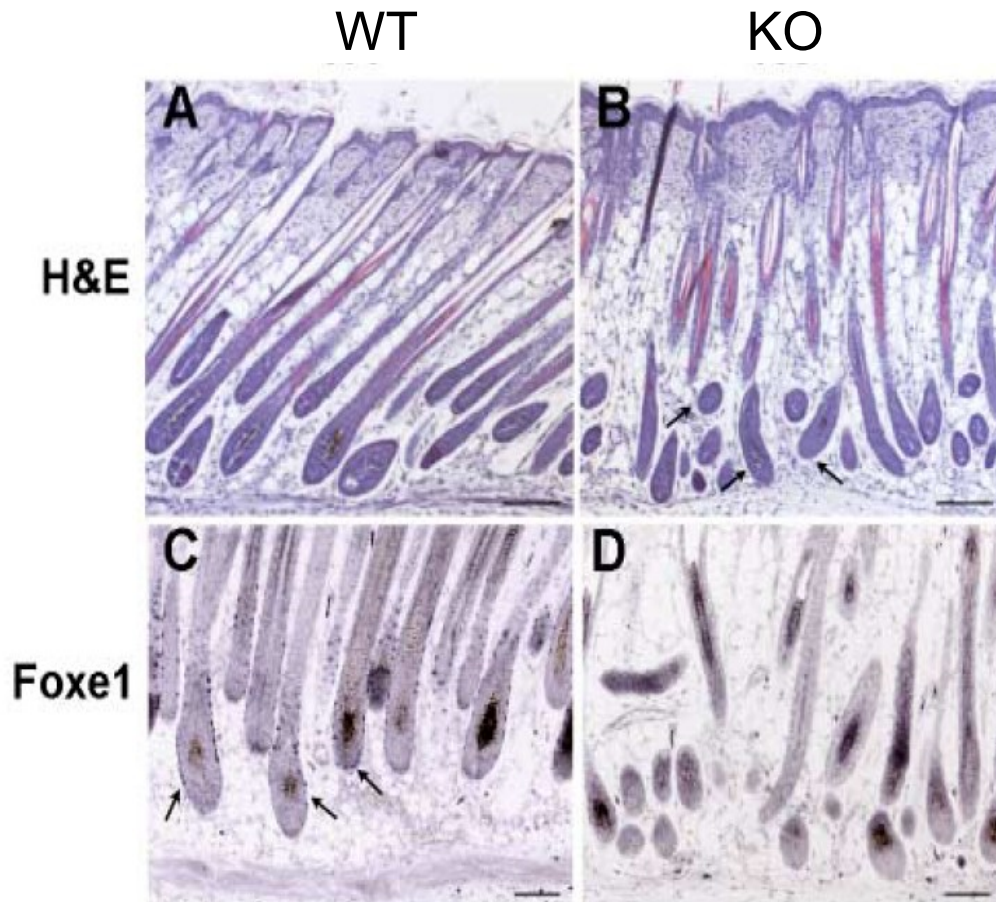


Figure 11. Hair follicle morphogenesis and downgrowth is impaired in Foxe1 null skin. Histological sections of wild-type (WT) (A) and Foxe12/2 skin grafts (KO) (B) were stained with hematoxylin and eosin (H&E) 2 weeks after transplantation. Hair follicles were uniformly sloped in the wild-type skin grafts, whereas in the Foxe12/2 skin grafts, hair follicles were disorganized and misshapen, and hair follicle bulbs pointed in different directions (see arrows). The increased thickness of the Foxe12/2 epidermis compared to the wild-type control was not consistently observed. As control immunohistochemistry was performed using anti-Foxe1 polyclonal antibodies, showing nuclear staining in the ORS in WT (C) (see arrows), but not in KO hair follicles (D) (Brancaccio et al., 2004).

A recent epigenomic, genetic, single-cell transcriptome approach have allowed to identify the spatiotemporal signals that converge on chromatin to elicit dynamic HF lineage changes (Adam, Yang et al. 2018). In this study four cell populations, representing sequential steps of lineage

progression, were isolated: (1) telogen-phase bulge stem cells, critical for long-term hair regeneration; (2) telogen-phase hair germ, critical for making MPPs and orchestrating the regenerative process; (3) proliferative basal TACs at the DP interface of mature (Ana-VI) HFs; and (4) suprabasal TACs, which are still proliferative, but have progressed further along their lineages than basal TACs. ATAC-seq profiles across the four purified cell populations of the HF-stem cell lineage, has allowed to obtain dynamic changes in chromatin during lineage progression. The clustered ATAC peaks identified binding sites for master transcription factors and assigned specific expressed genes to each of the four populations. Among these, *Foxe1* clusters in basal TACs (Fig.12) characterized by *Lgr5* positive cells typical of “lower proximal cup” (LPC), a term to indicate the cells at the very base of the HF bulb that bore similarities to HFSCs and ORS (Yang, Adam et al. 2017).

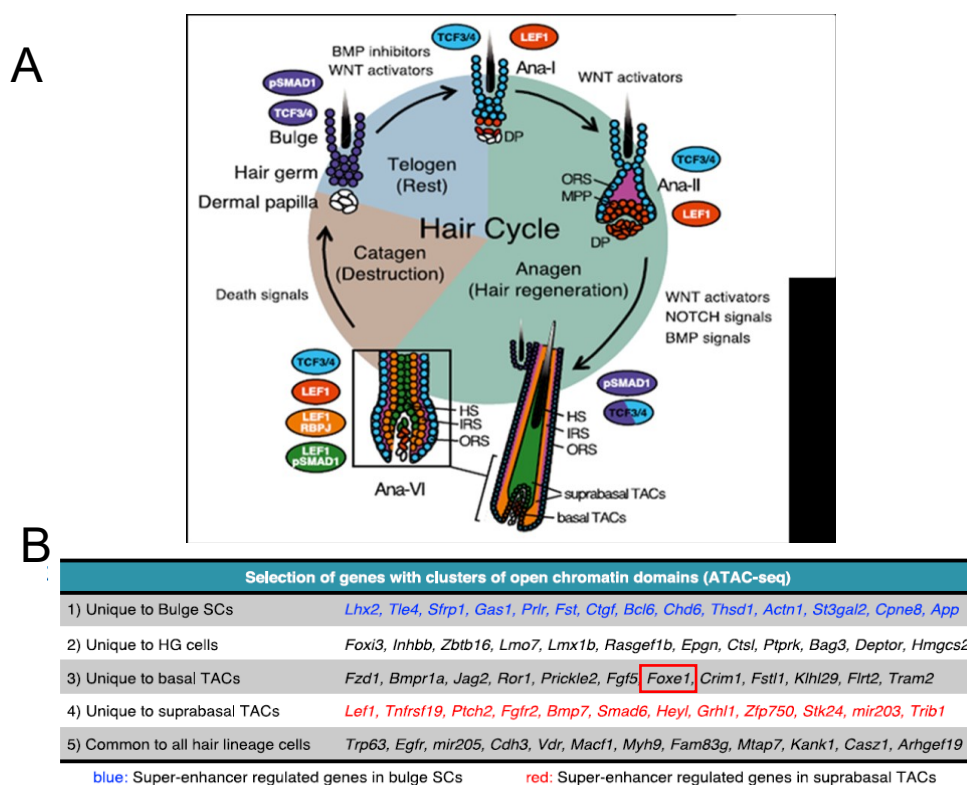


Figure 12. Transcriptional program regulating stem cell lineage progression during HF morphogenesis. A) Schematic depicting the phases of a cycling HF, with emphasis on the relevant lineage progression steps, signals, and associated DNA binding effectors B) ATAC-Seq identifies critical regulatory regions of Hair Lineage Cells. Selected genes with unique ATAC clusters in each population are shown (adapted from Adam et al., 2018).

1.12 FOXE1 expression in Non Melanoma Skin Cancers

The direct regulation of Foxe1 by the transcription factor Gli2, mediator of Shh signalling pathway (Brancaccio et al., 2004; Eichberger et al., 2004), explains the correlation between FOXE1 expression and the BCC tumorigenesis. Gene expression data analysis have clearly reported the specific induction of FOXE1 in BCC compared to normal skin (Fig.13,14).

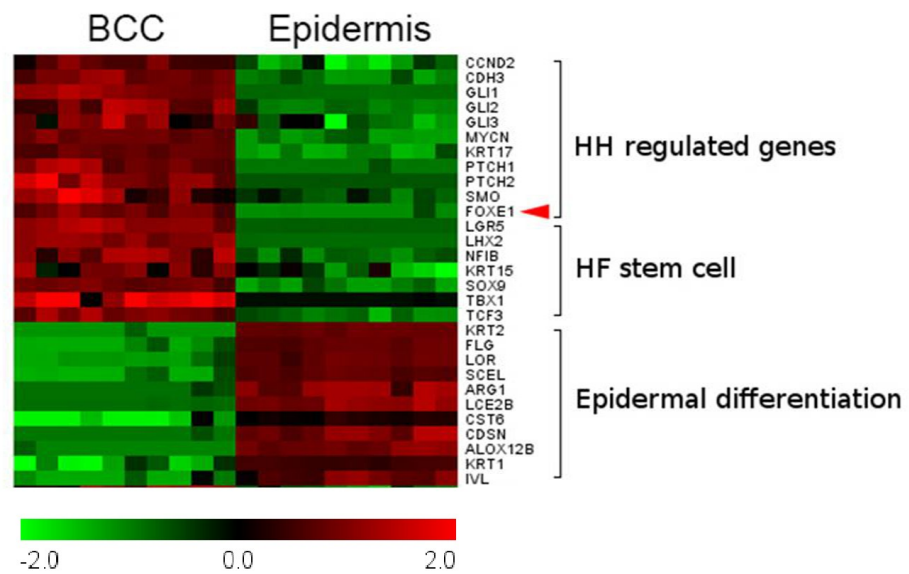


Figure 13. Foxe1 is among the most highly upregulated genes in BCC versus normal epidermis. Heat map derived from a comparative transcriptomic analysis of selected genes in skin BCCs versus normal skin epidermal cells (GSE42109 dataset). Retrieved from the Gene Expression Omnibus (GEO) database, using normalized expression values in log-2 scale (Ning, Mitsui et al. 2013).

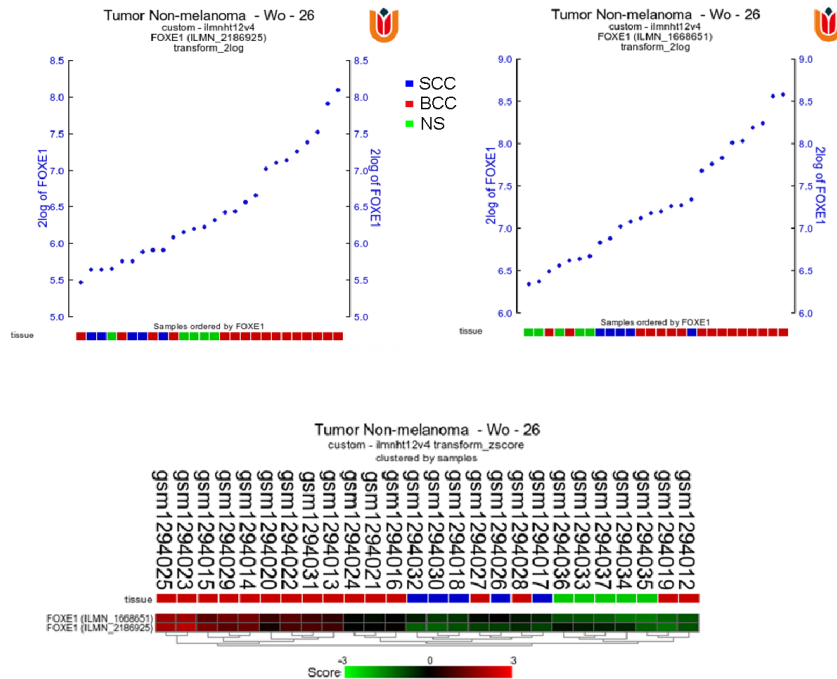


Figure 14. Correlation between FOXE1 expression and NMSCs. FOXE1 expression analysis using R2 platform. YY-graph generated from R2 tool from FOXE1 expression levels of all samples with expression levels ordered from left (low) to right (high). Underneath the X-axis, colored boxes represent clinical information of the samples in so called “tracks”. Below the graph are shown the two probeset reported for FOXE1 gene in R2 database. R2 platform contains mRNA gene expression profiles for more than 191.000 individual human samples and more 12.000 individual mouse samples. The samples are grouped in so called datasets. Each dataset has its own characteristics, such as tissue type, tumor type or from cell-line experiments. R2: Genomics Analysis and Visualization Platform (<http://r2.amc.nl>).

Preliminary data have shown that in BCC, in which the Shh signaling pathway is aberrantly activated, FOXE1 expression is abundantly induced as compared to normal skin in human samples (Fig.15). Similar data was obtained in mouse, by immunohistochemical analysis of BCC derived from Gli2 overexpressing transgenic mice which expressed high levels of Foxe1 in tumor cells. Foxe1 induced expression was confirmed in tumor cell lines derived from transgenic mice expressing a constitutively active form of Gli2 under the control of keratin 5 promoter (Gli2DN2) (Brancaccio et al., 2004) (Fig.16).

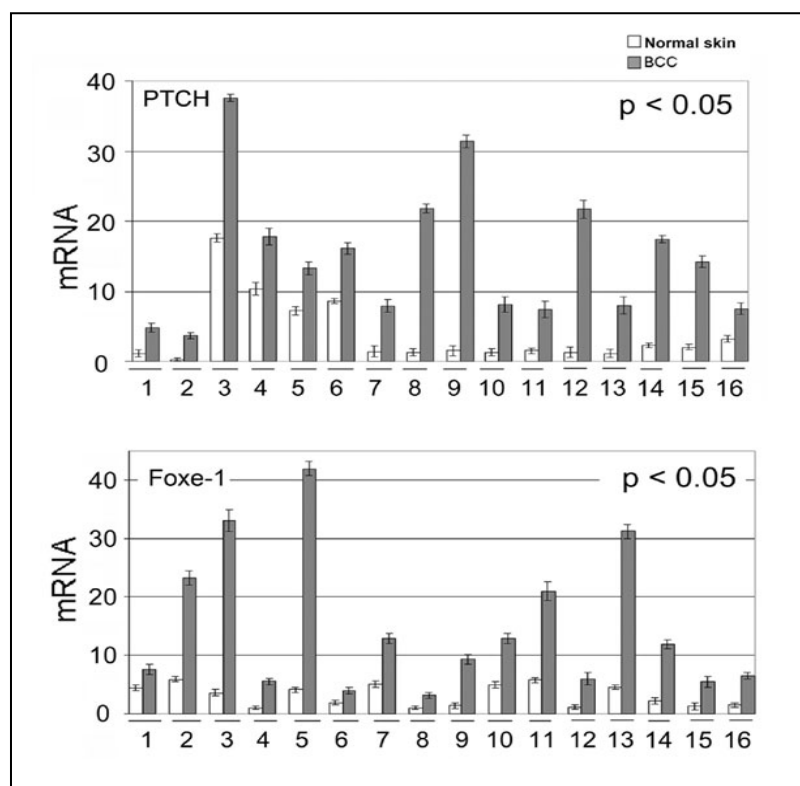


Figure 15. FOXE1 is a specific marker of human BCC. FOXE1 and PTCH mRNA levels were analyzed by real-time PCR in 16 human BCC samples and in the corresponding tumor-free skin from the same patients. Values were normalized to -actin mRNA levels. All samples were run in triplicate and referred to normal skin in sample 1 set arbitrarily as 1. P values were calculated by one-way ANOVA (Dentice, Luongo et al. 2007).

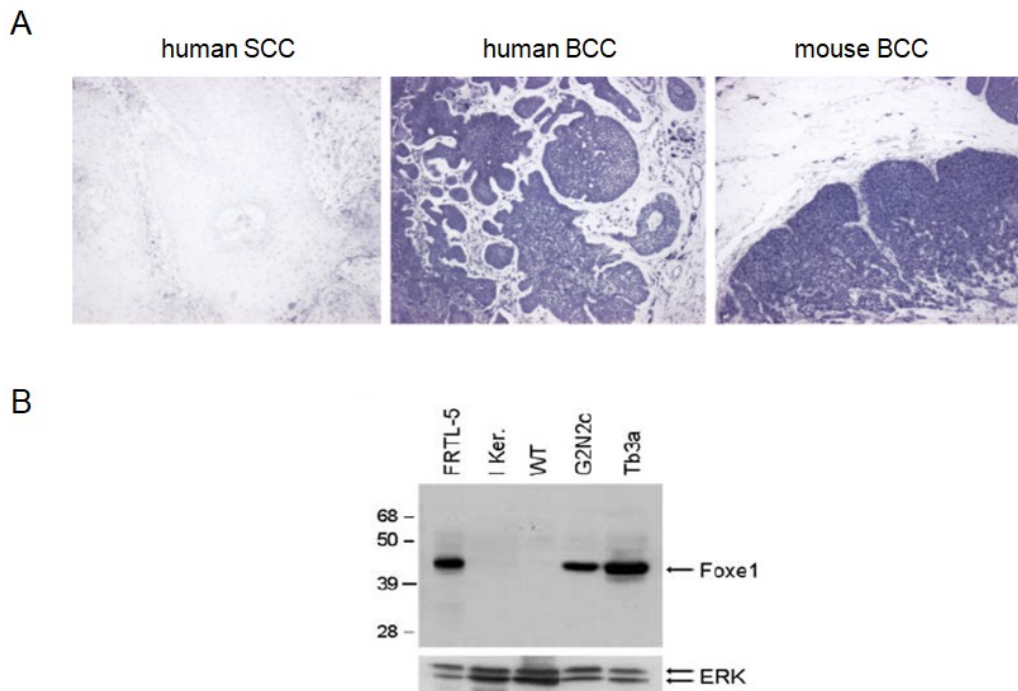


Figure 16. Foxe1 expression is induced in BCC. (A) Immunolocalization of Foxe1 in human and mouse skin tumors. Paraffin sections of human SCC and BCC, as well as of mouse BCC derived from transgenic mice expressing Gli2, were probed with polyclonal antibodies to Foxe1. This analysis revealed aberrant Foxe1 expression in BCC cells derived from both human and mouse origin. In contrast, SCC did not express Foxe1 at any detectable level. B) Foxe1 protein is strongly induced in trichoblastoma as compared with wild-type cells. An aliquot of 30 mg of total cell extract obtained from the rat thyroid cell line FRTL-5 used as positive control (FRTL-5), from mouse primary keratinocytes (I Ker.), from wt, as well as from trichoblastoma cells (G2N2c and Tb3a) were run on a 12% SDS–PAGE gel, and immunoblotted using anti-Foxe1 antibodies. ERK1 was used as a loading control (Brancaccio et al., 2004).

In contrast, its expression resulted absent in squamous cell carcinoma (SCC). It has been described that Foxe1 is downregulated or target of an aberrant methylation in its promoter (Venza et al., 2009), as well as observed in pancreatic and breast cancer (Sato et al., 2003) (Brune K et al., 2008). These observations may support the hypothesis that the transcriptional silencing Foxe1 may have a critical role in carcinogenesis and suggest that may be a cancer-related gene, in particular playing a crucial as-yet uncharacterized role of FOXE1 in NMSCs tumorigenesis.

1.13 Tbx1, another transcriptional regulator involved in BCC

The TBX1 gene is haploinsufficient in DiGeorge or 22q11.2 deletion syndrome, cardio-pharyngeal phenotype. Tbx1 encodes a T-box transcription factor and its loss in the second heart field (SHF), a population of cardiac progenitor cells destined to populate the cardiac outflow tract and the right ventricle, leads to reduced cell proliferation, premature differentiation and reduced contribution of cardiac progenitors to the heart. The molecular mechanism proposed for this transcription factor expected that Tbx1 is a priming factor that keeps targeted chromatin 'available' to other regulatory factors, which may be activators or repressors. This is an attractive hypothesis that is consistent with a role in cell lineage determination or maintenance (Fulcoli et al., 2016). Recently, Tbx1 expression has been positively associated to Sox9 induction during BCC tumorigenesis in SmoM2 transgenic mouse and has been defined as a promoter of stamness. ChIP-seq data have confirmed that it a direct Sox9 target gene (Larsimont et al., 2015, Caprio et al. 2020). Moreover, the correlation with Shh pathway was provided also by studies *in vivo* that recognized the presence of a genomic regulatory region upstream Tbx1, recognized by specific winged helix/forkhead box (Fox)-containing transcription factors, responsible of its responsiveness to Shh signalling during aortic arch development (Yamagishi et al., 2003). In addition, Tbx1 role has been associated to Wnt signalling pathway by which modulates cell polarity and migration, specifically, regulating at transcriptional level Wn5a gene in mouse cardiac progenitors (Chen et al., 2012). In the adult mouse, *Tbx1* is expressed in the hair follicle, where it plays a role in the maintenance of the stem cell pool (Chen et al., 2012).

2. AIM OF THE STUDY

My research activity aimed to investigate the molecular mechanisms underlying skin tumorigenesis in NMSC, mainly focusing on the biological function played by the forkhead transcription factor FOXE1. During my PhD, I identified the downstream transcriptional program regulated by FOXE1 in keratinocytes and in BCC cells and evaluated the effects of Foxe1 expression in key biological processes for cancer formation, such as cell proliferation, adhesion and cell migration. Moreover, using two distinct mouse models, I investigated the biological role of Foxe1 in BCC formation and maintenance, evaluating the effects of its depletion during skin tumorigenesis.

3.MATERIAL AND METHODS

3.1 Cell culture

SCC13 cell line, derived from human cutaneous Squamous Cell Carcinoma, were kindly provided by Dr. GP Dotto and cultured in Keratinocyte Serum Free Medium (KSFM; Thermo Fisher Scientific #17005042) supplemented with Bovine Pituitary Extracts (BPE; 30 µg/mL), Human Epidermal Growth Factor (EGF; 0.24 ng/mL) and Pen/Strep.

G2N2c and Tb3a cells were cultured under low calcium conditions in the presence of 8% Fetal Bovine Serum (Thermo Fisher Scientific, #26140079) that was chelated using Chelex 100 (Biorad) and 1.0 ng/mL of Keratinocyte Growth Factor (KGF; Sigma, #K1757) as described in Sheng et al., 2002. Cells were seeded on type I Collagen-coated tissue culture dishes.

HEK293T (Human Embryonic Kidney) cells were cultured at 37°C in a humidified condition of 95% air and 5% CO₂ in Dubecco's Modified Eagle Medium (DMEM), supplemented with 10% Fetal Bovine Serum and 4.0 mM L-Glutamine (L-Gln) and AA Non-Essential (1X; Thermo Fisher Scientific). All cell types were transfected using Lipofectamine 2000 (Thermo Fisher Scientific) following the manufacturer's protocol.

3.2 Primary mouse keratinocytes isolation and cell cultures

Primary keratinocytes were isolated from the epidermis of newborn mice. 2-3 days old mice were euthanized by hypothermia by placing them in a 100mm Petri Dish under ice for 30-45 minutes. Then mice were washed once with distilled water and twice with 70% ethanol, being careful to remove completely the ethanol after washing. The skin was removed from each mouse under a tissue culture hood using first sterile surgical scissors to amputate the limbs and the tail and then a sterile scalpel to cut the skin along the dorsal midline from the head to the tail. Using sterile forceps, the whole skin was removed, washed in HBSS and flatten with the dermis down on a petri dish. Then the skin was incubated overnight at 4°C floating on 2 ml of Dispase solution (0.80 U/mL Dispase II, 10 mM HEPES, 0.075% sodium bicarbonate, antibiotic/ antimycotic in HBSS) to obtain epidermis-dermis dissociation. Next day the epidermis was peeled away from dermis with forceps, placed in 2 ml of trypsin solution (0.125% trypsin, 0.1 mM EDTA in HBSS) and cut quickly into very small fragments with scissors to promote the enzymatic and mechanical dissociation of the tissue. The minced epidermis was incubated at 37°C for 5 minutes. Then trypsin was inactivated by adding DMEM medium supplemented with 10% of FBS and the cell suspension was filtered in 70 µm cell strainer to remove undigested tissue and floating fragments. The isolated keratinocytes were plated in collagen coated dishes in high calcium medium to enhance cell attachment. Next day, keratinocytes were washed twice with PBS to remove unattached cells and calcium residuals and grown at 34°C and 8% CO₂ in low calcium medium (0.05 mM CaCl₂) supplemented with 4% of calcium-chelated Fetal Bovine Serum (FBS) and Epidermal Growth Factor (EGF), changing medium every day.

3.3 Retroviral preparation

High-titer retroviruses were produced in HEK293T cells by transient co-transfection of pPINCO-GFP constructs or pPINCO-GFP-FOX E1 plasmid and amphotropic or ecotropic viral envelope plasmids (pAmpho/pEco), depending on the cell type to be infected. Cells were plated on collagen coated-60mm dishes the day before transfection. Subconfluent cells were co-transfected using 6µg of pPINCO-GFP (Empty control) or pPINCO-GFP-FOX E1 constructs and 6µg of pAmpho or pEco plasmids in the presence of 30ul of Lipofectamine 2000 (Thermo Fisher Scientific), according to the manufacturer's instructions. Cell supernatants containing the retroviruses were collected 48 hr after transfection, then fresh medium was added and collected again 72 hr after transfection. Finally, the retrovirus preparation was filtered using 0.45µm filters to remove cell debris.

3.4 Retroviral infection

Mouse primary keratinocytes freshly isolated from wild type mice (C57BL/6 strain) and SCC13 were infected the day after plating at 50% confluence in 35mm dish with retroviruses carrying FOX E1 or empty control, produced as described above, in the presence of 8 µg/ml Polybrene. Cells were incubated in the retrovirus mix for 2 hr at 34°C and 8% CO₂ or at 37°C and 5% CO₂. Since retroviruses were produced in the high-calcium medium of HEK293T cells, keratinocytes were washed twice with PBS after infection to remove calcium residuals and then low calcium medium was added. Cells were infected for two consecutive days and 48h after the second infection efficiency of retroviral incorporation was monitored evaluating the percentage of GFP positive cells. Infected cells were used for functional *in vitro* assays.

3.5 Lentiviral preparation and infection

High-titer lentiviruses were produced in HEK293T cells by transient co-transfection of pLKO.1 constructs or pLKO.1-shFOX E1 plasmid and psPAX2 (lentiviral packaging plasmid for expression of envelope and used with 2nd generation lentiviral vectors – Addgene #12260), pLP/VSVg (lentiviral packaging plasmid containing the HIV-1 gag and pol genes). Cells were plated on collagen coated-60mm dishes the day before transfection. Subconfluent cells were co-transfected using 2µg of pLKO.1 (empty control) or pLKO.1-shFOX E1 constructs, 3µg of psPAX2 and 1 µg of pLP/VSVg constructs in the presence of 15ul of Lipofectamine 2000 (Thermo Fisher Scientific), according to the manufacturer's instructions. Cell supernatants containing the lentiviruses were collected 72 hr after transfection. Finally, the lentivirus preparation was filtered using 0.45µm filters to remove cell debris.

3.6 Lentiviral infection

G2N2c and Tb3a cells were infected the day after plating at 50% confluence in 35mm dish with lentiviruses carrying shFOX E1 or empty control, produced as described above, in the presence of 8 µg/ml Polybrene (Sigma). Cells were incubated in the lentivirus mix O.N. at 37°C and 5% CO₂. Since lentiviruses were produced in the high-calcium medium of HEK293T cells, keratinocytes were washed twice with PBS after infection to remove calcium residuals and then low calcium medium was added. Cells were infected for two consecutive days and 48h after the second infection were selected with 0.75µg/ml puromycin. After 48 hr uninfected control keratinocytes were died and infected cells were collected for RT-qPCR and Western blot analysis and used for functional *in vitro* assays.

3.7 Western Blot

For SDS-PAGE, lysates were prepared in Laemmli buffer (10% glycerol, 0.01 % Bromophenol Blue, 0.0625 M Tris-HCl pH 6.8, 3 % SDS, 5 % βmercaptoethanol), boiled and loaded on denaturing SDS-PAGE gel. For Western Blot, proteins were transferred after running to Immobilon-P transfer membranes (Millipore) and probed with the antibodies diluted in PBS-0.2% Tween-20 with 5% nonfat-dry milk. The primary antibodies used for Western Blot analysis were: anti-β-Actin (AC-15, Santa Cruz Biotechnology), anti-α-Tubulin (Sigma-Aldrich), anti-FOX E1 (NBP1-30960, NovusBio). Secondary antibodies donkey anti-rabbit or sheep anti-mouse IgG conjugated to horseradish peroxidase (HRP) (GE Healthcare) were used and revealed by chemiluminescence (ECL, GE Healthcare Life Sciences).

3.8 RNA isolation and RT-qPCR

Total RNA was extracted from cells using TRIzol reagent (Thermo Fisher Scientific) and retro-transcribed to cDNA using SuperScript Vilo (Thermo Fisher Scientific). RT-qPCR was performed using the SYBR Green PCR master mix (Thermo Fisher Scientific) in an ABI PRISM 7500 (Thermo Fisher Scientific). Target genes were quantified using the following specific oligonucleotide primers and normalized for human RPLP0 expression or for mouse β-actin expression:

Oligonucleotide primers for Real Time RT-PCR in human samples

Gene	Forward 5'-3'	Reverse 5'-3'
hRPLP0	GACGGATTACACCTTCCCCTT	GGCAGATGGATCAGCCAAGA
hPDE5A	CCCAGATGTCAGTAAGGATAAAAGATT	TGCACTGCTGGTTTACATTTCC
hFZD5	TCGGTGCTGTGCTTCATCTC	TTCCATGTGATGAGGAAGGT
hCTGF	TGCACCGCCAAAGATGGT	GACTCTCCGCTGCGGTACAC
hNT5E	GGAGGACACTCCAACACATTTCT	CAGCAGGCACCTCTTTGGAA
hSDC4	TGATCGGCCCTGAAGTTGTC	GCCCTCTCAGGGATATGGTTATC
hGPC4	CTTAGCGGTTGCGGGAGAT	TCAACAGGGCATGGGTACACT
hRGS16	TGGGAGTACTGGCAAGTTCGA	CACCCCAGCACATCTTCTGA

Oligonucleotide primers for Real Time RT-PCR in mouse samples

Gene	Forward 5'-3'	Reverse 5'-3'
mActin	CTAAGGCCAACCGTGAAAAGAT	GCCTGGATGGCTACGTACATG
mPde5a	CGAGCCCTTGAACATCAAAGA	ATTTGGTCAACTTCTGCATTGAAC
mFzd5	CCCACCGCACGTTTTCC	GCTTTTCATTTGCTTCTTGTTATC
mCtgf	ACAAGGGCCTCTTCTGCGAT	ACCATCTTTGGCAGTGCACA
mNt5e	TGGCACACTTCATGAACATCCT	TCCACACCGTTATCAAATTCATGAT
mFoxe1	GGGATCTTGAGGAAGCAGTCG	GACAACCCCAAGAAGTGGCA
mGpc4	CTCTACGTGTCCAAAGGCTTCA	TTCAAATGGTCACCGTTGATCT

3.9 Microarray data Analysis

The total RNA samples were preprocessed for hybridization to Mouse Gene 2.0 ST Array (Affymetrix, Santa Clara, CA). The values of individual probes were summarized using the robust multi-array average (RMA) algorithm (Bolstad et al, 2003) embedded in the Expression Console software v.1.3 (Affymetrix), which comprises of convolution background correction, quantile normalization, and median polish summarization. Subsequently, differentially expressed genes (DEGs) were selected using P-values <0.05 and fold change FC: > or <1.0.

3.10 Cell proliferation assay (BrdU assay)

BrdU assay was performed using BrdU (ZYMED Labeling Reagent, Thermo Fisher Scientific). In brief, the labeling reagent was diluted 1:100 with complete tissue culture medium for 2h and then cells were fixed with 4% Paraformaldehyde (PFA) for 10 min at 37°C. Then cells were incubated with anti-BrdU mAb containing nucleases diluted in DNase Buffer (50mM MgCl₂, 250mM Tris pH7.5, 1M NaCl) and were treated with fluorescein-labeled secondary Ab and DAPI. The samples were imaged on a Leica DMI4000B inverted microscope, and five randomly selected areas were analyzed per sample (magnification, 20x). The cell number of DAPI-positive cells and BrdU-positive cells were counted for each area using ImageJ software, and the ratio of the cell number of BrdU-positive to DAPI-positive cells was calculated.

3.11 Wound Healing Assay

For scratch wound assay, cells were seeded in 12-well plates at confluence. The day after, cells were incubated treated with Mitomycin C (M4287-Sigma-Aldrich) diluted in medium (4 µg/mL) for 2 h at 37°C. Wounds were performed by dragging a sterile pipette tip across the monolayer and then imaged by time-lapse microscopy. During acquisition of movies, cells were incubated in a humidified chamber at 37 °C, 5% CO₂ in the complete medium and monitored for 96 h at 37 °C. In alternative, phase-contrast images were acquired in three regions along the wound every 24 h after wounding using a DMI4000B (Leica) inverted microscope (magnification, 5,10x). The percentage of wounded area was measured for each stack using ImageJ software. Experiment was performed in triplicate for each sample. Migrating cells were counted in five fields with a 4x objective. For each assay three independent experiments were carried out in triplicate

3.12 Boyden Chamber cell migration assay

SCC13, SCC028 and G2N2c cell cultures were cultured in 60mm dishes until reach 80% confluence. Then cells were starved for 24h with serum-free medium at 37°C. Cells (1.5×10^5) were plated without serum on 8-µm pore size Transwell filters (Corning, Corning, NY, USA) using 12-weel inserts. Cells were allowed to migrate for 30h (G2N2c) or 40h (SCC13, SCC028), then the assay was terminated and stained with Crystal Violet Stain Solution (20% ethanol, 1% crystal violet). Migrated cells were counted capturing five randomly selected areas of the transwell surface (magnification, 5x) and using ImageJ software. Experiment was performed in triplicate for each sample.

3.13 Tumorsphere assay with Matrigel coating

Cells grown as monolayer were trypsinized and resuspended in cold DMEM medium supplemented with 2 % of Matrigel (Matrigel®Matrix-Basement Membrane, Corning). A final

concentration of 21×10^2 cells/well were plated on top of pre-coated Matrigel surface in 12-well plates. Then, cells were incubated at 37°C to let them to fully settle down before refreshing medium 48h after seeding. Tumorspheres were cultured for 10 days, changing medium every two days. Phase-contrast images of each well were acquired using a DMI4000B (Leica) inverted microscope (magnification, 5-10x). Tumorsphere-forming efficiency was measured as total number of spheres formed/total number of single cells seeded ratio. Tumorspheres area was measured using ImageJ software. Experiment was performed in triplicate for each sample.

3.14 Tumorsphere assay with Ultra-low attached plates

G2N2c and Tb3a cells, grown as monolayer, were trypsinized and resuspended in spheroid media (DMEM/F12, 2% B27, 0.4% BSA, 20ng/mL EGF, 4 $\mu\text{g}/\text{mL}$ Insulin) at final concentration of 7×10^4 cells/mL. Then, 7×10^2 cells/well were seeded in Ultra-Low Attachment Multiple Well Plate (96-well, flat bottom - Corning) and allowed to grow for 10 days w/o any medium change. Tumorsphere-forming efficiency was measured as the total number of spheres formed/total number of single cells seeded ratio. Automated analysis was performed with ZEISS ZEN Intellesis Image Segmentation model (ZEN Blue 3.0 software). Experiment was performed seeding twenty wells for each sample.

3.15 Adhesion assay

Cells grown as monolayer were trypsinized to single cell suspension and seeded in 48-well-plates at final concentration of 5×10^4 cells/well (SCC13) or 15×10^4 cells/well (G2N2c). Cells were allowed to attach in growth media for different time points at 37°C and then washed twice with PBS1X to remove the non-adherent cells. Then, cells were fixed and stained with Crystal Violet Staining Solution. For quantification, cells were lysed with methanol (100%) and cell density was measured by value of absorbance (570nm) with the plate reader EnSpire® (Multimode Plate Reader-PerkinElmer-Corning). Experiment was performed in triplicate for each sample and for each time point analyzed.

3.16 Histology and Immunostaining

Ear and tail skin was dissected, fixed in 4% paraformaldehyde (PFA) and embedded in paraffin, from which 7 μm sections were cut and stained with Haematoxylin and Eosin (H&E) and immunofluorescence according to standard methods. For paraffin sections, permeabilization for antigen retrieval was performed by microwaving samples in 0.01 M citrate buffer at pH 6.0. The following antibodies were used: anti-Foxe1, keratin 14 (BioLegend), keratin 17 (P.Coulomb Lab), Ecadherin (Zymed laboratories-Invitrogen), keratin 6 (Progen), Sox9 (Santa Cruz). The following

secondary antibodies were used for immunofluorescence staining: Alexa Fluor® 488 goat anti-mouse (Invitrogen), Alexa Fluor® 594 goat anti-rabbit (Invitrogen), Alexa Fluor® 488 goat anti-rabbit. Nuclear staining was performed using DAPI reagent. Fluorescent signals were monitored under a Zeiss Axioskop2 plus image microscope.

3.17 Mouse genotyping

The conditional Foxe1 knockout mouse (K14-Cre/Foxe1flox/flox), K14-CREER/RosaSmoM2/Foxe1flox/flox, K14-CreER/Foxe1flox/flox, K5-Gli2, K5-Gli2/K14-Cre/Foxe1flox/flox and Cre negative mice genotyping was performed by PCR using DNA isolated from mouse tails.

The oligonucleotides primers used for the screening of K5-Gli2 transgenic mouse model are:

K5Gli2_Foward primer (5'-3'): TGCATATAAATTCTGGCTGGCG

K5Gli2_Reverse primer (3'-5'): GCATGAACATGGTTAGCAGAGGG

A 166bp band is expected for the transgenic mouse.

The oligonucleotides primers used for the screening of LoxP locus in Foxe1 conditional knockout (Foxe1 fl/fl) mouse model are:

Cond-FOXE1_Foward primer (5'-3'): ACTTCGGGACAGACCAGGAACCTGG

Cond-FOXE1_Reverse primer (3'-5'): AACTGGACTAAAGTGGGGCGCG

A 344bp band is expected for the presence of recombinant allele, whereas a 235bp band is expected for the wt allele.

The oligonucleotides primers used for the screening of SmoM2 oncogene are:

Rosa1_Foward primer (5'-3'): AAAGTCGCTCTGAGTTGTTAT

Rosa3_Reverse primer (3'-5'): GGAGCGGGAGAAATGGATATG

Rosa2_Reverse primer (3'-5'): GCGAAGAGTTTGTCTCAACC

To screen mice for the presence of Cre-ER and/or Cre-recombinase, the following oligonucleotides primers were used:

Cre_Reverse primer (3'-5'): TAACATTCTCCCACCGTCAGTA

Cre_Foward primer (5'-3'): FGGCAGTAAAACTATCCAGCAACA

A 300 bp band is expected for the K14-Cre and K14-Cre-ER mice.

3.18 Tumour induction

For tumour induction, *K14-CREER/RosaSmoM2*, *K14-CREER/RosaSmoM2/Foxe1flox/flox*, *K14-CreER/Foxe1flox/flox*, *Cre negative* mice were treated with tamoxifen (Sigma T-5648) (0,5 mg, diluted in corn oil, Sigma-Aldrich) by intraperitoneal injection in mice aged 28 day. Five mice for each group were sacrificed at different time –points after treatment (5, 8 and 16 weeks) to collect samples from ear, tail and dorsal skin.

4. RESULTS

4.1 Identification of Foxe1 putative target genes in WT keratinocytes and BCC cells.

While a set of Foxe1 downstream target genes, involved in differentiation and organogenesis of thyroid development, have been identified (Zannini et al., 1997) (Fernandez, Lopez-Marquez et al. 2013), mediators of Foxe1 functions in skin have yet to be defined. To identify potential Foxe1 effectors in keratinocytes, we performed a genome-wide expression analysis using microarrays to study gene expression profiling modulated by Foxe1 in two different systems of epithelial cells: wild type primary mouse keratinocytes (mKer) and a mouse BCC cell line (G2N2c). Foxe1 expression was modulated in these cell systems in order to identify the differentially expressed genes (DEGs) comparing treated groups to their relative controls. Specifically, mKer, in which FOXE1 is absent, were infected with a retrovirus carrying exogenous FOXE1 to obtain its overexpression (mKer-FOXE1 OE); while in BCC cells Foxe1 knockdown was achieved by transient transfection with a specific Foxe1-siRNA (G2N2c-Foxe1 KD). Statistically significant DEGs were identified with P-values <0.05 and fold change FC: >1.0 (induced) or FC: <1.0 (inhibited) (Fig.17 A, B).

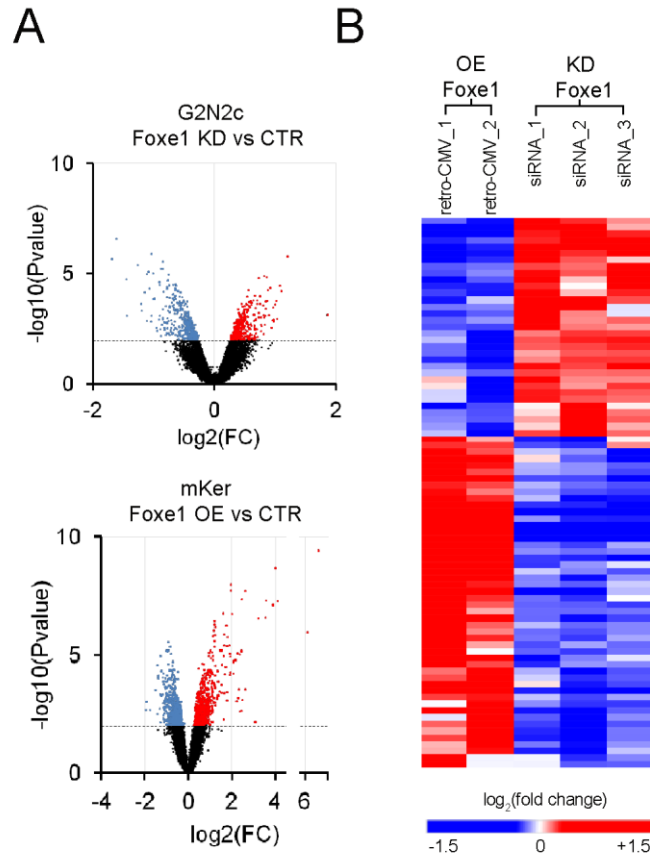


Figure 17. Identification of differentially expressed genes by Foxe1 in keratinocytes. A) Volcano plots representing DEGs of the two experiments. The significantly up-regulated and down-regulated genes are indicated with red and blue dots, respectively, while non-significant genes are shown as black dots. B) Heatmap representing differentially expressed genes between treated samples and control samples. FOXE1 OE: mKer overexpressing FOXE1 (n=2 replicates); Foxe1 KD: G2N2c Foxe1 knockdown cells (n=3 replicates). Red, upregulation; Blu, downregulation.

Data analysis of gene expression profiles in FOXE1 overexpressed mKer resulted in 3,289 DEGs, of which 1,585 upregulated and 1,704 downregulated compared to control cells. Genes induced by FOXE1 overexpression were significantly enriched in biological processes associated to regulation of cell adhesion (e.g. integrins *Itga2*, *Itga5*, *Itgav*, *Itgb1*, and laminins *Lama5*, *Lamb1*), actin cytoskeleton organization (Rictor and downstream Rho GEFs such as *Arhgef2*, *Arhgef5*, *Arhgef17*, *Arhgef19*), and regulation of extracellular matrix structure (*Gpc4*, *Sdc4*, *Tnc*).

Among the downregulated genes an even more significant enrichment was observed for genes associated to regulation of keratinocyte differentiation, consistent with a putative role of Foxe1 in suppressing epidermal cell fate, and cell cycle progression (Fig.18).

In BCC cells the gene signature regulated by Foxe1 expression was at least partially overlapping. In G2N2c Foxe1 knockdown cells, we identified 2,583 DEGs, of which 1,403 were upregulated and 1,180 downregulated compared to controls. Gene ontology analysis showed that reduced Foxe1 expression in BCC cells lead to increased expression of genes associated to cell cycle, moreover the gene expression profile resulted associated to unfolded protein response and regulation of cell-substrate adhesion (Fig.19).

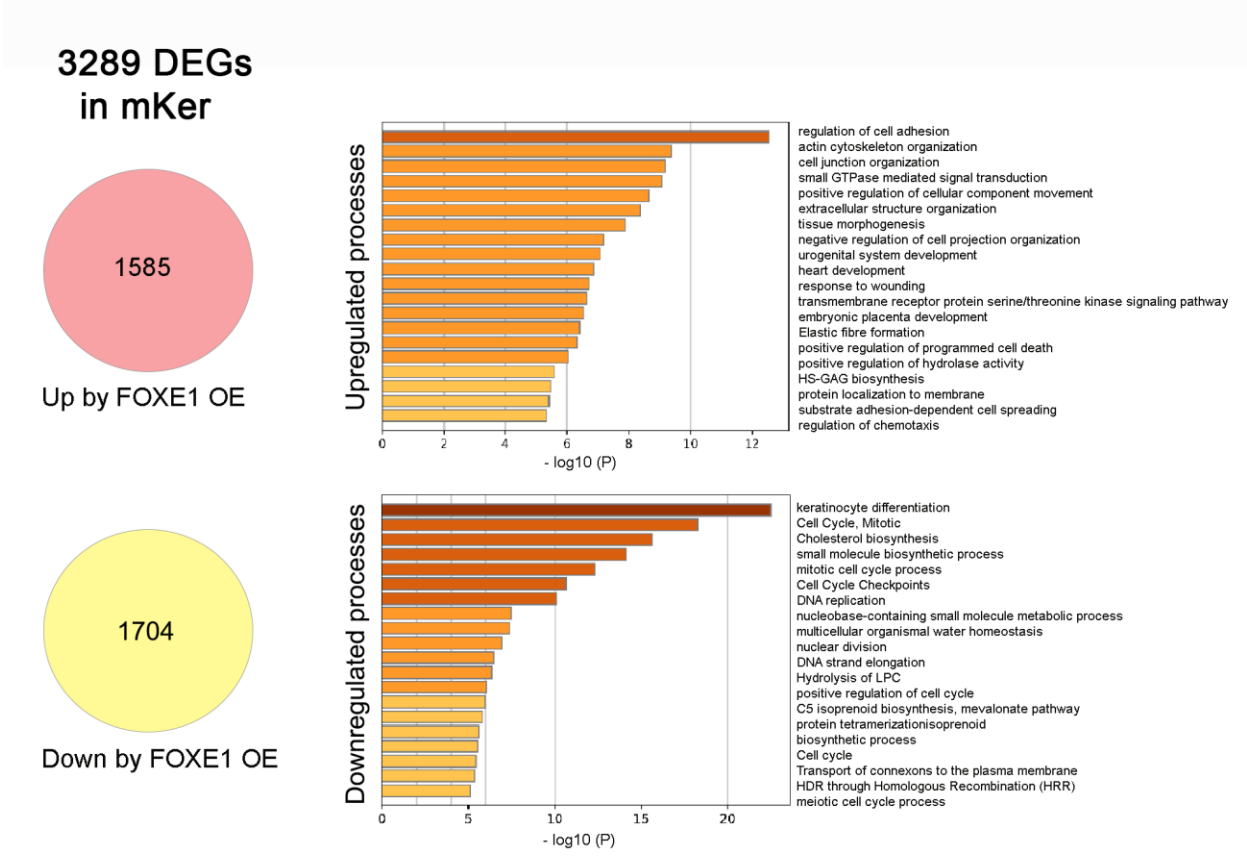
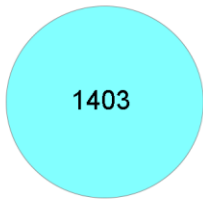
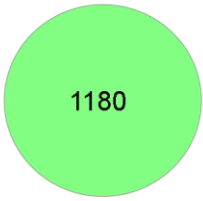


Figure 18. FOXE1 overexpression regulates subset of genes related to cell movement and cell proliferation in mouse keratinocytes. Gene enrichment analyses determined by Metascape of the 3,289 DEGs in primary mouse keratinocytes overexpressing FOXE1: 1,585 putative target genes resulted upregulated (red circle); 1,704 genes are downregulated (yellow circle).

**2583 DEGs
in G2N2c**



Up by Foxe1 KD



Down by KD Foxe1

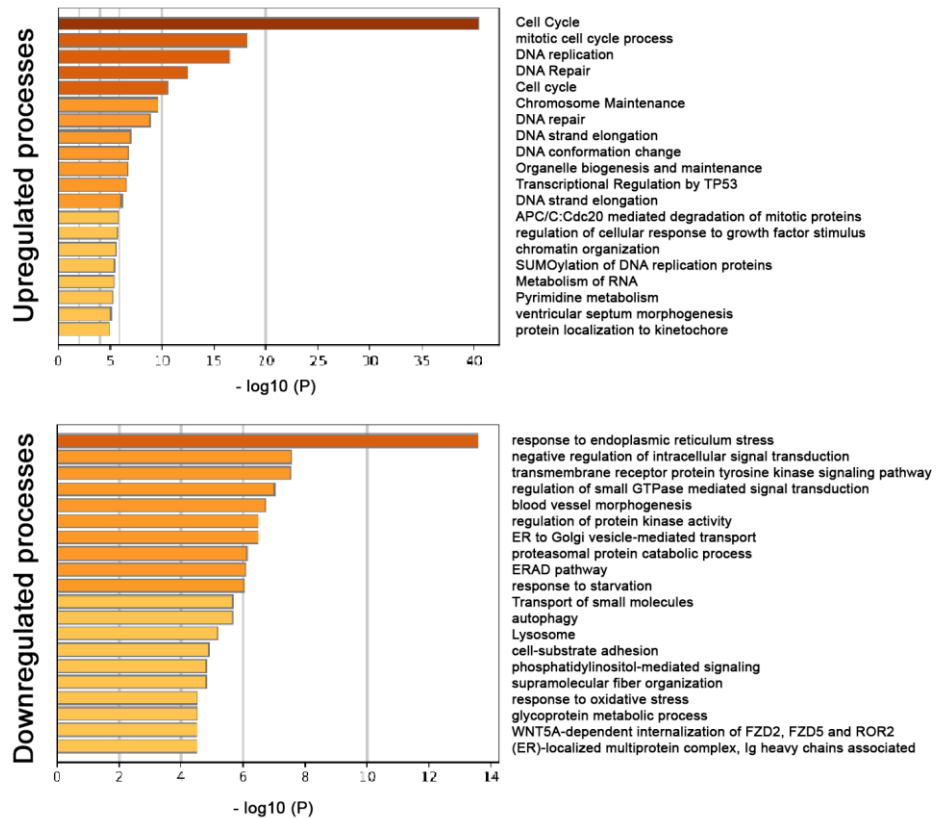


Figure 19. Foxe1 knockdown increases a gene expression profile related to cell cycle progression and proliferation in BCC cells. Gene enrichment analyses of the 2,583 DEGs in G2N2c Foxe1 knockdown: 1,403 putative target genes resulted upregulated (blue circle); 1,180 genes are downregulated (green circle) as determined by Metascape.

Then, we compared the DEGs identified in mKer to those identified in G2N2c cells in order to isolate a specific subset of putative downstream mediators of FOXE1 common to both cell types. 185 genes were upregulated by FOXE1 overexpression in keratinocytes and downregulated by Foxe1 knockdown in BCC cells. The most enriched category was the negative regulation of intracellular signal transduction and the negative regulation of kinase activity (e.g. Dusp6 and Dusp8), consistent with cell cycle arrest. In addition, wound healing and negative regulation of the Rho pathway and the WNT non-canonical pathway were also enriched. A subset of these positively regulated genes encoded membrane glycoproteins (SDC4, GPC4), transmembrane receptors (such as FZD5-6, LGR4), regulators of epithelial cell migration (EPCAM), modulators of extracellular matrix composition and its structural organization (FN1,CTGF) (Fig.20). Some of these putative FOXE1 regulated genes were also validated in human cutaneous squamous cell

carcinoma (SCC13) overexpressing FOXE1 as well as in G2N2c cells in which Foxe1 knockdown was obtained via lentiviral infection of shRNA against FOXE1 (Fig.21).

Taken together these data indicate that Foxe1 plays a major function in negatively regulating signal transduction pathways that lead to cell cycle progression, and induce cell adhesion.

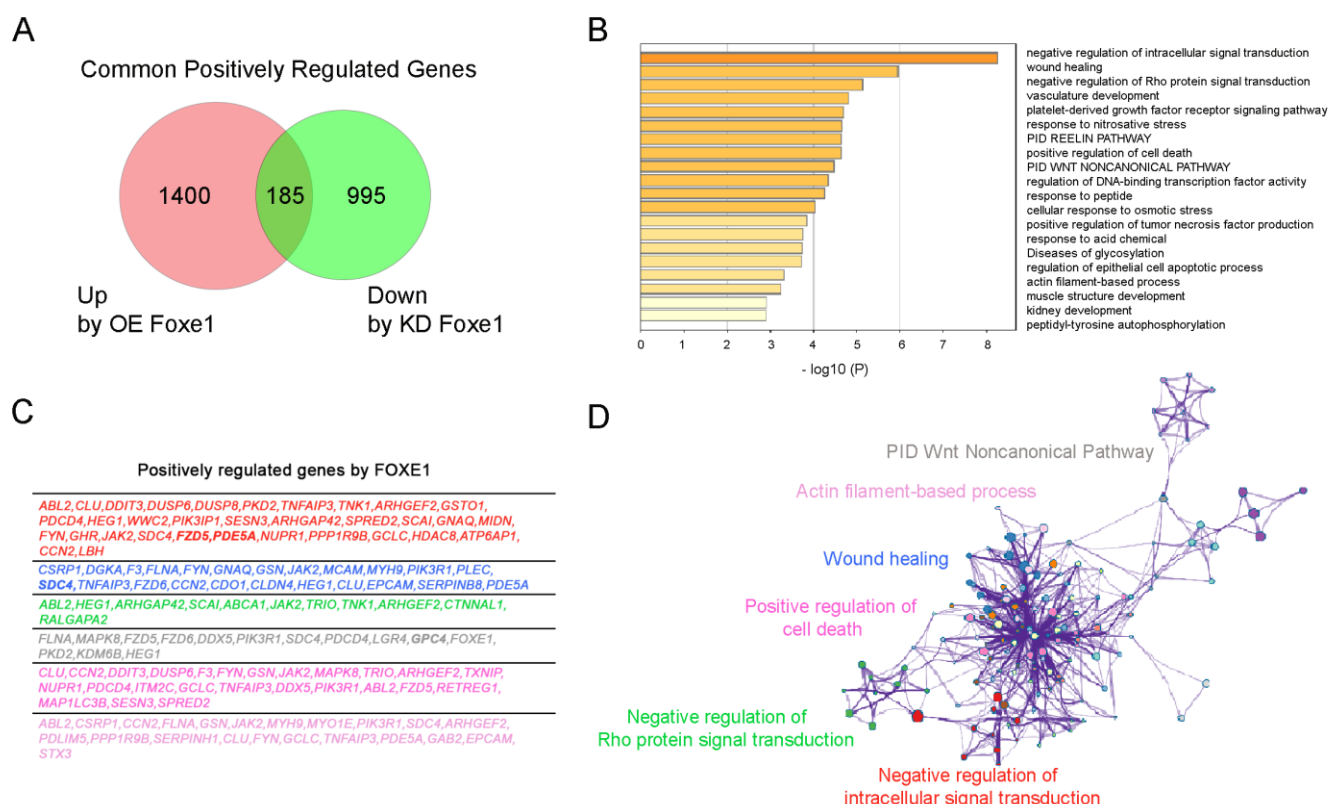


Figure 20. Positively regulated genes by Foxe1. A) Venn diagram illustrating overlap between changes identified with Foxe1 overexpression (OE Foxe1) in primary keratinocytes and Foxe1 knock-down (KD Foxe1) in G2N2C cell line. The red circle represents all the genes that change significantly by >1-fold when Foxe1 is overexpressed compared to control in primary keratinocytes (1585 upregulated genes). The green circle represents the genes that change significantly <1-fold when Foxe1 is knocked down in G2N2C cells compared to control cells (1180 downregulated genes). The overlap (185 genes) shows the FOXE1-positively regulated genes in keratinocytes. B) Enrichment analyses of putative FOXE1 positively regulated genes, as determined by Metascape, q-values < 0.05. C) Table of genes list representative for each cluster ID, coloured according to network showed in (D). D) Network of enriched terms across positively regulated genes. The most significantly enriched terms are indicated and coloured by cluster ID. (Zhou et al. Nature Commun. 2019 10(1):1523)

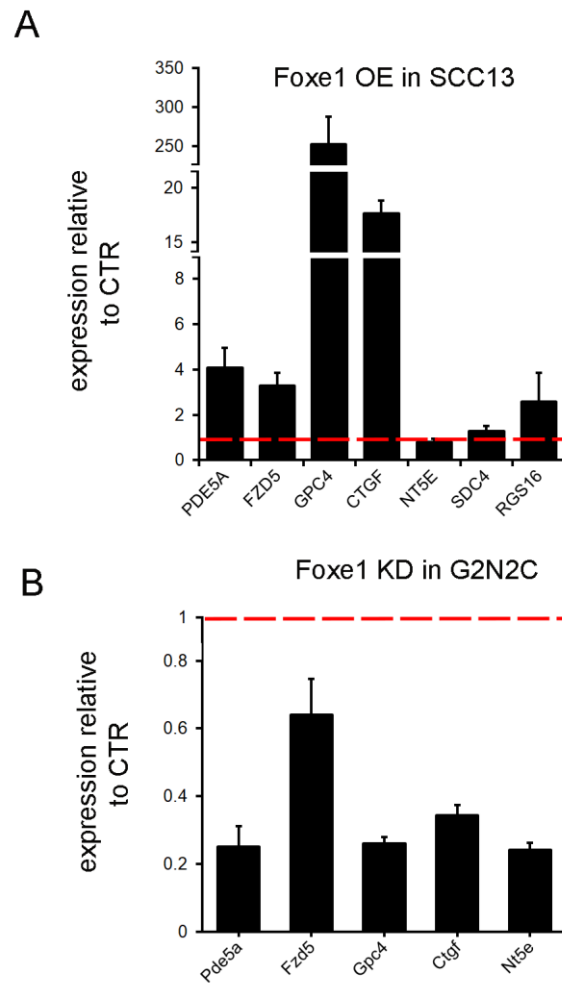


Figure 21. Positive regulation mediated FOXE1 of putative target genes in NMSC cell lines. Real-time PCR validation of newly identified putative FOXE1 targets in a human squamous cell carcinoma cell line (SCC13) exogenously expressing Foxe1 and in a mouse BCC cell line using a shRNA-mediated silencing of Foxe1 expression. mRNA levels were quantified using qRT-PCR and normalized to RPLP0 in human samples and to β -Actin in mouse samples. mRNA levels are shown as fold change relative to the relative control. The red line corresponds to a 1-fold change in expression. Error bars represent standard deviation (SD).

On the other hand, 194 genes were negatively regulated by Foxe1. These putative mediators were strongly enriched for genes coding for crucial components of the cell cycle regulatory (Fig.22). This transcriptome analysis reveals that in keratinocytes Foxe1 participate to the positive regulation of a subset of genes involved in cell motility, adhesion and extracellular matrix organization and to inhibition of cell processes related to cell cycle progression, chromosome segregation and DNA synthesis.

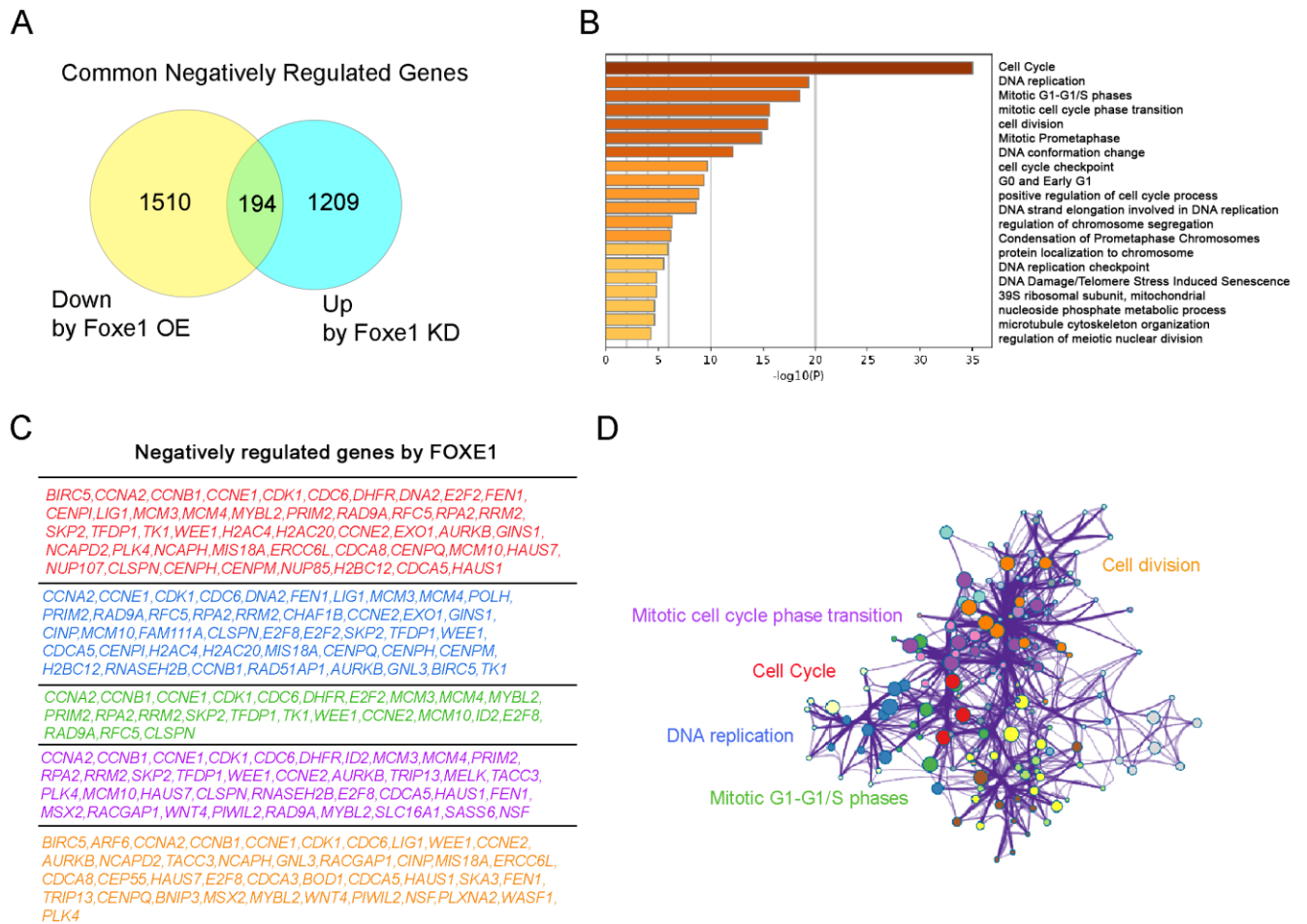


Figure 22. Negatively regulated genes by Foxe1. A) Venn diagram illustrating overlap between changes identified with Foxe1 overexpression (OE Foxe1) in primary keratinocytes and Foxe1 knock-down (KD Foxe1) in G2N2C cell line. The yellow circle represents all the genes that change significantly by <1-fold when Foxe1 is overexpressed compared to control in primary keratinocytes (1,704 genes downregulated). The blue circle represents the genes that change significantly >1-fold when Foxe1 is knocked down in G2N2C cells compared to control cells (1,403 genes upregulated). The overlap (194 genes) shows the FOXE1-negatively regulated genes in keratinocytes. B) Enrichment analyses of putative FOXE1 negatively regulated genes, as determined by Metascape, q-values < 0.05. C) Table of genes list representative for each cluster ID, colored according to network showed in (D). D) Network of enriched terms across negatively regulated genes. The most significantly enriched terms are indicated and coloured by cluster ID. (Zhou et al. Nature Commun. 2019 10(1):1523).

4.2 FOXE1 negatively regulates keratinocyte proliferation.

To test the effects of FOXE1 on keratinocyte proliferation, we firstly assessed the effects of modulating FOXE1 expression on DNA synthesis by BrdU incorporation. In a mouse BCC cell line (G2N2c), Foxe1 knockdown was achieved by parallel transient transfection with two independent siRNA. Both siRNA caused a drastic increased in DNA synthesis compared to control (Fig.23 A). Conversely, FOXE1 overexpression in primary mouse keratinocytes, which do not express endogenous Foxe1, caused inhibition of BrdU incorporation (Fig.23 B, C).

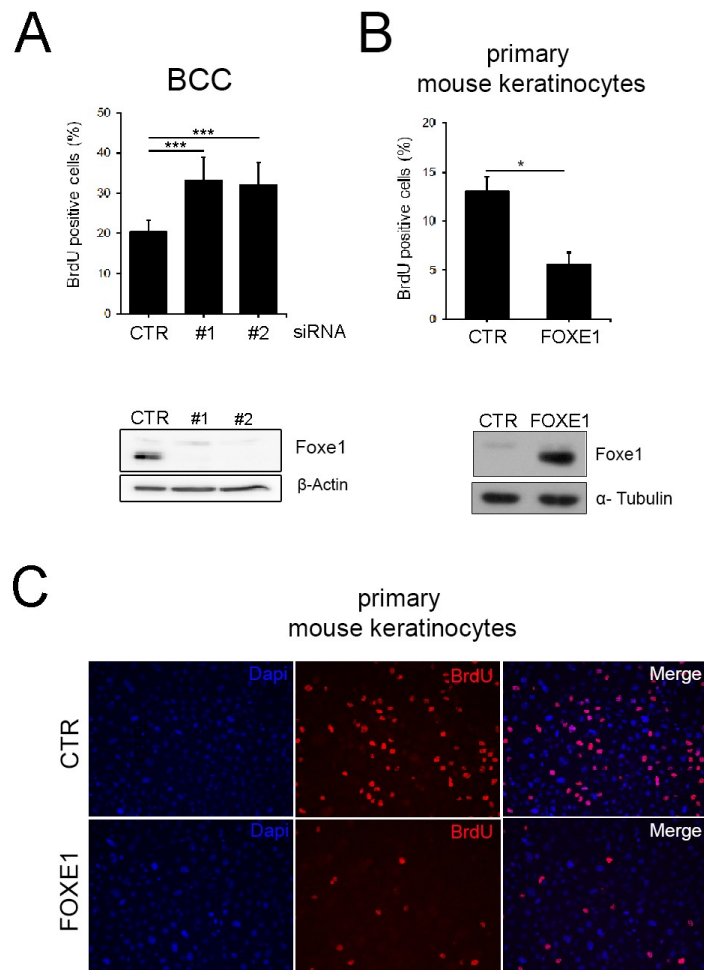


Figure 23. Foxe1 expression leads to impaired cell proliferation. A) Upper panel: Cell proliferation was measured by BrdU incorporation assay in G2n2c cells 48h hours upon transfection of two different Foxe1-specific siRNA (#1, #2) or a negative control (CTR, scrambled siRNA). Data are shown as mean \pm SEM of 5 independent experiments. Statistical significance was calculated using paired two-tailed t-test (***) $P \leq$

0.001; n=5). Lower panel: SDS-PAGE followed by Western blot for FOXE1 in G2n2c cells. β -Actin was used as loading control. B) Upper panel: BrdU incorporation assay performed in primary mouse keratinocytes after infection with a retrovirus (PINCO) carrying exogenous Foxe1 (FOXE1) or empty virus as control (CTR). Data are shown as mean \pm SEM of 3 independent experiments. Statistical significance was calculated using paired two-tailed t-test (* $P \leq 0.05$; n=3). Lower panel: SDS-PAGE followed by Western blot for FOXE1 in mKer cells. α -Tubulin was used as loading control. C) Representative images of immunofluorescence staining using anti-BrdU antibody (red signal) performed in primary mouse keratinocytes treated as in (B). DAPI (4',6-diamidino-2-phenylindole) was used to stain DNA (blue signal). Magnification, 20x.

Next, we investigated if Foxe1 affects tumorigenic keratinocyte stem cells or progenitor activity by measuring the ability of cells to generate clonogenic spheres in suspension (tumorspheres) (Pastrana et al., 2011; Liu JC et al., 2007). For this assay, we used two independent mouse BCC cell lines: G2N2c and Tb3a (Sheng et al., 2002), which were both able to form large spheres in non-adherent conditions. Foxe1 knockdown was obtained by transduction with a lentiviral vector carrying a FOXE1 specific shRNA, corresponding to siRNA #1 sequence (Fig.24 A, D). In both cell lines, the total number of tumorspheres was increased in Foxe1 knockdown cells compared to controls, increasing the tumorsphere-forming efficiency (Fig. 24 B,C, E, F).

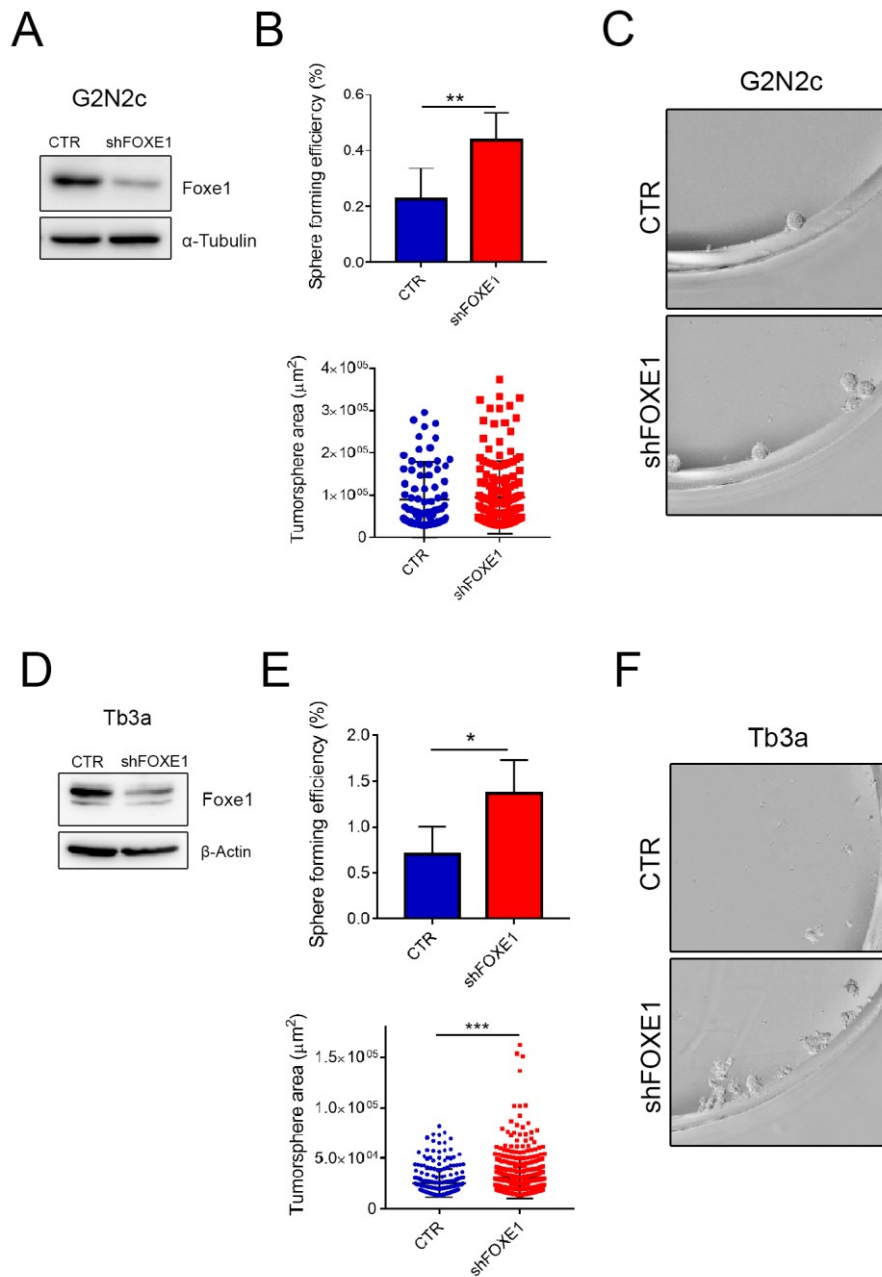


Figure 24. Foxe1-knockdown increases the self-renewal capacity in BCC cells. A, D) SDS-PAGE followed by Western blot for Foxe1 in G2N2c and Tb3a cells transduced with a lentiviral vector carrying a specific Foxe1-shRNA (shFOXE1) or sh-RNA control (CTR), α -tubulin and β -actin were used as loading control. B, E) Upper panel: Quantification of tumor-sphere assay performed in BCC cell lines treated as in (A,D). Cells were seeded into ultra-low attachment 96-well plate and the total number of tumorspheres formed in each wells was counted 10 days after seeding. Sphere-forming efficiency (SFE, %) represents the ratio between the average number of tumorspheres formed and the total number of seeded cells. Lower panel: Quantification of tumorsphere area (μm^2). Data are shown as mean \pm SEM of 3 independent experiments (G2N2c) or 2 independent experiments (Tb3a). Significance was calculated using unpaired two-tailed Student's t-test (*** $P \leq 0.001$; ** $P \leq 0.01$; * $P \leq 0.05$, $n=3$ or $n=2$). C, F) Representative phase contrast images of G2N2c and Tb3a tumorspheres formed 10 days after seeding. Magnification, 5x.

Conversely, we assessed the effect of FOXE1 over-expression (Fig. 25 A) on tumorsphere formation in a human cutaneous squamous cell carcinoma cell line (SCC13) (James G. Rheinwald and Michael A. Beckett *Cancer Res* 1981). FOXE1 expression in SCC cells caused a reduction in tumorspheres area, without affecting tumorsphere number compared to control cells (Fig. 25 B, C), suggesting that FOXE1 negatively impacts on the self-renewing capacity of SCC cells. Together these findings indicate that FOXE1 negatively regulates cell proliferation and may cause an impairment in cancer stem-like cell renewal potential, thus supporting the hypothesis that Foxe1 induced expression in BCC tumor may explain at least in part the slow growth rate of this cutaneous tumor.

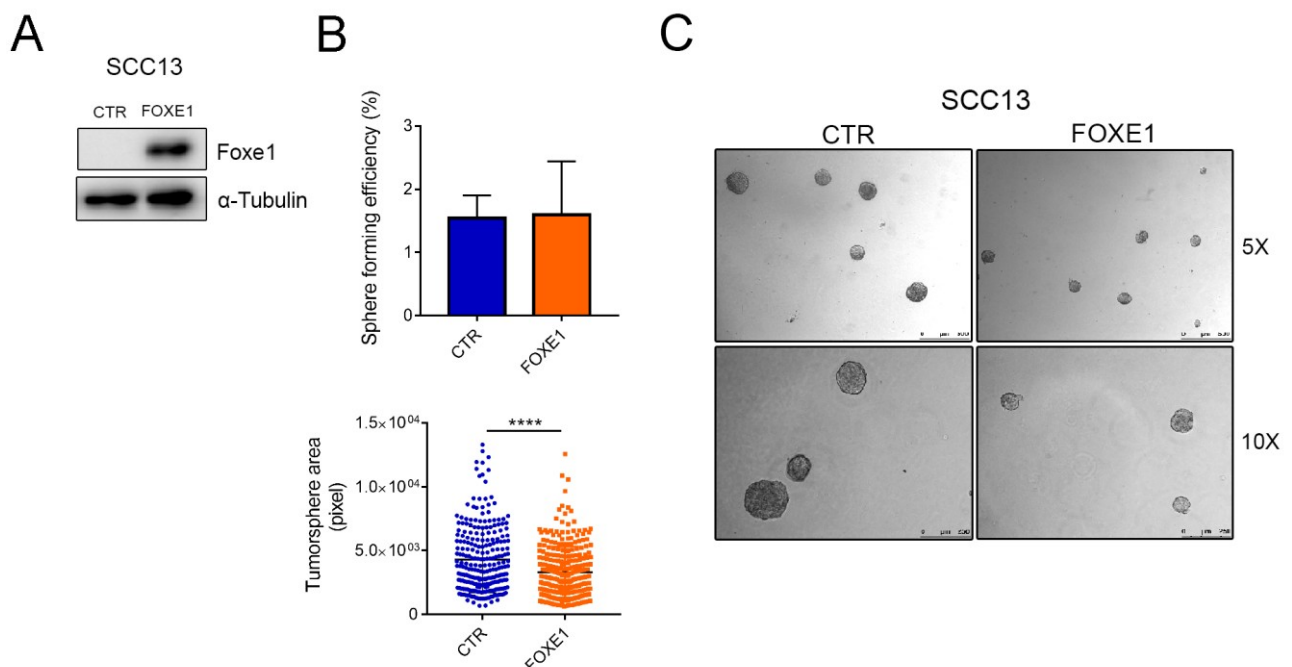


Figure 25. Foxe1 over-expression in SCC negatively impacts on tumor sphere forming efficiency. A) SDS-PAGE followed by Western blot for Foxe1 in SCC13 cells transduced with a retroviral vector carrying Foxe1 (FOXE1) or empty-control (CTR), α -tubulin was used as loading control. B) Upper panel: Quantification of tumor-sphere assay performed in SCC cell lines treated as in (A). Human SCC13 were seeded onto Matrigel pre-coated wells and Sphere-forming efficiency (SFE, %) was calculated counting the total number of tumorspheres formed 10 days after seeding. Lower panel: Quantification of tumorsphere area (pixels). Total area of tumorspheres was calculated using ImageJ software. Data are shown as mean \pm SEM of 3 independent experiments. Significance was calculated using unpaired two-tailed Student's t-test (* $P < 0.0001$; $n=3$). C) Representative phase contrast images of human SCC13 spheres seeded onto Matrigel pre-coated wells either infected with a retroviral vector carrying exogenous Foxe1 (FOXE1) or with an empty control (CTR). Magnification, 5-10X.

4.3 FOXE1 expression impairs cell migration and affects cell adhesion in cultured NMSC cell lines.

Gene expression analysis suggested an involvement of FOXE1 in regulating a set of genes and signalling pathways required in cell adhesion, motility and extracellular matrix composition, prompting us to test the possibility that FOXE1 may affect these processes. So, we investigated whether modulation of FOXE1 expression in keratinocytes is able to affect cell migration. Firstly, confluent cultures of BCC cell lines were tested for their ability to migrate in a scratch assay in the presence of endogenous Foxe1 levels or upon Foxe1 knockdown. To avoid any confounding effect, cells were mitomycin-treated to block DNA synthesis. In both G2N2C and TB3A cells, Foxe1-knockdown significantly increased cell migration independently of its effect on cell proliferation (Fig.26 A, B). Similarly, Foxe1-knockdown also led to increased cell migration in a transwell migration assay (Fig. 26 C).

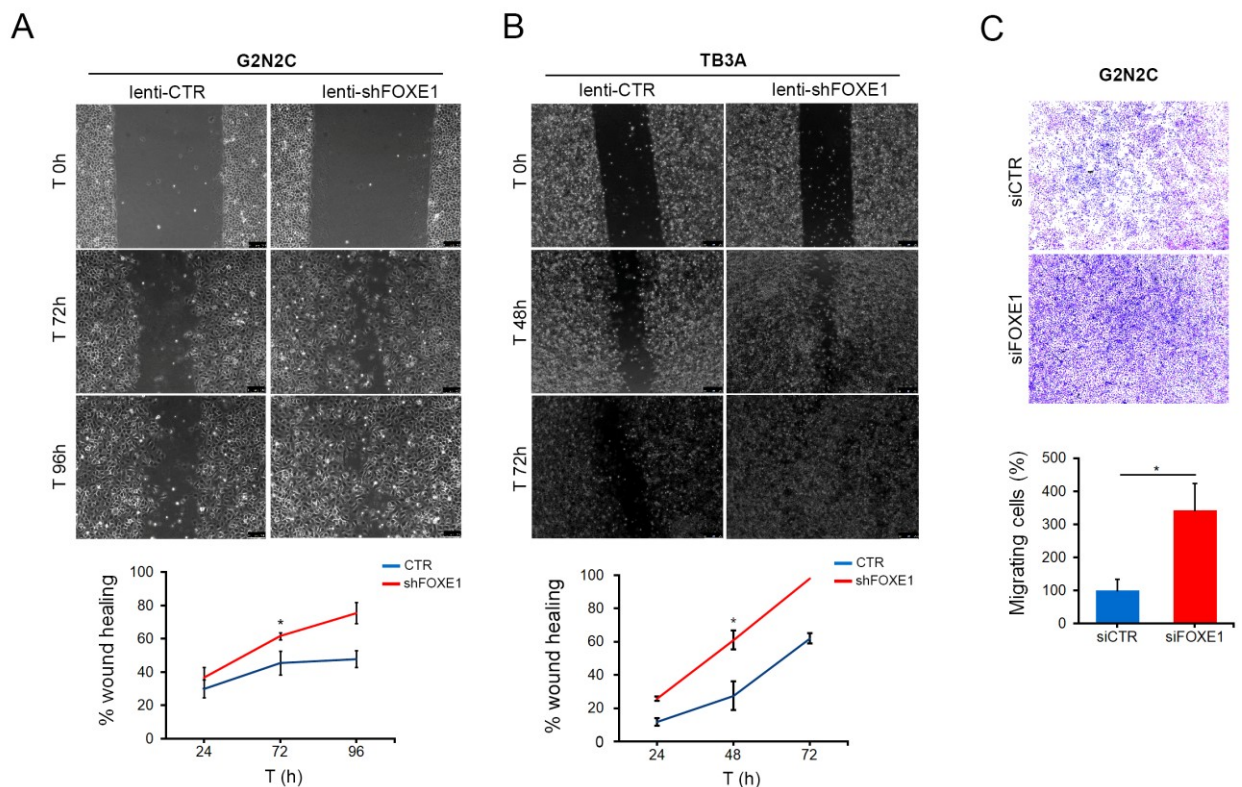


Figure 26. Foxe1-knockdown in BCC cell lines causes an increase in cell migration. A, B) Wound healing assay showing the scratch at indicated time points in G2N2c (A) and Tb3a (B) cell lines

transduced with a lentiviral vector carrying a specific Foxe1-shRNA (lenti-shFOXE1) or sh-RNA control (lenti-CTR). Quantification of wound healed area (%) was obtained by ImageJ software. Data are shown as mean \pm SEM of 2 independent experiments. Statistical significance was calculated using unpaired two-tailed t-test ($*P < 0.05$, $n=2$). C) Cell migration was measured in G2N2c cells 48h upon transfection of a specific Foxe1-specific siRNA or negative control in transwell chambers (8 μ m). Representative fields of migrated cells on the bottom side of the membrane (Magnification, 5x). After staining migrated cells were counted and quantitative data are reported as percentage of migrated cells. Results were quantified using the ImageJ software. Data are shown as mean \pm SEM of 3 independent experiments. Statistical significance was calculated using unpaired two-tailed t-test ($*P < 0.05$; $n=3$).

Consistent with these observations, FOXE1 over-expression severely impaired the migration in SCC13 cells and in primary mouse keratinocytes in response to wounding. While control cells closed the wound in approximately 24 h, the margins of the wound in FOXE1 OE cells remained far apart (Fig.27 A, B). As expected, the inhibitory effect on cell motility was observed also in transwell assays, in which the number of migrating cells was significantly reduced in SCC13. Similar results were observed also by FOXE1 OE in the human laryngeal squamous cell carcinoma SCC-028 (Fig.27 C).

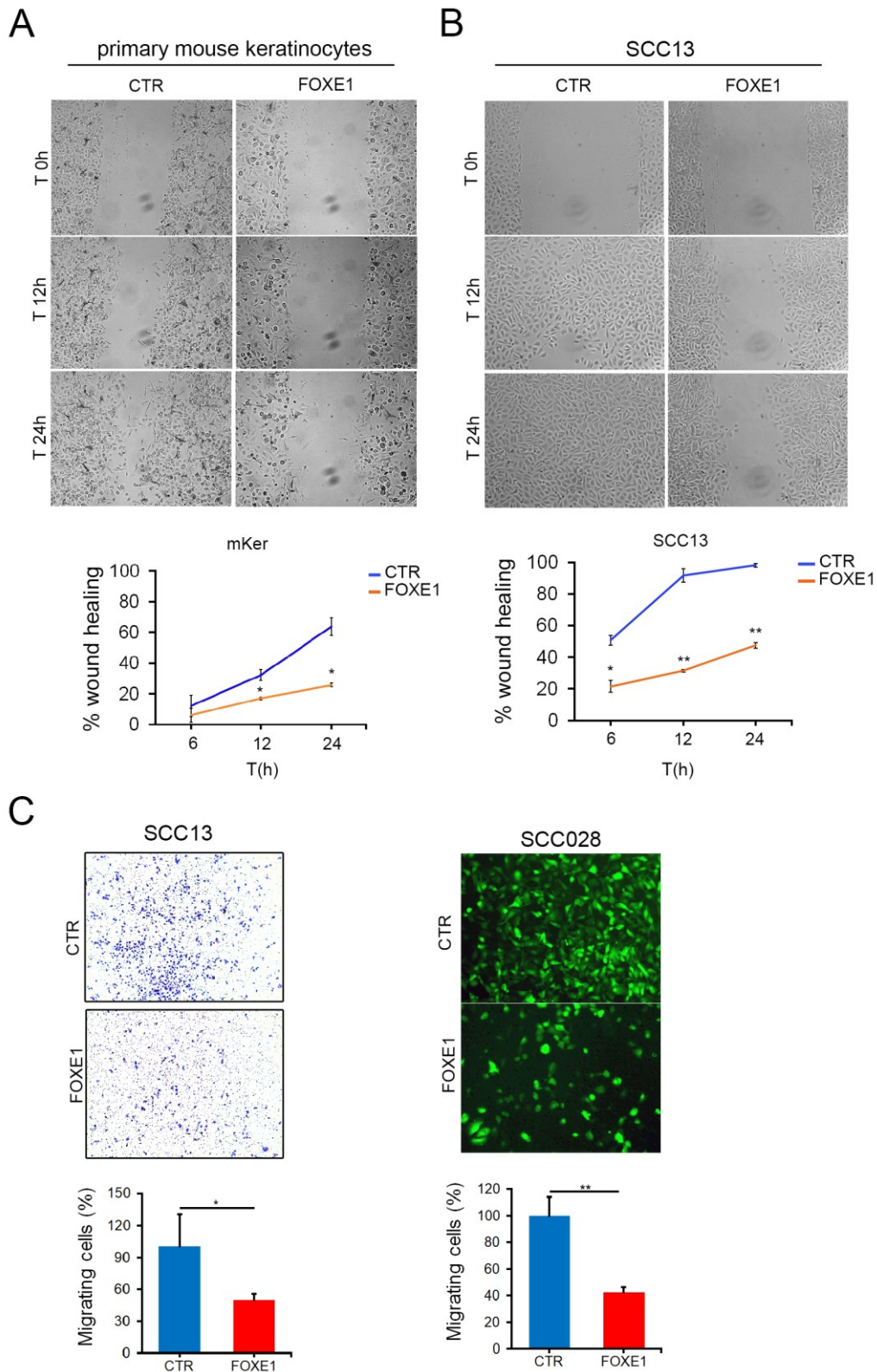


Figure 27. Foxe1 over-expression leads to impaired cell migration. A) and B) Wound healing assay showing the scratch at indicated time points in primary mouse keratinocytes (A) and in a human cutaneous SCC derived cell line (B) infected with a retroviral vector carrying exogenous Foxe1 (FOXE1) or empty controls (CTR). Cell migration was monitored by time-lapse microscopy for 30h. Quantification of wound healed area (%) was obtained by ImageJ software. Data are shown as mean \pm SEM of 2 independent experiments (mKer) or of 5 independent experiments (SCC13). Statistical significance was calculated using

unpaired two-tailed t-test ($*P<0.05$; $n=2$; $**P<0.01$; $n=5$). C) Boyden chambers assay was performed in SCC13 and SCC028 cell lines over expressing FOXE1 (FOXE1) or expressing the empty retroviral vector (CTR). Migrating cells were imaged with a bright-field (SCC13, on the left) or by fluorescence microscopy as the retroviral vector PINCO carries GFP ORF under the CMV promoter (SCC028, on the right) (5x magnification). Photos were representative fields. Migrated cells were counted and quantified using ImageJ software. Quantitative data are reported as percentage of migrated cells. Data are shown as mean \pm SEM of 3 independent experiments. Statistical significance was calculated using unpaired two-tailed t-test ($*P<0.05$; $**P<0.01$, $n=3$).

To test whether cell adhesion is also affected by FOXE1 expression, we performed an adhesion assay in which cells were allowed to attach onto uncoated surface for different time points and after removing non adherent cells by washing, attached cells were quantified by colorimetric assay. Both human SCC13 and mouse BCC cell lines were more adhesive when FOXE1 was highly expressed compared to controls (Fig.28 A, B).

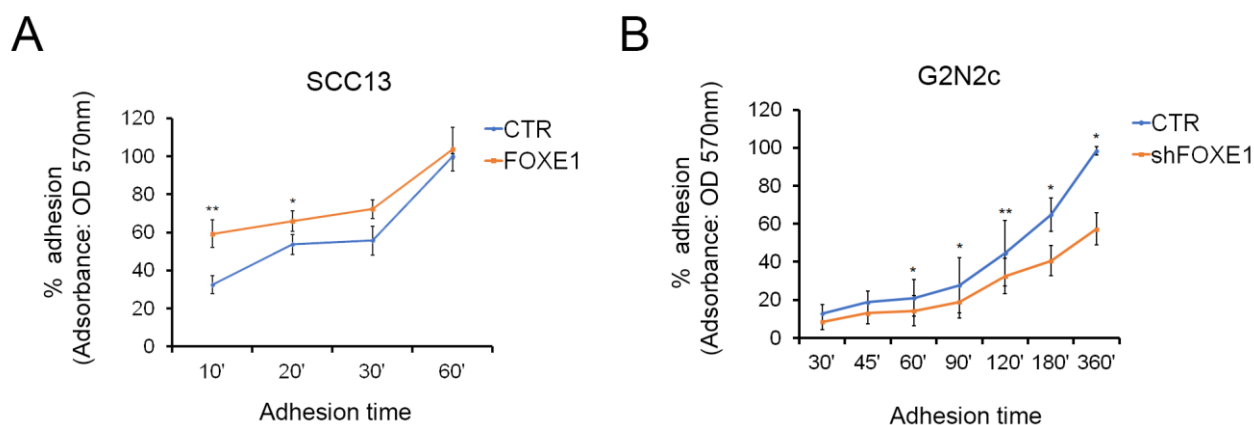


Figure 28. Foxe1 expression enhances cell adhesion in NMSC cell lines. Cell adhesion assay was performed in human cutaneous SCC derived cell line infected with a retroviral vector carrying exogenous Foxe1 (FOXE1) or empty control (CTR) and in mouse BCC cells line Foxe1-silenced cells (shFOXE1) and its related control (CTR). Cells were allowed to attach for the indicated time points. After washing, the percentage of adherent cells were quantified by a colorimetric assay. Data are shown as mean \pm SEM of 3 independent experiments. Statistical significance was calculated using unpaired two-tailed t test ($*P<0.05$; $**P<0.01$, $n=3$).

Moreover, we observed that Foxe1 silencing in BCC cells influences the actin polymerization, causing a disassembly of F-actin filaments (Fig.29). Taken together, these results suggest that FOXE1 expression leads to an adhesive, anti-migratory epithelial behaviour, which could limit the potential aggressiveness of BCC cell lines compared to the more invasive and motile SCC cells.

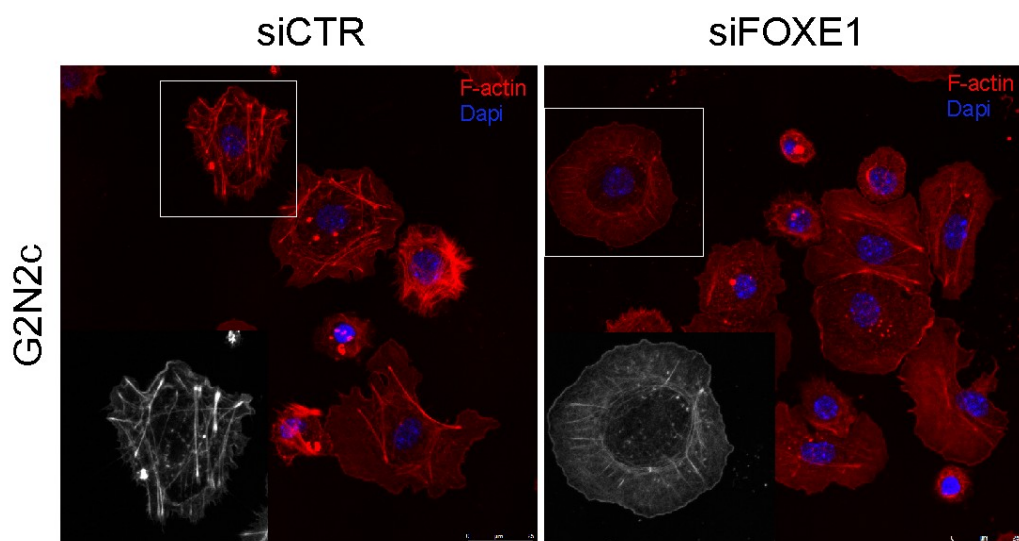


Figure 29. Foxe1 knockdown affects F-actin cytoskeleton in BCC cells. Immunofluorescence images visualized by confocal microscopy of F-actin (rhodamine phalloidin, red signal) in G2N2c cells 48h after siRNA transfection. DAPI (4',6-diamidino-2-phenylindole) was used to stain DNA (blue signal). Magnification, 63X. Scale bar is 25 μ m.

4.4 Tbx1 positively regulates cell migration in BCC cells.

In parallel with my studies on Foxe1, I also contributed to understanding the function of another transcription factor, Tbx1, in BCC. Similar to Foxe1, Tbx1 is specifically expressed in the hair follicle. Tbx1 is a marker of HFSC niche where it acts as a promoter of stem cell self-renewal and tissue regeneration (Chen T. et al., 2012). Interestingly, similar to Foxe1, Tbx1 is aberrantly expressed in BCC tumorigenesis, probably contributing to the transcriptional program of BCC. In the heart TBX1 has been associated to regulation of cell motility and cytoskeletal organization, via Wnt signalling pathway (Chen L. et al, 2012). Therefore, we investigated the effects of Tbx1 modulation on cell migration in BCC cells (G2N2c cell line) with a similar approach to that used for Foxe1. Wound healing assay revealed that at 48h after transfection of specific Tbx1 siRNA cell motility of BCC cells is strongly impaired. These observations suggests that the biological role of this gene in BCC cells has an opposite effect to that of Foxe1, acting as a promoter of cell motility and not as an inhibitor (Fig.30) (Caprio C. et al., 2020).

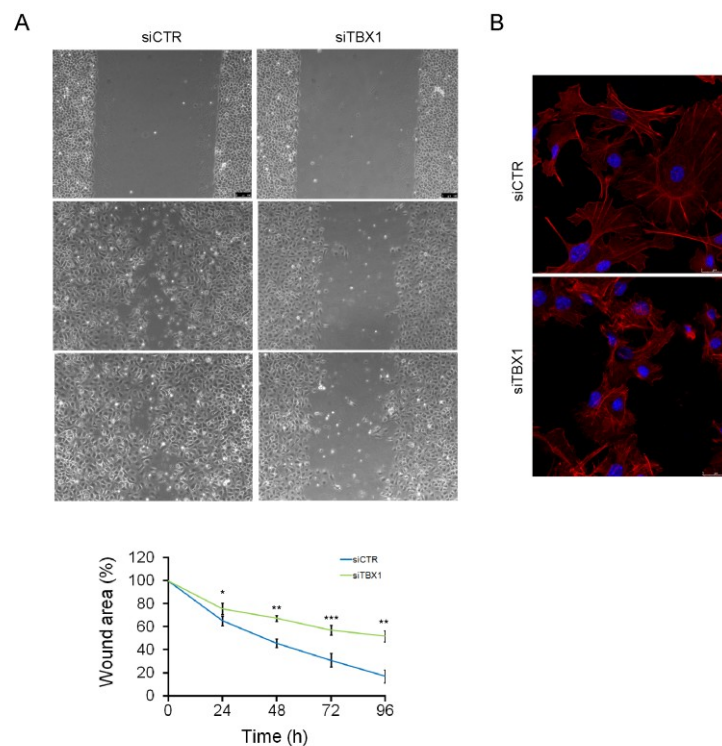


Figure 30. Tbx1-knockdown in BCC cell lines causes an inhibition of cell migration. A) Wound healing assay showing the scratch at indicated time points in G2N2C cells transfected with a specific Tbx1 siRNA (siTBX1) or siRNA control (siCTR). Quantification of wound healed area (%) was obtained by ImageJ software. Data are shown as mean \pm SEM of 4 independent experiments. Statistical significance was calculated using unpaired two-tailed t-test (* $P \leq 0.05$, ** $P \leq 0.01$, *** $P \leq 0.001$, $n=4$). B) Immunofluorescence images visualized by confocal microscopy of F-actin (rhodamine phalloidin, red) and nuclei (DAPI, blue) in G2N2c cells 48h after siRNA transfection. Magnification, 63X. Scale bar is 25 μ m.

4.5 Depletion of Foxe1 expression in K5-Gli2 model results in severe tumorigenic skin lesions.

Our laboratory has previously demonstrated that Foxe1 is highly expressed in human and mouse BCC, but not in SCC (Brancaccio et al., 2004).

To define the role of *Foxe1* in BCC tumorigenesis, we firstly assessed the expression of Foxe1 in a BCC mouse model exogenously expressing the transcription effector of the SHH pathway Gli2 under the control of the keratin 5 promoter (K5-Gli2) (Grachtchouk M. et al., 2000). In a C57BL/6 genetic background, Gli2 expression lead to BCC formation at 3-4 months of age on the ear and tail. Gli2 expressing mice were readily distinguishable from their wild-type littermate for their sparse hair coat from 1 month of age. By 9 months of age, the average number of visible globular tail BCC was 2 (n=12), whereas ears developed clusters of small BCC-like lesion on the edges. Using polyclonal antibodies specific for Foxe1, we tested its expression in fully developed BCCs. As shown in Fig. 31, Foxe1 expression was detected in most if not all the nuclei of the BCC cells, whereas it was absent in the stroma and in the epidermis.

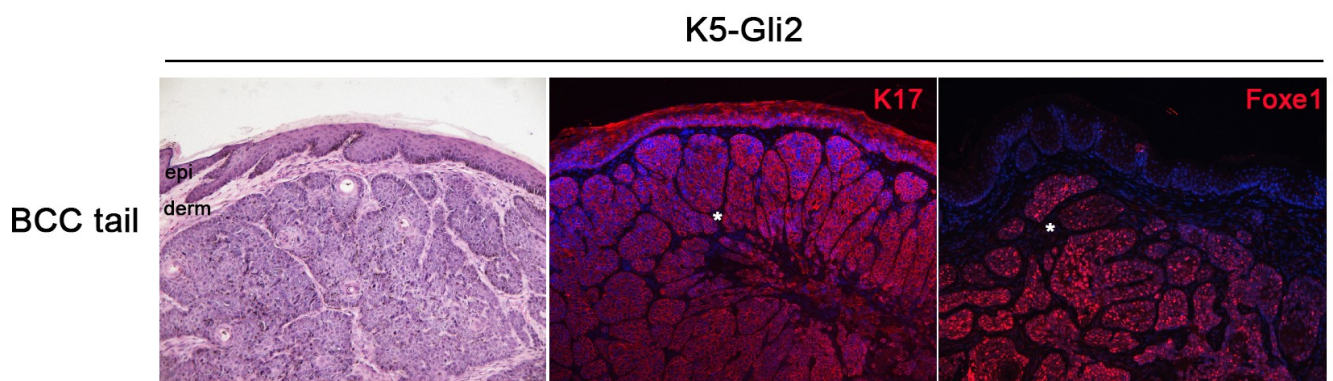


Figure 31. Foxe1 is abundantly induced in nodular BCCs of K5-Gli2 mouse. H&E staining of nodular BCC developed on tail skin of K5-Gli2 mouse at 9 months of age (left). Immunofluorescence staining showing K17 expression, present in nearly all tumor cells and in hyperplastic epidermis (centre), and Foxe1 positive cells (red signal) (right). Epi: epidermis. Derm: derma. Asteriks (*): tumor stroma. Magnification, 10x.

To test the function of *Foxe1* in BCC tumorigenesis, K5-Gli2 mice were crossed with K14-Cre *Foxe1* fl/fl in which *Foxe1* is specifically deleted in stratified epithelia including the epidermis and its derivative.

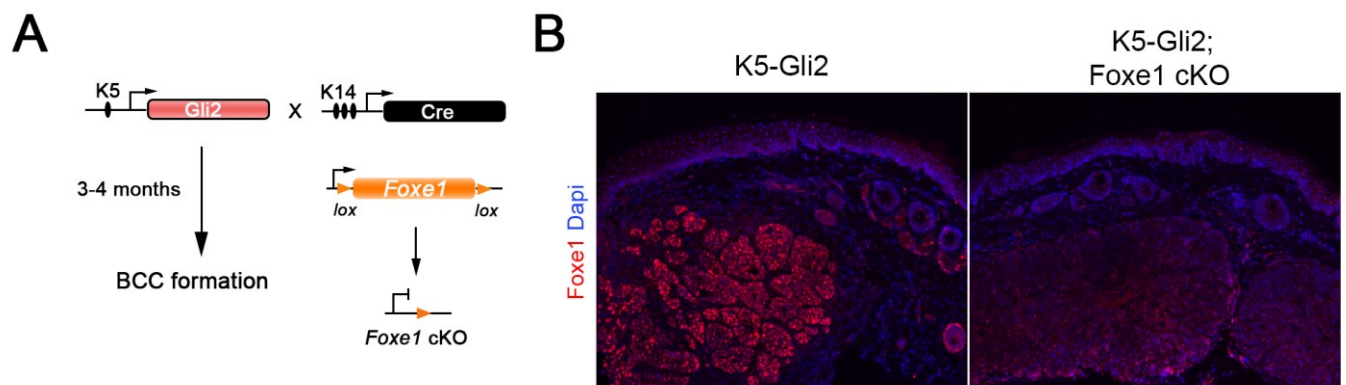


Figure 32. Conditional deletion of *Foxe1* during BCC tumorigenesis in K5-Gli2 model. A) Genetic strategy used to obtain BCC formation in K5-Gli2 mouse model in absence of *Foxe1* (single exon, orange) expression in epidermis. B) Immunofluorescence staining showing absence of *Foxe1* expression in K5-Gli2; K14-Cre *Foxe1*fl/fl mouse model compared to control mice (K5-Gli2) in skin sections from nodular BCC (tail). Magnification, 10x.

No statistical differences were detected in the average number of tumors and in their appearance in either tail or ears. This is may be due at least in part to the low and variable number and size of tumors that were obtained in this mouse model.

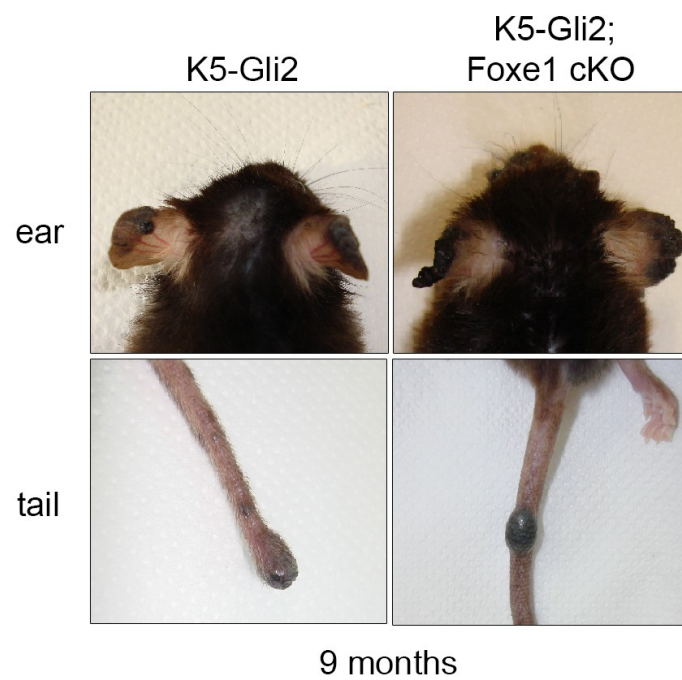


Figure 33. Typical BCC tumors in K5-Gli2 mouse model. Macroscopic pictures of nodular BCCs developed on ear (photos on top) and tail (photos below) of K5-Gli2 mice (control group) and K5-Gli2; K14-Cre Foxe1 fl/fl mice at 9 months of age.

Interestingly, however, mice lacking Foxe1 expression were all affected by moderate to severe ventral alopecia (n=13 Foxe1 cKO mice versus n=12 control mice), and 77% of them developed severe facial tumorigenic lesions, which in severe cases led to eye loss (Fig.34).



Figure 34. Foxe1 depletion in skin of K5-Gli2 mouse causes more severe skin lesions. Macroscopic appearance of K5-Gli; K14-Cre Foxe1fl/fl showing an aggressive phenotype of skin with ventral alopecia and tumorigenic lesions in face area not present in control group (K5-Gli2 mice).

Histological analyses revealed the presence of hyperplastic and hyperproliferative invaginating lesions resembling the upper portion of the hair follicles with hyperplastic sebaceous glands and

were characterized by infiltration of many inflammatory cells in the dermis and in the epidermis (Fig.35).

Taken together these data indicate that loss of the hair follicle marker Foxe1 in BCC leads to a more severe and aggressive phenotype at least in some area of the body that are usually not affected by BCC in this mouse model.

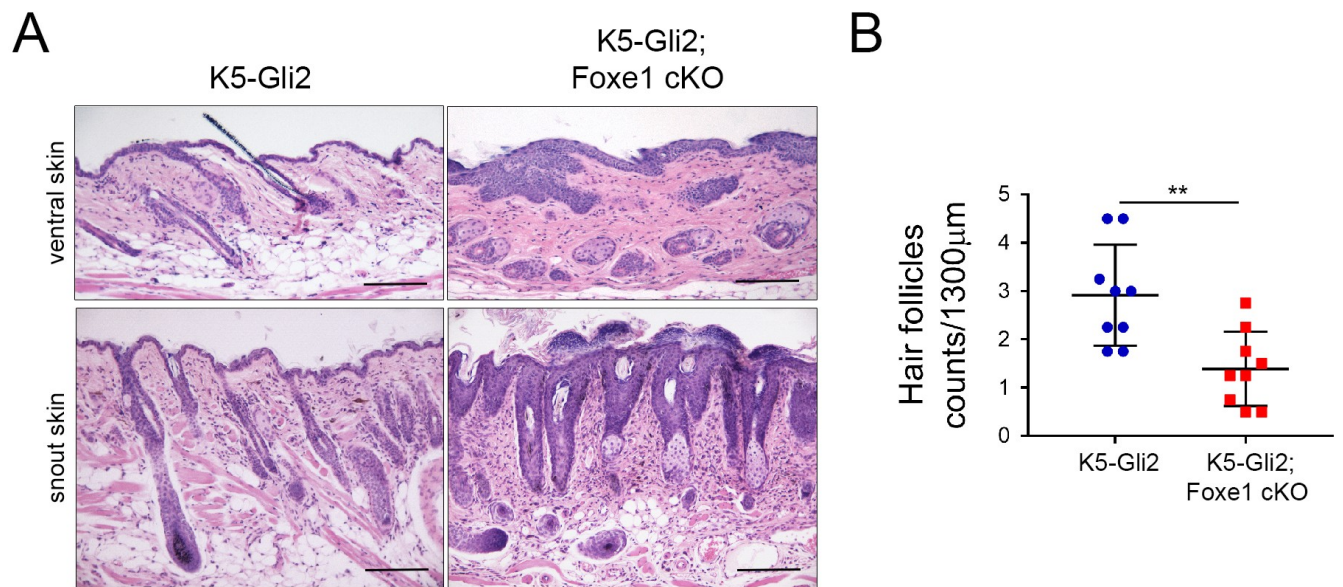


Figure 35. Absence of Foxe1 expression in HF of K5-Gli2 mice induces hyperproliferation and strong inflammation of epidermis. A) Histological appearance of ventral and snout skin of K5-Gli2 mice in the presence or in the absence of Foxe1. Magnification, 10x. B) Relative quantification of hair loss in ventral skin. Scatter plot showing mean of hair follicles number counted in K5-Gli2 (n=9) and K5-Gli2; K14-Cre Foxe1 fl/fl (n=9) mice. ****P<0.01** (t-test). Scale bar, 200µm.

4.6 Foxe1 depletion in BCC leads to more disorganized skin lesions in SmoM2 expressing BCCs.

To explore further the function of Foxe1 in BCC further, we took advantage of an inducible BCC mouse model in which SmoM2 oncogene is expressed under the control of the ROSA26 promoter upon the conditional deletion of Lox-STOP-Lox cassette (Mao et al.; 2006). SmoM2 was induced in a temporal and skin-specific manner by crossing the SmoM2 with K14-Cre-ER mice, as previously reported (Youssef et al., 2010). The advantage of this model is that BCC formation occurs earlier in 8-10 weeks upon tamoxifen administration.

We first induced SmoM2 expression in most epidermal cells by administering tamoxifen (5 consecutive days, 10 mg total) to K14-CREER/RosaSmoM2 mice starting from day 28 after birth (P28). Macroscopically visible lesions were clearly detectable 6-8 weeks after treatment, preferentially in the tail and ear skin as previously reported (Youssef et al.; 2010), although no globular BCCs were observed in the tails in contrast to the K5-Gli2 mouse model. Haematoxylin-eosin staining revealed hyperplastic epidermal lesions invading the underlying dermis with a typical appearance of branched basal hair follicle like structures (Fig. 36 A). BCCs express hair follicle markers such as Krt17 and Sox9. Accordingly, immunofluorescence staining revealed that Sox9, a transcription factor expressed in the bulge and in early outer root sheath progenitors (Kadaja M Fuchs G&D, 2014), was expressed in most cells of the lesions, as previously shown (Vidal et al., 2008; Larsimont et al., 2015). Similarly, Foxe1 was also expressed in strands of epithelial cells invading the dermis (Fig. 36 B). Spatial distribution of Foxe1 positive cells was mainly restricted to the lower regions of fully developed BCCs and was not detected in the hyperplastic interfollicular epidermis, consistent with its physiological expression in the hair follicle of adult skin, where it is limited to the lower portion of the most undifferentiated layer (outer root sheath, ORS) (Brancaccio et al., 2004). These *in vivo* findings indicate that FOXE1 expression is a common feature observed during BCC formation in mouse skin, irrespective of the oncogenic hit.

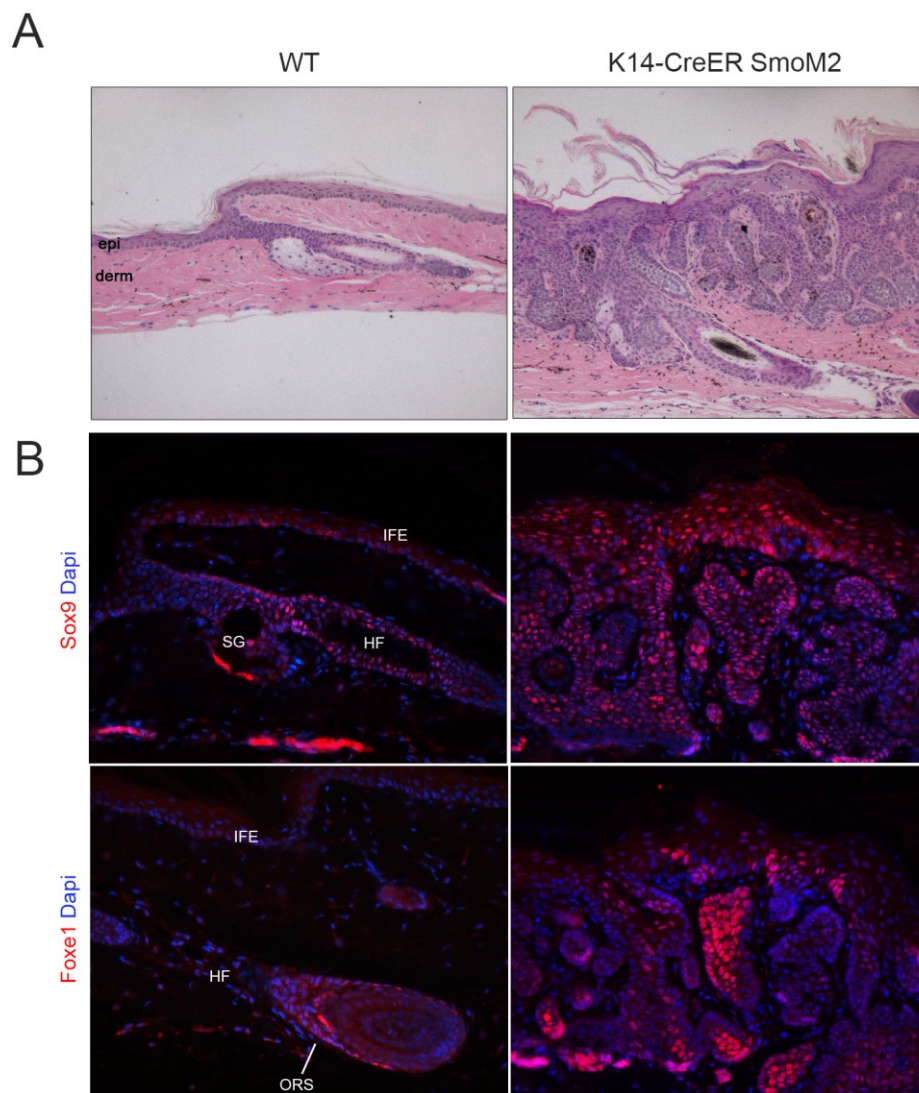


Figure 36. Induction of Foxe1 expression in BCC lesions of K14-Cre-ER; SmoM2-YFP mice. A) Haematoxylin–eosin staining of tail sections from WT and K14–CREER/RosaSmoM2 mice 10 weeks after TAM (10 mg) administration. B) Immunofluorescence staining showing Sox9 (on the left) and Foxe1 (on the right) positive cells in skin section of tail from WT and K14–CREER/RosaSmoM2 mice 10 weeks after TAM (10 mg) administration. epi: epidermis. derm: dermis. SG, sebaceous gland. IFE, interfollicular epidermis; HF, hair follicle; ORS, outer root sheath.

To determine the role of Foxe1 during BCC formation, we performed concomitant conditional deletion of *Foxe1* and overexpression of SmoM2 and examined the impact of *Foxe1* deletion on BCC formation. To this aim, we crossed K14-CREER/RosaSmoM2 model with a conditional

Foxe1 knockout mouse ($Foxe1^{fl/fl}$). The resulting K14-CREER/RosaSmoM2/Foxe1 $^{fl/fl}$ model (K14-CreER SmoM2 Foxe1cKO) was compared to control mouse (K14-CreER SmoM2) for their ability to generate BCC on time (Fig.37 A). Similar to K5-Gli2 mice no differences could be detected in BCC formation in the tail, whereas the ear lesions developed few days earlier and were more severe in mice lacking Foxe1 rather than controls. Importantly, mice lacking Foxe1 also developed lesions in the snout, reproducing what has already been observed during K5-Gli2-induced BCC in absence of Foxe1 (Fig.37 B).

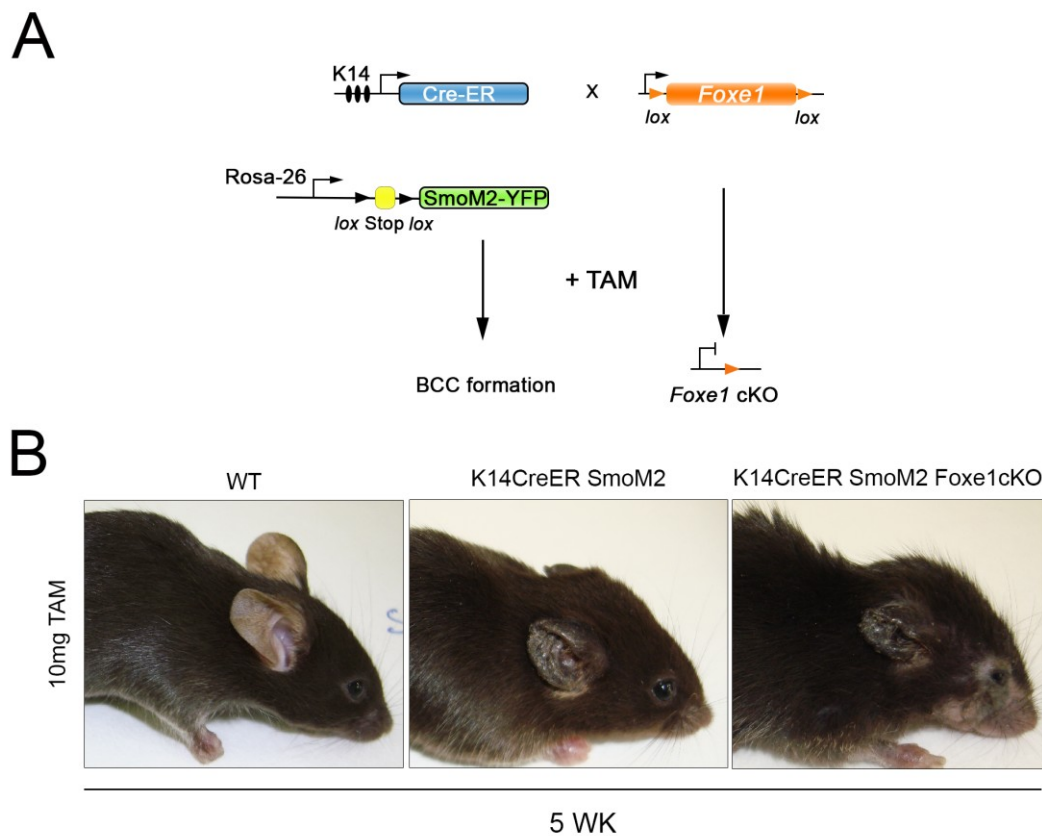


Figure 37. Foxe1 deletion in skin of K14-CreER; SmoM2 mouse model causes more severe skin lesions than controls. A) Scheme representing the genetic strategy used to induce BCC in mouse epidermis together with conditional deletion of *Foxe1* (single exon, orange). B) Macroscopic appearance of BCC lesions developed on ears of Cre negative mice (left), K14-CreER; SmoM2 (centre) and K14-CreER; SmoM2; Foxe1 $^{fl/fl}$ (right) at 5 weeks after tamoxifen administration (TAM 10 mg). Experiment was performed using four mice for each experimental group.

Since high dose of tamoxifen lead to a poor health conditions after 8 weeks of age, we performed experiments at low dose (0.5 mg total injected 28 days after birth) to expand the time of observation of BCC evolution after oncogene induction. Possible alterations during BCC tumorigenesis were investigated comparing BCC lesions originated in presence or absence of Foxe1 expression at different time points during tumor evolution. In particular, early stages, tumor progression and advanced stages were analyzed collecting skin samples at 5, 8 and 16 weeks, respectively, after tamoxifen administration. Cre-recombinase negative mice and K14-CreER/Foxe1flox/flox mouse model were treated with tamoxifen as negative controls (Fig.38).

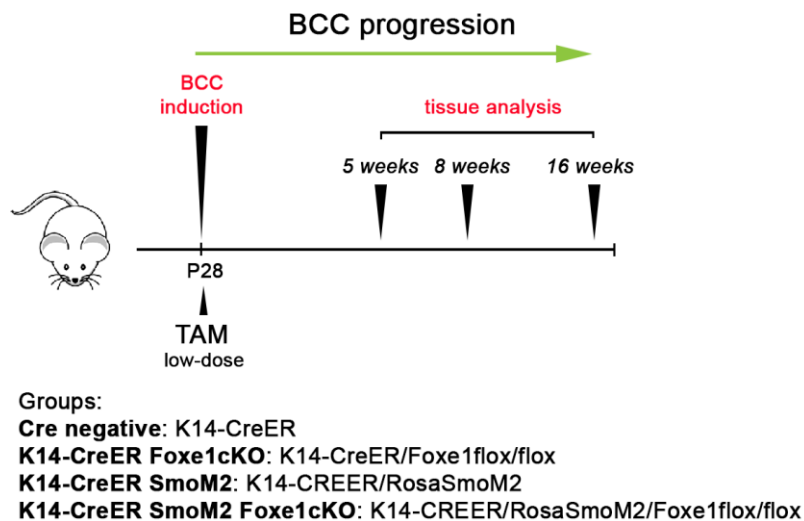


Figure 38. Study of BCC formation, progression and late stages of skin tumorigenesis in presence and absence of Foxe1 expression. Experimental plan to study phenotypic effects of Foxe1 deletion on BCC tumorigenesis with low dose of tamoxifen (TAM 0,5mg).

Five weeks following TAM administration, K14-CreER;SmoM2;Foxe1cKO mice developed macroscopic ear lesions earlier than the K14-CreER; SmoM2. As expected, no lesions were observed in skin in the two negative control groups (Fig.39). In addition, at 8-16 weeks Foxe1 depleted mice expressing SmoM2 developed BCC-like lesions in the snout as observed at 5 weeks at higher tamoxifen doses and consistent with the phenotype in K5-Gli2; K14-Cre Foxe1fl/fl mice.

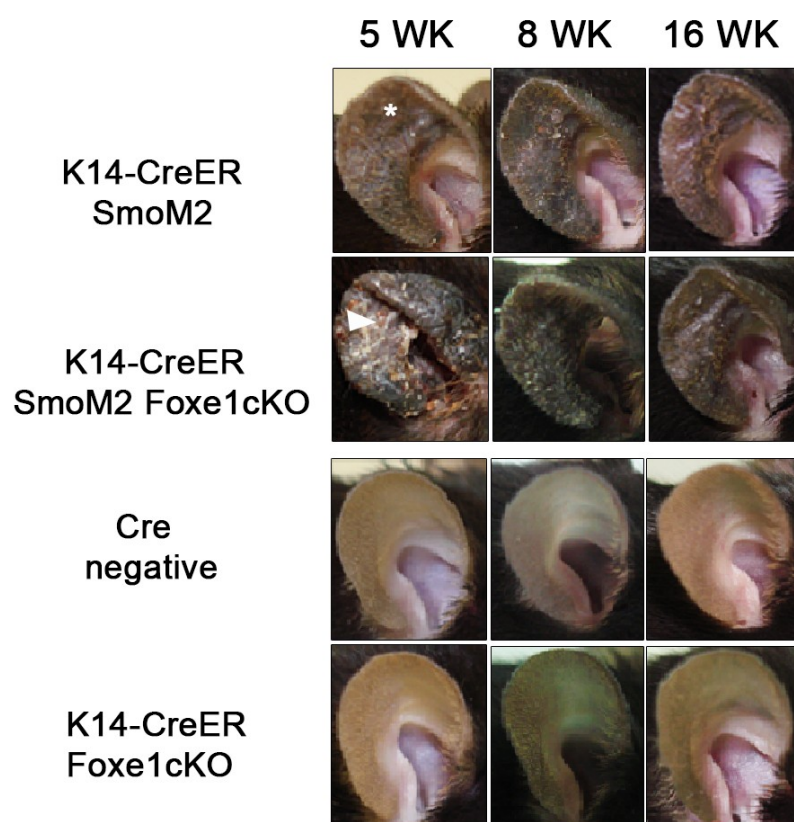


Figure 39. Foxe1 deletion resulted in more severe skin lesions than control in BCC. Representative macroscopic pictures of ears taken at 5, 8, 16 weeks after TAM administration (0,5 mg) show the absence of tumor induction in Cre-negative, K14-CreER/Foxe1flox/flox mice and macroscopic tumor burdens readily visible on ear of K14-CREER/RosaSmoM2/Foxe1flox/flox mice. Note the advanced stage of skin lesions in Foxe1 depleted mice (white arrow) compared to control: K14-CREER/RosaSmoM2 (white asterisk). All groups are treated with a single injection 28 days after birth. The experiment was performed using five mice for each experimental group and for each time analyzed.

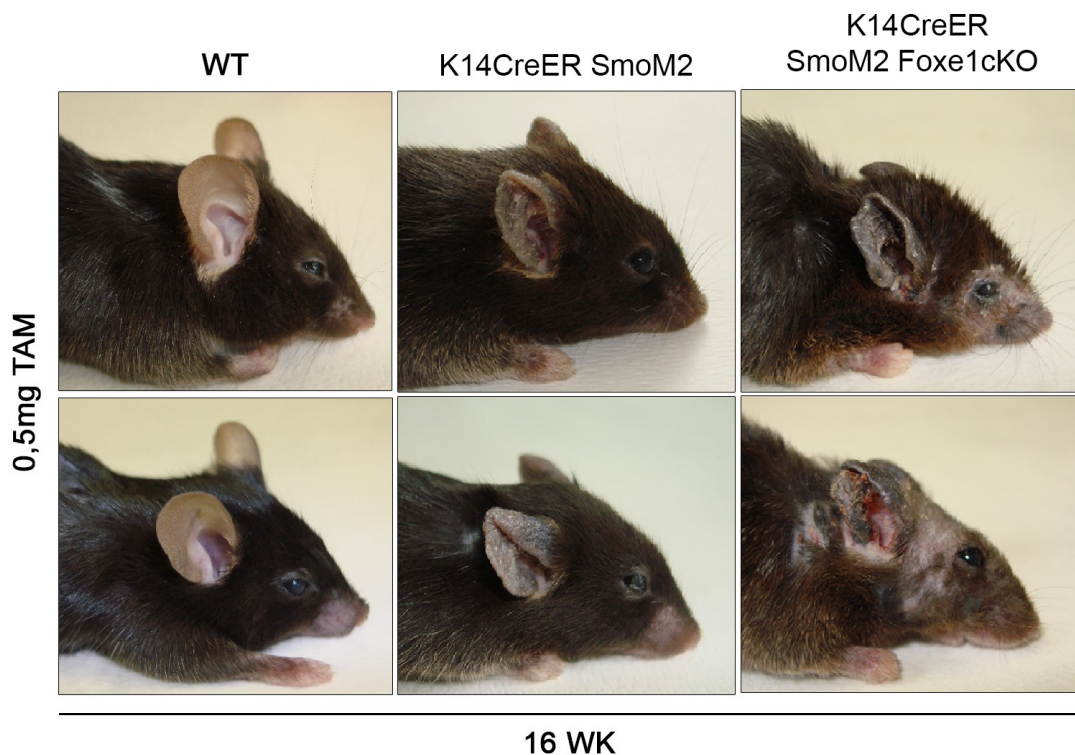


Figure 40. Foxe1 deletion in skin of K14-CreER; SmoM2 mouse model reproduces tumorigenic snout lesions of K5-Gli2; K14-Cre Foxe1fl/fl model. Representative macroscopic appearance of BCC lesions developed in the snouts of Cre negative mice (indicated as WT in figure), K14-CreER; SmoM2 and K14-CreER; SmoM2; Foxe1flox/flox at 16 weeks after tamoxifen administration (TAM 0,5 mg). Experiment was performed using five mice for each experimental group.

Interestingly, microscopic examination of the ear epidermis at 8 weeks after TAM administration revealed that K14-CreER SmoM2 mice formed well-organized multifocal nodular islands with a palisade arrangement of nuclei at the periphery of the nodules separated from the surrounding stroma by clearly visible empty spaces, whereas Foxe1 depleted lesions were larger and less organized (Fig.41 A). In nodular BCC formations, basaloid wells were elongated and lacking of the typical organization of darkly stained basaloid cells with a palisade arrangement of nuclei at the periphery of the clusters.

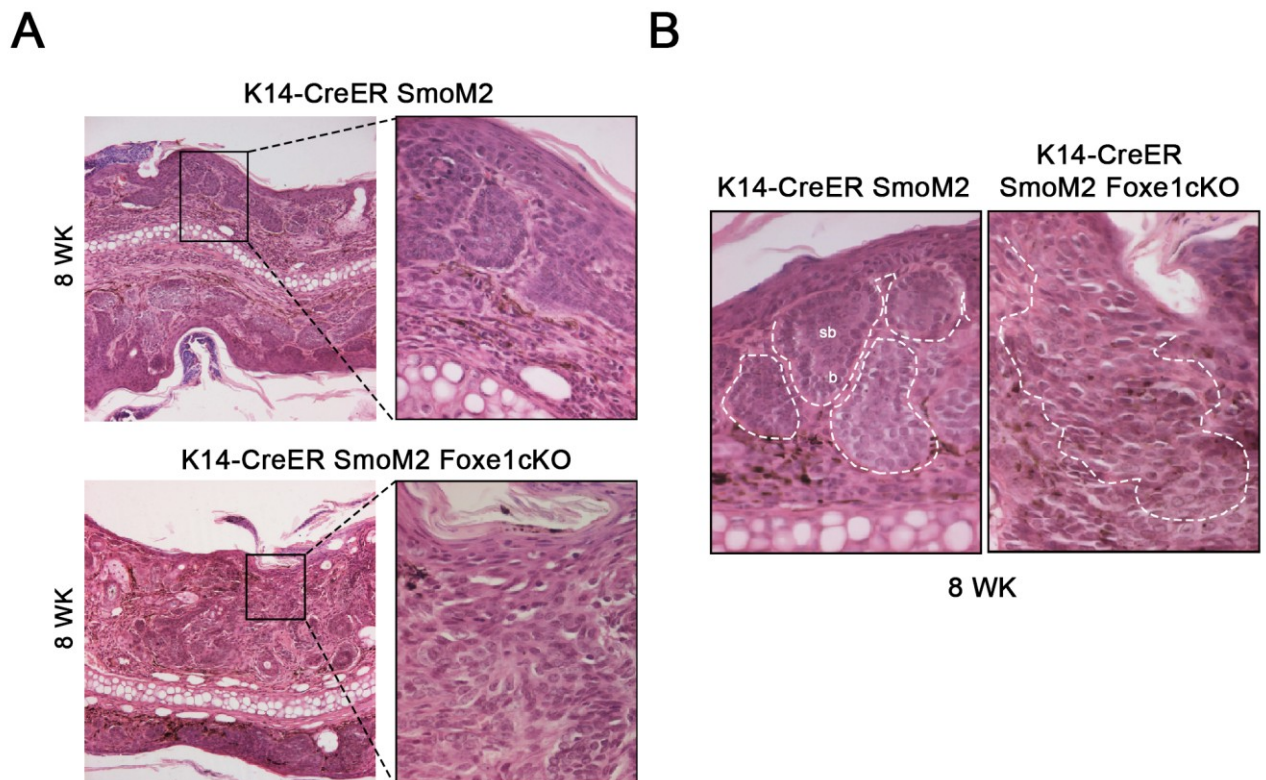


Figure 41. Foxe1 seems to be a determinant of BCC architecture in skin lesions from K14-CreER SmoM2 mouse model. A) Hematoxylin and eosin staining of the BCC lesions from ears of K14-CreER SmoM2 and K14-CreER SmoM2; Foxe1^{flox/flox}. Magnified views of BCC lesions (black box) are depicted in images on right. B) Particulars of BCC lesions developed on ears. Note the more disorganized structure in lesions lacking Foxe1. Magnification, 40 x. sb: suprabasal. b: basal.

Moreover, very often not clustered tumors are observed, in which it was not possible to distinguish basal from suprabasal compartments (Fig.41 B). These *in vivo* observations suggest that Foxe1 may affect tumor architecture of BCC originated in K14-CreER SmoM2 model and the spatial organization of basaloid cells in tumor burdens.

5. DISCUSSION

Non melanoma skin cancers (NMSCs) are the most common type of human cancers worldwide and their incidence is increasing at high rate. Therefore, studies and a lot of efforts are needed to understand the molecular mechanisms underlying tumor formation and to define new strategies to prevent these tumors and to overcome the occurrence of drug resistance and relapse. This class of skin tumors includes Basal Cell Carcinoma (BCC) and cutaneous Squamous Cell Carcinoma (SCC). BCCs are locally invasive epithelial tumors, characterized by inappropriate activation of the Hedgehog (HH) pathway. SCC is less common but more aggressive than BCC, tending to have a more heterogeneous genetic background with a higher incidence of metastasis.

BCC carcinogenesis is characterized by an interruption of canonical differentiation processes of IFE progenitors and consequent deregulation of early-stage follicle lineage markers. This transcriptional reprogramming is orchestrated by Hh and Wnt/b-catenin pathway cooperation (Yang, Andl et al. 2008, Youssef et al., 2012, Larsimont, Youssef et al. 2015).

Here, we investigated the biological function of the forkhead transcription factor Foxe1 in NMSC tumorigenesis in order to define its role in this process. Our previous observations demonstrated that this evolutionarily conserved transcriptional regulator is a specific marker of the Outer Root Sheath (ORS) compartment of HF and that it is positively regulated by the Shh/Gli pathway. Accordingly, Foxe1 expression is involved in this tumorigenic transcriptional reprogramming and its deregulation is associated with BCC, in humans and mice (Brancaccio, et al. 2004; Eichberger, T., et al. 2004). In sharp contrast, Foxe1 is absent or undetectable in more aggressive skin cancers such as SCCs, where its promoter is often hypermethylated (Venza, Visalli et al. 2010).

Downregulation or absence of Foxe1 expression levels has been recognized, by recent studies, as a determinant of thyroid carcinomas susceptibility, consistent with its pro-differentiation role in the developing thyroid and in the adult thyroid (Landa I., et al. 2009; Lidral et al., 2015; He H., et al. 2015). Here we show that, in BCC, the transcriptional program modulated by Foxe1 seems to be contrasting with the concept of a gene overexpressed in cancer. In BCC cells and in WT keratinocytes, Foxe1 controls a subset of genes regulating crucial biological processes. We found that it affects positively genes required for extracellular matrix structure and deposition. ECM constitutes a crucial component of the cell migratory machinery, influencing cell motility and cell-ECM interactions, also in tumor cells. Observations *in vitro* confirmed this biological effect, since Foxe1 causes an impairment of cell migration in NMSC cells, associated to an increase in cell adhesion, as demonstrated both in BCC and SCC cells. Increased cell migration and reduced cell adhesion are hallmarks of tumor cell invasion and tumor spreading. Therefore, our findings support a role for Foxe1 in promoting an adhesive, anti-migratory phenotype of BCC cancer cells, compared to the more motile and invasive behaviour of SCC cells.

The correlation between Foxe1 and cell migration is not a new concept, however its function as a pro-migratory or an inhibitor of migration is still controversial. On one hand, it has been reported that its physiological role during thyroid organogenesis is to drive the correct migration of thyroid buds from the pharyngeal ectoderm to its final destination in the throat (De Felice Nature Genetics 1998; Parlato et al Dev Biology 2004). Moreover, we reported that in skin the ablation of this factor caused an aberrant morphogenesis of the hair follicle (Brancaccio et al., 2004) likely due to

defects of the ORS cells to descend correctly into the dermis. But, on the other hand, recent data obtained in papillary thyroid tumors demonstrate that Foxe1 knockdown leads to increased proliferation, cell migration and invasion consistent with loss of Foxe1 in advanced tumor stages (Ding Z et al Molecular and Cellular Endocrinology 2019), in line with our results. Indeed, we find that Foxe1 restoration in SCC cells caused a strong impairment of cell motility. Similar data are obtained in BCC cells, in which the depletion of Foxe1 caused a gain in cell migration. This unexpected function for a gene overexpressed in cancer can be explained by the induction of putative target genes involving in regulating cell-cell and cell-substrate adhesion. An additional explanation can be found in modulation of putative downstream pathways identified by the gene expression analysis. Among these, we found that “negative regulation of the Rho pathway” and the “WNT non-canonical pathway” are the most enriched biological processes modulated by Foxe1. Our hypothesis is that the migratory defect of tumor cells expressing Foxe1 is caused by a positive modulation of the non-canonical Wnt/PCP signalling, which antagonize the canonical β -catenin cascade causing the inhibition of cell migration, possibly through inactivation of Rac1 via ROCK (Topol, Jiang et al. 2003, Kremenevskaja, von Wasielewski et al. 2005, Toyama, Lee et al. 2010, Rapp, Kiss et al. 2016). In addition, gene expression analysis indicate that Foxe1 plays a major function in negatively regulating signal transduction pathways. This aspect can explain, at least in part, the inhibitory effect of Foxe1 expression observed in cell cycle progression in keratinocytes and in BCC cells, possibly consistent with the indolent nature of this tumor. These *in vitro* findings indicate that Foxe1 negatively regulates cell proliferation and may cause an impairment in cancer stem-like cell renewal potential, as demonstrated by tumorspheres assays. These data, other than confirm the results obtained from genome expression analysis in BCC cells and keratinocytes, support an intriguing contribution in skin tumorigenesis, which could limit the potential aggressiveness of BCC cell lines compared to the more aggressive SCC.

In agreement with the data *in vitro*, we obtained significant results in BCC initiation and maintenance. We took advantages of two distinct mouse models for BCC, the inducible K14-Cre-ER; Rosa-SmoM2-YFP constitutively expressing an active Smo (Mao et al.; 2006, Youssef NCB 2010), and K5-Gli2 that constitutively expresses an active Gli2 (Grachtchouk M. Et al., 2000). In both mouse models, the aberrant activation of the Shh pathway leads to Foxe1 expression, indicating that Foxe1 expression is a common feature observed during BCC development irrespective of the oncogenic hit. Its expression was abundant as that of another HF markers, the transcription factor Sox9 (Kadaja M Fuchs G&D 2014). In both models Foxe1 was expressed in the tumors and not in the hyperplastic interfollicular epidermis, and in SmoM2 mice the spatial distribution of Foxe1 positive cells was mainly restricted to the lower regions of fully developed BCCs, consistent with its physiological expression in the hair follicle of adult skin where it is limited to the lower portion of the most undifferentiated layer (outer root sheath, ORS) (Brancaccio et al., 2004).

In the constitutively mouse model K5-Gli2, the evaluation of the effect of Foxe1 depletion on BCC tumorigenesis, was complicated by late onset and the low and variable tumor number and size formed in this specific mouse model. However, Foxe1 depletion lead to tumorigenic lesions in the snout, a skin area not usually associated to BCC development in this mouse model. In addition, the depletion of Foxe1 in ventral skin caused complete alopecia associated with a general

hyperplasia of the epithelium, hyperplastic sebaceous glands, and loss of the lower portion of the hair follicle, a phenotype not observed in K14-Foxe1 alone.

Importantly, a similar phenotype was observed when we depleted Foxe1 in the inducible BCC model K14-CreER SmoM2, as mice lacking Foxe1 developed lesions in the snout skin.

Moreover, the characteristic superficial BCCs developed in the ear of K14-CreER SmoM2 had a more aggressive and less organized phenotype compared to control mice.

These *in vivo* observations suggest that Foxe1 may affect tumor architecture of BCC originated in K14-CreER SmoM2 model and the spatial organization of basaloid cells, probably affecting ECM assembly and cell-ECM adhesion as indicated by global gene expression analyses.

In conclusion, our study indicates that the transcription factor Foxe1, a marker of the lower portion of the HF, orchestrate an interesting transcriptional program when deregulated in human and mouse BCC. In contrast to what it would be expected for a gene overexpressed in a tumor context, its role affects negatively key biological processes involved in tumorigenesis, such as cell proliferation and migration. The results obtained *in vitro* and *in vivo* are in agreement with very recent results obtained in thyroid cancer (Ding et al 2019) and the concept that this gene seems to be a determinant of the indolent behaviour of BCC tumors as compared to more aggressive SCC in which its expression is silenced by methylation (Venza I, British Journal Dermat 2010). Therefore, we propose that Foxe1 plays a role as crucial modulator of BCC architecture and that its expression is likely to have a significant impact on BCC formation and maintenance by conferring at least in part the well-organized poorly invasive structure of this tumor.

6. LIST OF PUBLICATIONS

TBX1 and Basal Cell Carcinoma: Expression and Interactions with Gli2 and Dvl2 Signaling. Caprio C., Varricchio S., Bilio M., **Feo F.**, Ferrentino R., Russo D., Staibano S., Alfano D., Missero C., Ilardi G. and Baldini A. *Int. J. Mol. Sci.* 2020, 21, 607; doi:10.3390/ijms21020607.

Loss of the SHH effector Foxe1 leads to a more aggressive phenotype in basal cell carcinoma. **Federica Feo**, Simona Ferraioli, Dario Antonini, Claudia Russo, Marina Grachtchouk, Gabriella De Vita, Andrzej Dlugosz, Mario De Felice, Caterina Missero. Manuscript in preparation.

7. REFERENCES

Adam, R. C., H. Yang, Y. Ge, W. H. Lien, P. Wang, Y. Zhao, L. Polak, J. Levorse, S. C. Baksh, D. Zheng and E. Fuchs (2018). "Temporal Layering of Signaling Effectors Drives Chromatin Remodeling during Hair Follicle Stem Cell Lineage Progression." *Cell Stem Cell* 22(3): 398-413 e397.

Ahtiainen, L., Lefebvre, S., Lindfors, P.H., Renvoise', E., Shirokova, V., Vartiainen, M.K., Thesleff, I., and Mikkola, M.L. (2014). Directional cell migration, but not proliferation, drives hair placode morphogenesis. *Dev. Cell* 28, 588–602.

Andl, T., Reddy, S.T., Gaddapara, T., and Millar, S.E. (2002). WNT signals are required for the initiation of hair follicle development. *Dev. Cell* 2, 643–653.

Anna Brancaccio, Annunziata Minichiello, Marina Grachtchouk, Dario Antonini, Hong Sheng, Rosanna Parlato, Nina Dathan³, Andrzej A. Dlugosz and Caterina Missero. Requirement of the forkhead gene *Foxe1*, a target of sonic hedgehog signaling, in hair follicle morphogenesis. *Human Molecular Genetics*, 2004, Vol. 13, No. 21

Bamforth JS, Hughes IA, Lazarus JH, Weaver CM, Harper PS. Congenital hypothyroidism, spiky hair, and cleft palate. *J Med Genet* 1989; 26:49-51.

Carlsson, P. and M. Mahlapuu (2002). "Forkhead transcription factors: key players in development and metabolism." *Dev Biol* 250(1): 1-23.

Chen, L.; Fulcoli, F.G.; Ferrentino, R.; Martucciello, S.; Illingworth, E.A.; Baldini, A. Transcriptional control in cardiac progenitors: *Tbx1* interacts with the BAF chromatin remodeling complex and regulates *Wnt5a*. *Plos Genet.* 2012, 8, e1002571.

Chen, T.; Heller, E.; Beronja, S.; Oshimori, N.; Stokes, N.; Fuchs, E. An RNA interference screen uncovers a new molecule in stem cell self-renewal and long-term regeneration. *Nature* 2012, 485, 104–108

Chen, Y. H. and Y. Q. Zhang (2018). "Exploration of the association between *FOXE1* gene polymorphism and differentiated thyroid cancer: a meta-analysis." *BMC Med Genet* 19(1): 83.

Cinzia Caprio, Silvia Varricchio, Marchesa Bilio, Federica Feo, Rosa Ferrentino, Daniela Russo, Stefania Staibano, Daniela Alfano, Caterina Missero, Gennaro Ilardi and Antonio Baldini. *1TBX1* and Basal Cell Carcinoma: Expression and Interactions with *Gli2* and *Dvl2* Signaling. *Int. J. Mol. Sci.* 2020, 21, 607; doi:10.3390/ijms21020607.

Cotsarelis G, Sun, TT, Lavker, RM. Label-retaining cells reside in the bulge area of pilosebaceous unit: Implications for follicular stem cells, hair cycle, and skin carcinogenesis. *Cell* 1990 61: 1329–1337

Dathan Nina, Rosanna Parlato, Annamaria Rosica, Mario de Felice, Roberto di Lauro. Distribution of the *titf2/foxe1* Gene Product Is Consistent With an Important Role in the Development of Foregut Endoderm, Palate, and Hair. *DEVELOPMENTAL DYNAMICS* 224:450–456 (2002)

Daya-Grosjean, L. & Couve-Privat, S. Sonic hedgehog signaling in basal cell carcinomas. *Cancer Lett.* 225, 181–192 (2005).

De Felice M, Ovitt C, Biffali E, Rodriguez-Mallon A, Arra C, Anastassiadis K, Macchia PE, Mattei MG, Mariano A, Schöler H, Macchia V, Di Lauro R. A mouse model for hereditary thyroid dysgenesis and cleft palate. *Nat Genet.* 1998 Aug;19(4):395-8.

De Felice, M. and R. Di Lauro (2004). "Thyroid development and its disorders: genetics and molecular mechanisms." *Endocr Rev* 25(5): 722-746.

Dentice, M., C. Luongo, S. Huang, R. Ambrosio, A. Elefante, D. Mirebeau-Prunier, A. M. Zavacki, G. Fenzi, M. Grachtchouk, M. Hutchin, A. A. Dlugosz, A. C. Bianco, C. Missero, P. R. Larsen and D. Salvatore (2007). "Sonic hedgehog-induced type 3 deiodinase blocks thyroid hormone action enhancing proliferation of normal and malignant keratinocytes." *Proc Natl Acad Sci U S A* 104(36): 14466-14471.

Eichberger T et al. FOXE1, a new transcriptional target of GLI2 is expressed in human epidermis and basal cell carcinoma. *J Invest Dermatol.* 2004 May;122(5):1180-7.

Ervin H. Epstein. Basal cell carcinomas: attack of the hedgehog. *Nat Rev Cancer.* 2008 October ; 8(10): 743–754. doi:10.1038/nrc2503.

Fernandez, L. P., A. Lopez-Marquez, A. M. Martinez, G. Gomez-Lopez and P. Santisteban (2013). "New insights into FoxE1 functions: identification of direct FoxE1 targets in thyroid cells." *PLoS One* 8(5): e62849.

Fuchs E, Green H. 1980.Changes in keratin gene expression during terminal differentiation of the keratinocyte. *Cell* 19:1033-1042.

Fuchs E, Horsley V. More than one way to skin . . . *Genes Dev.* 2008 Apr 15;22(8):976-85.

Fulcoli, F.G.; Franzese, M.; Liu, X.; Zhang, Z.; Angelini, C.; Baldini, A. Rebalancing gene haploinsufficiency in vivo by targeting chromatin. *Nat. Commun.* 2016, 7, 11688.

Gat, U., DasGupta, R., Degenstein, L., and Fuchs, E. (1998). De Novo hair follicle morphogenesis and hair tumors in mice expressing a truncated beta-catenin in skin. *Cell* 95, 605–614.

Glick, S. E. Millar and A. A. Dlugosz (2008). "Pathological responses to oncogenic Hedgehog signaling in skin are dependent on canonical Wnt/beta3-catenin signaling." *Nat Genet* 40(9): 1130-1135.

Golson, M. L. and K. H. Kaestner (2016). "Fox transcription factors: from development to disease." *Development* 143(24): 4558-4570.

Grachtchouk M, Mo R, Yu S, Zhang X, Sasaki H, Hui CC, et al. Basal cell carcinomas in mice overexpressing Gli2 in skin. *Nature genetics* 2000;24(3):216-7.

Grachtchouk M, Pero J, Yang SH et al. (2011) Basal cell carcinomas in mice arise from hair follicle stem cells and multiple epithelial progenitor populations. *J Clin Invest* 121:1768–81.

Grachtchouk V, Grachtchouk M, Lowe L et al. (2003) The magnitude of hedgehog signalling activity defines skin tumor phenotype. *EMBO J* 22:2741–51.

Halasi, M. and Gartel, A. L. (2013). FOX(M1) news—it is cancer. *Mol. Cancer Ther.* 12, 245-254.

Hannenhalli, S. and Kaestner, K. H. (2009). The evolution of Fox genes and their role in development and disease. *Nat. Rev. Genet.* 10, 233-240.

He H, Li W, Liyanarachchi S, Jendrzewski J, Srinivas M, Davuluri RV, et al. Genetic predisposition to papillary thyroid carcinoma: involvement of FOXE1, TSHR, and a novel lincRNA gene, PTCSC2. *The Journal of clinical endocrinology and metabolism* 2015;100(1):E164-72.

Huelsken, J., Vogel, R., Erdmann, B., Cotsarelis, G., and Birchmeier, W. (2001). beta-Catenin controls hair follicle morphogenesis and stem cell differentiation in the skin. *Cell* 105, 533–545.

Jamora, C., DasGupta, R., Kocieniewski, P., and Fuchs, E. (2003). Links between signal transduction, transcription and adhesion in epithelial bud development. *Nature* 422, 317–322.

Kaestner, K. H., Katz, J., Liu, Y., Drucker, D. J. and Schutz, G. (1999). Inactivation of the winged helix transcription factor HNF3ALPHA affects glucose homeostasis and islet glucagon gene expression in vivo. *Genes Dev.* 13, 495-504.

Kasper, M., V. Jaks, D. Hohl and R. Toftgard (2012). "Basal cell carcinoma - molecular biology and potential new therapies." *J Clin Invest* 122(2): 455-463.

Kremenevskaja, N., R. von Wasielewski, A. S. Rao, C. Schofl, T. Andersson and G. Brabant (2005). "Wnt-5a has tumor suppressor activity in thyroid carcinoma." *Oncogene* 24(13): 2144-2154.

Landa I, Ruiz-Llorente S, Montero-Conde C, Inglada-Perez L, Schiavi F, Leskela S, et al. The variant rs1867277 in FOXE1 gene confers thyroid cancer susceptibility through the recruitment of USF1/USF2 transcription factors. *PLoS genetics* 2009;5(9):e1000637.

Larsimont, J. C., K. K. Youssef, A. Sanchez-Danes, V. Sukumaran, M. Defrance, B. Delatte, M. Liagre, P. Baatsen, J. C. Marine, S. Lippens, C. Guerin, V. Del Marmol, J. M. Vanderwinden, F. Fuks and C. Blanpain (2015). "Sox9 Controls Self-Renewal of Oncogene Targeted Cells and Links Tumor Initiation and Invasion." *Cell Stem Cell* 17(1): 60-73.

Lehmann, O.J., Sowden, J.C., Carlsson, P., Jordan, T. and Bhattacharya, S.S. (2003) Fox's in development and disease. *Trends Genet.*, 19, 339–344.

Li, C. M.-C., Gocheva, V., Oudin, M. J., Bhutkar, A., Wang, S. Y., Date, S. R., Ng, S. R., Whittaker, C. A., Bronson, R. T., Snyder, E. L. et al. (2015a). Foxa2 and Cdx2 cooperate with Nkx2-1 to inhibit lung adenocarcinoma metastasis. *Genes Dev.* 29, 1850-1862.

Lidral AC, Liu H, Bullard SA, Bonde G, Machida J, Visel A, et al. A Single Nucleotide Polymorphism Associated with Isolated Cleft Lip and Palate, Thyroid Cancer and Hypothyroidism Alters the Activity of an Oral Epithelium and Thyroid Enhancer Near FOXE1. *Human molecular genetics* 2015.

Ma, J., X. Huang, Z. Li, Y. Shen, J. Lai, Q. Su, J. Zhao and J. Xu (2019). "FOXE1 supports the tumor promotion of Gli2 on papillary thyroid carcinoma by the Wnt/beta-catenin pathway." *J Cell Physiol* 234(10): 17739-17748.

Maglic, D., K. Schlegelmilch, A. F. Dost, R. Panero, M. T. Dill, R. A. Calogero and F. D. Camargo (2018). "YAP-TEAD signaling promotes basal cell carcinoma development via a c-JUN/AP1 axis." *EMBO J* 37(17).

Mill P et al. Sonic hedgehog-dependent activation of Gli2 is essential for embryonic hair follicle development. *Genes Dev.* 2003 Jan 15;17(2):282-94.

Millar SE. Molecular mechanisms regulating hair follicle development. *J Invest Dermatol.* 2002 Feb;118(2):216-25.

Missero C. The genetic evolution of skin squamous cell carcinoma: tumor suppressor identity matters. *Exp Dermatol.* 2016 May 19. doi: 10.1111/exd.13075.

Missero Caterina and Antonini Dario. Crosstalk among p53 family members in cutaneous carcinoma. *Experimental Dermatology*, 2014, 23, 143–146 143. 2014

Nikitski, A., V. Saenko, M. Shimamura, M. Nakashima, M. Matsuse, K. Suzuki, T. Rogounovitch, T. Bogdanova, N. Shibusawa, M. Yamada, Y. Nagayama, S. Yamashita and N. Mitsutake (2016). "Targeted Foxe1 Overexpression in Mouse Thyroid Causes the Development of Multinodular Goiter But Does Not Promote Carcinogenesis." *Endocrinology* 157(5): 2182-2195.

Ning, H., H. Mitsui, C. Q. Wang, M. Suarez-Farinas, J. Gonzalez, K. R. Shah, J. Chen, I. Coats, D. Felsen, J. A. Carucci and J. G. Krueger (2013). "Identification of anaplastic lymphoma kinase as a potential therapeutic target in Basal Cell Carcinoma." *Oncotarget* 4(12): 2237-2248.

Ouspenskaia et al., 2016, *Cell* 164, 156–169 January 14, 2016 ©2016 Elsevier Inc.

Pasca di Magliano M, Hebrok M. Hedgehog signalling in cancer formation and maintenance. *Nat Rev Cancer*. 2003 Dec;3(12):903-11.

Rapp, J., E. Kiss, M. Meggyes, E. Szabo-Meleg, D. Feller, G. Smuk, T. Laszlo, V. Sarosi, T. F. Molnar, K. Kvell and J. E. Pongracz (2016). "Increased Wnt5a in squamous cell lung carcinoma inhibits endothelial cell motility." *BMC Cancer* 16(1): 915.

Rook A and Burns T (2004) *Rook's textbook of dermatology* (Blackwell Science, Malden, Mass.) 7th Ed. p 4 v. (paged continuously).

Ruiz i Altaba A, Sánchez P, Dahmane N. Gli and hedgehog in cancer: tumours, embryos and stem cells. *Nat Rev Cancer*. 2002 May;2(5):361-72.

S. Y. and A. A. Dlugosz (2014). "Basal cell carcinoma, Hedgehog signaling, and targeted therapeutics: the long and winding road." *J Invest Dermatol* 134(e1): E18-22.

Sasaki, H.; Hui, C.; et al. Dissecting the oncogenic potential of Gli2: Deletion of an NH(2)-terminal fragment alters skin

Schmidt-Ullrich R, Paus R. Molecular principles of hair follicle induction and morphogenesis. *Bioessays*. 2005 Mar;27(3):247-61.

Schneider MR, Schmidt-Ullrich R, Paus R. The hair follicle as a dynamic miniorgan. *Curr Biol*. 2009 Feb 10; 19(3):R132-42.

Shelby C. Peterson, Markus Eberl, Andrzej A. Dlugosz, Sunny Y. Wong Basal Cell Carcinoma Preferentially Arises from Stem Cells within Hair Follicle and Mechanosensory Niches. *Cell Stem Cell* 16, 400–412, April 2, 2015 ©2015 Elsevier

Shen Q, Jin H, Wang X. 2013. Epidermal stem cells and their epigenetic regulation. *Int J Mol Sci.* 2013 Aug 30;14(9):17861-80. doi: 10.3390/ijms140917861.

Sheng, H.; Goich, S.; Wang, A.; Grachtchouk, M.; Lowe, L.; Mo, R.; Lin, K.; de Sauvage, F.J.; Simpson CL, Patel DM, Green KJ. 2011. Deconstructing the skin: cytoarchitectural determinants of epidermal morphogenesis. *Nat Rev Mol Cell Biol* 12:565-580.

Sonic hedgehog signaling is essential for hair development. *Curr. Biol.* 8, 1058–1068. Woo, W.M., Zhen, H.H., and Oro, A.E. (2012). Shh maintains dermal papilla identity and hair morphogenesis via a Noggin-Shh regulatory loop. *Genes Dev.* 26, 1235–1246.

St-Jacques, B., Dassule, H.R., Karavanova, I., Botchkarev, V.A., Li, J., Danielian, P.S., McMahon, J.A., Lewis, P.M., Paus, R., and McMahon, A.P. (1998).

Sugimachi, K., T. Matsumura, T. Shimamura, H. Hirata, R. Uchi, M. Ueda, S. Sakimura, T. Iguchi, H. Eguchi, T. Masuda, K. Morita, K. Takenaka, Y. Maehara, M. Mori and K. Mimori (2016). "Aberrant Methylation of FOXE1 Contributes to a Poor Prognosis for Patients with Colorectal Cancer." *Ann Surg Oncol* 23(12): 3948-3955.

Topol, L., X. Jiang, H. Choi, L. Garrett-Beal, P. J. Carolan and Y. Yang (2003). "Wnt-5a inhibits the canonical Wnt pathway by promoting GSK-3-independent beta-catenin degradation." *J Cell Biol* 162(5): 899-908.

Toyama, T., H. C. Lee, H. Koga, J. R. Wands and M. Kim (2010). "Noncanonical Wnt11 inhibits hepatocellular carcinoma cell proliferation and migration." *Mol Cancer Res* 8(2): 254-265.

van Genderen, C., Okamura, R.M., Farin~ as, I., Quo, R.G., Parslow, T.G., Bruhn, L., and Grosschedl, R. (1994). Development of several organs that require inductive epithelial-mesenchymal interactions is impaired in LEF-1-deficient mice. *Genes Dev.* 8, 2691–2703.

Venza, I., M. Visalli, B. Tripodo, G. De Grazia, S. Loddo, D. Teti and M. Venza (2010). "FOXE1 is a target for aberrant methylation in cutaneous squamous cell carcinoma." *Br J Dermatol* 162(5): 1093-1097.

Wang GY, Wang J, Mancianti ML et al. (2011) Basal cell carcinomas arise from hair follicle stem cells in *ptch1*(β -/-) mice. *Cancer Cell* 19:114–24.

Wang, J., Zhu, C.-P., Hu, P.-F., Qian, H., Ning, B.-F., Zhang, Q., Chen, F., Liu, J., Shi, B., Zhang, X. et al. (2014b). *Foxa2* suppresses the metastasis of hepatocellular carcinoma partially through matrix metalloproteinase-9 inhibition. *Carcinogenesis* 35, 2576-2583.

Watt, FM. The stem cell compartment in human interfollicular epidermis. *J Dermatol Sci* 2002 28: 173–180.

Wong, S. Y. and A. A. Dlugosz (2014). "Basal cell carcinoma, Hedgehog signaling, and targeted therapeutics: the long and winding road." *J Invest Dermatol* 134(e1): E18-22.

Yamagishi, H.; Maeda, J.; Hu, T.; McAnally, J.; Conway, S.J.; Kume, T.; Meyers, E.N.; Yamagishi, C.; Srivastava, D. *Tbx1* is regulated by tissue-specific forkhead proteins through a common Sonic hedgehog-responsive enhancer. *Genes Dev.* 2003, 17, 269–281.

Yang, H., R. C. Adam, Y. Ge, Z. L. Hua and E. Fuchs (2017). "Epithelial-Mesenchymal Micro-niches Govern Stem Cell Lineage Choices." *Cell* 169(3): 483-496 e413.

Yang, S. H., T. Andl, V. Grachtchouk, A. Wang, J. Liu, L. J. Syu, J. Ferris, T. S. Wang, A. B. Glick, S. E. Millar and A. A. Dlugosz (2008). "Pathological responses to oncogenic Hedgehog signaling in skin are dependent on canonical Wnt/beta3-catenin signaling." *Nat Genet* 40(9): 1130-1135.

Youssef KK, Van KA, Lapouge G et al. (2010) Identification of the cell lineage at the origin of basal cell carcinoma. *Nat Cell Biol* 12: 299–305.

Zannini M, Avantiaggiato V, Biffali E, Arnone MI, Sato K, Pischetola M, Taylor BA, Phillips SJ, Simeone A, Di Lauro R. TTF-2, a new forkhead protein, shows a temporal expression in the developing thyroid which is consistent with a role in controlling the onset of differentiation. *EMBO J.* 1997 Jun 2;16(11):3185-97.

Zhang J, Yang Y, Yang T, Yuan S, Wang R, Pan Z, et al. Double-negative feedback loop between microRNA-422a and forkhead box (FOX) G1/Q1/E1 regulates hepatocellular carcinoma tumor growth and metastasis. *Hepatology.* 2015;61(2):561-573. doi: 10.1002/hep.27491

Zhang Y et al. Reciprocal requirements for EDA/EDAR/NF-kappaB and Wnt/beta-catenin signaling pathways in hair follicle induction. *Dev Cell.* 2009 Jul;17(1):49-61.

Zhu, H. (2016). Forkhead box transcription factors in embryonic heart development and congenital heart disease. *Life Sci.* 144, 194-201.